NAVAL POSTGRADUATE SCHOOL

MONTEREY, CALIFORNIA

THESIS

NUMERICAL PERFORMANCE PREDICTION OF A MINIATURE RAMJET AT MACH 4

by

Bingqiang Chen

September 2012

Thesis Advisor:	Garth V. Hobson
Second Reader:	Christopher M. Brophy

THIS PAGE INTENTIONALLY LEFT BLANK

REPORT DOCUMENTATION PAGE			*Form Approved OMB No. 0704-0188*
Public reporting burden for this collection of information is estimated to average 1 hour per response, including the time for reviewing instruction, searching existing data sources, gathering and maintaining the data needed, and completing and reviewing the collection of information. Send comments regarding this burden estimate or any other aspect of this collection of information, including suggestions for reducing this burden, to Washington headquarters Services, Directorate for Information Operations and Reports, 1215 Jefferson Davis Highway, Suite 1204, Arlington, VA 22202-4302, and to the Office of Management and Budget, Paperwork Reduction Project (0704-0188) Washington DC 20503.			
1. AGENCY USE ONLY *(Leave blank)*	**2. REPORT DATE** September 2012	**3. REPORT TYPE AND DATES COVERED** Master's Thesis	
4. TITLE AND SUBTITLE Numerical Performance Prediction of a Miniature at Mach 4			**5. FUNDING NUMBERS**
6. AUTHOR(S) Bingqiang Chen			
7. PERFORMING ORGANIZATION NAME(S) AND ADDRESS(ES) Naval Postgraduate School Monterey, CA 93943-5000			**8. PERFORMING ORGANIZATION REPORT NUMBER**
9. SPONSORING /MONITORING AGENCY NAME(S) AND ADDRESS(ES) N/A			**10. SPONSORING/MONITORING AGENCY REPORT NUMBER**
11. SUPPLEMENTARY NOTES The views expressed in this thesis are those of the author and do not reflect the official policy or position of the Department of Defense or the U.S. Government.			
12a. DISTRIBUTION / AVAILABILITY STATEMENT Approved for public release; distribution is unlimited.			**12b. DISTRIBUTION CODE** A

13. ABSTRACT (maximum 200 words)

Using a 3-D axis-symmetric model, the cold-flow performance of a miniature ramjet in Mach 4 flow was predicted with the computational fluids dynamic (CFD) code from ANSYS-CFX. The nozzle-throat area was varied to increase the backpressure and this pushed the normal shock that was sitting within the inlet, out to the lip of the inlet cowl.

Using the eddy dissipation combustion model in ANSYS-CFX, a combustion analysis was performed on the miniature ramjet. The analysis involved the single-step, stoichiometric combustion of hydrogen and oxygen within the combustion chamber of the ramjet.

The drag force induced on the miniature ramjet when subjected to Mach 4 flow in a supersonic wind tunnel was measured using cryogenic strain gauges arranged in a Wheatstone bridge. A CFD cold-flow drag prediction was compared against this measured drag force to establish the former's accuracy in drag prediction.

For all CFD predictions, the two-equation Shear-Stress-Transport (SST) turbulence model was used. The SST turbulence model blends the k-epsilon and k-omega turbulence model and effects the transportation of the turbulent shear stress for improved accuracy in turbulence modeling.

14. SUBJECT TERMS Mach 4, Ramjet, Drag, Turbulence Modeling, Simulation, ANSYS CFX			**15. NUMBER OF PAGES** 131
			16. PRICE CODE
17. SECURITY CLASSIFICATION OF REPORT Unclassified	**18. SECURITY CLASSIFICATION OF THIS PAGE** Unclassified	**19. SECURITY CLASSIFICATION OF ABSTRACT** Unclassified	**20. LIMITATION OF ABSTRACT** UU

NSN 7540-01-280-5500

Standard Form 298 (Rev. 8-98)
Prescribed by ANSI Std. Z39.18

THIS PAGE INTENTIONALLY LEFT BLANK

Approved for public release; distribution is unlimited

NUMERICAL PERFORMANCE PREDICTION OF A MINIATURE RAMJET AT MACH 4

Bingqiang Chen
Major, Singapore Armed Forces
B.Eng., Nanyang Technological University, 2007

Submitted in partial fulfillment of the
requirements for the degree of

MASTER OF SCIENCE IN ENGINEERING SCIENCE (MECHANICAL ENGINEERING)

from the

NAVAL POSTGRADUATE SCHOOL
September 2012

Author: Bingqiang Chen

Approved by: Garth V. Hobson
Thesis Advisor

Christopher M. Brophy
Second Reader

Knox T. Milsaps
Chair, Department of Mechanical
and Aerospace Engineering

THIS PAGE INTENTIONALLY LEFT BLANK

ABSTRACT

Using a 3-D axis-symmetric model, the cold-flow performance of a miniature ramjet in Mach 4 flow was predicted with the computational fluids dynamic (CFD) code from ANSYS-CFX. The nozzle-throat area was varied to increase the backpressure and this pushed the normal shock that was sitting within the inlet, out to the lip of the inlet cowl.

Using the eddy dissipation combustion model in ANSYS-CFX, a combustion analysis was performed on the miniature ramjet. The analysis involved the single-step, stoichiometric combustion of hydrogen and oxygen within the combustion chamber of the ramjet.

The drag force induced on the miniature ramjet when subjected to Mach 4 flow in a supersonic wind tunnel was measured using cryogenic strain gauges arranged in a Wheatstone bridge. A CFD cold-flow drag prediction was compared against this measured drag force to establish the former's accuracy in drag prediction.

For all CFD predictions, the two-equation Shear-Stress-Transport (SST) turbulence model was used. The SST turbulence model blends the k-epsilon and k-omega turbulence model and effects the transportation of the turbulent shear stress for improved accuracy in turbulence modeling.

THIS PAGE INTENTIONALLY LEFT BLANK

TABLE OF CONTENTS

THIS PAGE INTENTIONALLY LEFT BLANK

LIST OF FIGURES

LIST OF TABLES

LIST OF ACRONYMS AND ABBREVIATIONS

CFD	Computational Fluid Dynamics
EDM	Eddy Dissipation Model
RANS	Reynolds-Averaged Navier-Stokes
RMS	Root-Mean-Square
SST	Shear Stress Transport
SSWT	Supersonic Wind Tunnel
atm	Unit: Atmosphere
$CD_{k\omega}$	Cross-Diffusion Term [Pa s]
P_t	Total Pressure [Pa]
ε	Turbulence Dissipation [$m^2\ s^{-3}$]
k	Turbulence Kinetic Energy [$J\ kg^{-1}$]
μ_t	Turbulence Eddy Viscosity [Pa s]
ω	Turbulence Frequency [s^{-1}]
Ω	Vorticity [s^{-1}]
y	Dimensionless distance to the nearest wall

THIS PAGE INTENTIONALLY LEFT BLANK

ACKNOWLEDGMENTS

I would like to extend warm appreciation in acknowledging several people whose efforts greatly contributed to the successful completion of this thesis.

A sincere thank you to Mr. John Mobley, of the mechanical-engineering machine shop. His dedication and precision in building the ramjet were indispensable.

Many thanks also to Mr. Douglas Seivwright, who, despite his busy schedule, took time off to help bond the strain gauges onto the flexures, a delicate job that he has mastered over many years.

I am grateful to Mr. John Gibson for his help in putting the ramjet together and setting up the wind tunnel for experiments. Without his skills, the experiments would never have run smoothly.

And finally, I thank my advisor, Professor Garth Hobson, for the opportunity to work with him and the close guidance he provided from start to finish.

THIS PAGE INTENTIONALLY LEFT BLANK

I. INTRODUCTION

In 1913, René Lorin, a French inventor, conceived the concept of the ramjet, a rotor-less air-breathing jet engine. While he did not succeed in building a prototype, he understood that there would be insufficient pressure to operate a ramjet in subsonic flight. The interest in ramjets picked up, and in 1938, a French engineer, René Leduc, sent the Leduc 0.10, the first ramjet-powered aircraft, into the skies. The Leduc 1.0, achieved a Mach number of 0.85, remarkable for its time.

The capability of ramjets delivering high speed flights has always been an area of interest to the military. In 1976, the turbo-ramjet powered SR-71, a military reconnaissance plane made its maiden flight, achieving Mach 3.3+ with a top speed of over 3500 m/s. While it is still the fastest manned aircraft, the bigger significance to the military is its ability to outfly almost any threat launched against it. In 2006, the ramjet-powered BrahMos cruise missile was introduced. At Mach 3, it is the world's fastest cruise missile. This essentially translates to high survivability rate against any interceptor, and hence a higher possibility of hitting the target.

While these ramjet engines powering military flight have been huge, there are many potential uses for miniaturized ramjets in defense technologies. Possibilities include employment as an anti-material kinetic round at standoff distances and even to power the flight of mini/micro unmanned, aerial vehicles (UAV). However, before these ideas turn into reality, there must be sufficient knowledge of the performance envelope involved.

This thesis takes on the work of Fergurson [1] and Khoo [2]. In [1], a miniature ramjet was designed for flight at Mach 4 and the cold-flow performance of the ramjet was evaluated using Overflow computational fluid dynamics (CFD) code and partially validated through tests in a supersonic wind tunnel (SSWT). A follow-up of the analysis was performed in [2] with the CFD-FASTRAN code in an attempt to model the combustion process in the ramjet. However, due to limited computing power and limitations in the CFD code used, the analysis did not cover the operating conditions of the ramjet.

In [1] and [2], the cold-flow CFD analyses showed an oblique shock forming at the inlet cowl where a normal shock was expected. In [2], it was hypothesized that this observation was due to the nozzle's throat being too wide. The current research attempts to investigate this with variations in nozzle-throat sizing.

In the design of the ramjet in [1], fuel ports were added to the nose cone of the ramjet to induce early fuel-air mixing. However, computationally, the impact of fluid injections through these tip ports were not analyzed. The current research aims to determine how the flow field will be affected by fluid injection through these tip ports.

Exploiting the power of parallel processing, the present study revisits the analysis performed in [1] and [2] using CFD code by ANSYS-CFX to perform 3-D combustion analysis of the ramjet. Hydrogen fuel was injected through the rear fuel ports on the struts for combustion.

Finally, in [2], the CFD predictions and experimental results in wind-tunnel testing showed a disparity in the drag profiles observed. The present study revisits this with a new model and sensors in a wind-tunnel experiment.

Work done in this thesis will provide a better understanding of the miniature ramjet and lay the foundations required for a flight test.

II. NUMERICAL PERFORMANCE PREDICTION WITH ANSYS-CFX

A. ANSYS-CFX

In [1] and [2], the CFD codes used for the numerical performance predictions were NASA Overflow code and the CFDRC-FASTRAN code, respectively.

For this thesis, version 14 of the ANSYS Workbench suite of tools by ANSYS, Inc., was used. The ANSYS Workbench suite provides a simple workflow for the management of the project, from mesh generation (ANSYS-Meshing) to problem setup, numerical simulation, and post-processing of the simulation results.

ANSYS-CFX, a finite-volume-based CFD code by ANSYS, Inc., was used for numerical performance predictions. ANSYS-CFX comprises CFX-PRE, CFX-SOLVER, and CFX-POST.

In the CFD analysis with ANSYS-CFX, the meshed model was transferred into CFX-PRE, where the problem was set up and the implicit boundary conditions were applied. Thereafter, the CFX-SOLVER was invoked for flow computation, where the Navier-Stokes equation was solved in its conservative form [3].

The CFX-SOLVER supports parallel processing for complex models requiring high computational powers. Additionally, ANSYS-CFX can analyze reacting flows with its combustion model. For this study, the eddy dissipation model (EDM) was used with the shear stress transport (SST) turbulence model. The results of the flow computation were then flowed to CFX-POST for viewing and post processing.

B. TURBULENCE MODELLING

At high Reynolds numbers, turbulence develops in flows; motion of the fluid particles becomes random, with velocities and pressures varying with time [3]. For the prediction of turbulence effects, ANYS-CFX supports numerous Reynolds-Averaged Navier-Stokes (RANS) equation-based turbulence models. Based upon the turbulent eddy viscosity concept, two-equation turbulence model represents the turbulence properties of the flow with two additional transport equations. The k-epsilon (k-ε) and k-omega (k-(ω) turbulence models belong to the class of two-equation models and are used for many common engineering problems.

In the k-ε model, the two additional equations involve the transport of turbulence kinetic energy (k) and turbulence dissipation (ε). In general, the model gives reasonable predictions for free-shear-layer flow with relatively low pressure gradients and is insensitive to free-stream conditions. The near-wall high grid sensitivity and limited accuracy in wall-bounded flows with large pressure gradients are known weaknesses of the model [4].

The k-ω model involves the transportation of k and the turbulence frequency (ω). Unlike the k-ε model, the k-ω model does not employ explicit wall-dampening functions for near-wall treatment. Numerically stable, it performs very well in the logarithmic region and is the preferred model in the sub-layer of the boundary layer. However, the k-ω model is very sensitive to free-stream conditions [4].

Like many other turbulence models based on the eddy viscosity concept, both the k-ε and k-ω turbulence models falter in the prediction of flow separations from smooth surfaces [3] [4].

The SST turbulence model integrates the accuracy of the k-ω turbulence model in the near-wall region, with the free-stream independence of the k-ε model. In addition, for improved flow-separation prediction from smooth surfaces, the transport effect of the principal turbulent shear stress is incorporated [4].

Transforming the k-ε model to include a cross-diffusion term, and combining with the k-ω model, the two-equation SST model takes the form:

$$\frac{D\rho k}{Dt} = \tau_{ij}\frac{\partial u_i}{\partial x_j} - \beta^* \rho\omega k + \frac{\partial}{\partial x_j}\left[\left(\mu + \sigma_k \mu_t\right)\frac{\partial k}{\partial x_j}\right]$$

$$\frac{D\rho\omega}{Dt} = \frac{\gamma}{v_t}\tau_{ij}\frac{\partial u_i}{\partial x_j} - \beta\rho\omega^2 + \frac{\partial}{\partial x_j}\left[\left(\mu + \sigma_\omega \mu_t\right)\frac{\partial \omega}{\partial x_j}\right] + 2\left(1 - F_1\right)\rho\sigma_{\omega 2}\frac{1}{\omega}\frac{\partial k}{\partial x_j}\frac{\partial \omega}{\partial x_j}$$

where

$$\tau_{ij} = \mu_t \left(\frac{\partial u_i}{\partial x_j} + \frac{\partial u_j}{\partial x_i} - \frac{2}{3} \frac{\partial u_k}{\partial x_j} \delta_{ij} \right) - \frac{2}{3} \rho k \delta_{ij}$$

The turbulent eddy viscosity is obtained from a limiter to turbulent shear stress:

$$\mu_t = \rho v_t = \frac{a_1 k \rho}{\max\left(a_1 \omega; \Omega F_2\right)}$$

where Ω is the absolute value of vorticity. The blending of the k-ε and k-ω model is achieved through the blending functions F_1 and F_2, which evaluates to 1 in the near-wall region and 0 when away from the surface.

$$F_1 = \tanh\left(\left[\min\left(\max\left(\frac{\sqrt{k}}{0.09\omega y}, \frac{500v}{y^2\omega}\right), \frac{4\rho\sigma_{\omega 2} k}{CD_{k\omega} y^2}\right)\right]^4\right)$$

$$F_2 = \tanh\left(\left[\max\left(\frac{2\sqrt{k}}{0.09\omega y}, \frac{500v}{y^2\omega}\right)\right]^2\right)$$

y is the distance to the nearest wall and $CD_{k\omega}$ is the cross-diffusion term:

$$CD_{k\omega} = \max\left(2\rho\sigma_{\omega 2} \frac{1}{\omega} \frac{\partial k}{\partial x_j} \frac{\partial w}{\partial x_j}, 10^{-20}\right)$$

The SST turbulence model is the default turbulence model used in this thesis. Full derivation of the SST turbulence model is available in [5].

C. COMBUSTION MODELING

The combustion model used in the thesis is the Eddy Dissipation Model (EDM). In the EDM, the fast chemical rate of reaction has direct relation to the molecular-level mixing rate of the reactants. Relative to the flow transport process, the chemical reaction rates are fast and products are formed instantaneously when mixing of the reactants take place at the molecular level. In a turbulent flow, the eddy properties dominate the mixing time and the molecular level mixing is defined by:

$$rate \propto \frac{\varepsilon}{k}$$

D. RAMJET NOMENCLATURE

For ease of reference, the various parts of the ramjet and its associated stations are defined in Figure 1.

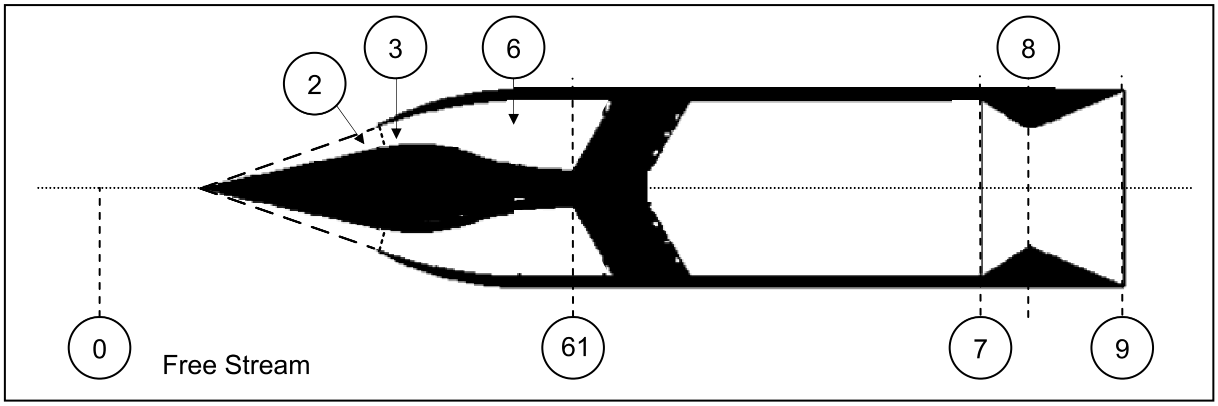

Figure 1. Schematic of ramjet with associated stations

III. COLD-FLOW CFD ANALYSIS

A. BACKGROUND AND METHODOLOGY

In [1] and [2], for efficiency, a 2-D axis-symmetrical model was used for the cold-flow analysis of the ramjet. However, to maintain the axissymmetry, the internal struts of the ramjet were not included in the 2-D computational model of the ramjet. In this thesis, a more realistic 3-D computational model of the ramjet was used for the CFD cold-flow analysis. The conditions for the simulation were set to those in the wind tunnel for subsequent comparisons.

From [1] and [2], while a normal shock was expected to form at the inlet cowl, an oblique shock system was instead observed. It was hypothesized that this could be due to a non-optimized nozzle-throat diameter (too large). To investigate this, CFD analyses were performed on the ramjet models with the nozzle-throat area of the base model reduced by 10% to 40%, in 10% steps. The reduction of the throat areas was aimed at increasing backpressure, thereby forcing the observed oblique shock system into a normal shock that sits at the lip of the inlet cowl.

For the steady-state cold-flow CFD analyses, the models used were first created in SolidWorks and then imported into ANSYS Workbench for mesh generation with the ANSYS-Meshing utility. The meshed model then flowed into ANSYS-CFX through the CFX-PRE – CFX-SOLVER – CFX-POST workflow previously described.

Parallel computing with over ten computers was employed to allow for faster computation of each simulation. Typical run times of over 72 hours were experienced on the NPS computer cluster, named “Hamming".

B. COMPUTATIONAL MODEL SETUP FOR COLD-FLOW ANALYSES

1. Three-Dimensional Computational Model

Exploiting the two axes of symmetry (Figure 2), the computational domain of the ramjet was modeled to consist of a "quarter-cut" of the ramjet in a block of fluid (Figure 3). Similar to [1] and [2], to simplify the computation for the cold-flow analysis, the fuel-injection ports on the ramjet were not modeled.

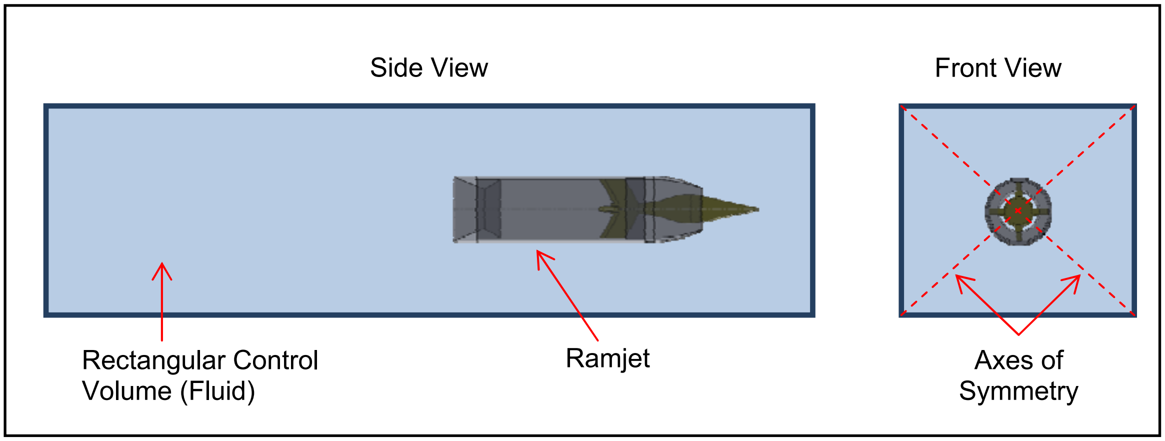

Figure 2. Geometry of ramjet with two axes of symmetry

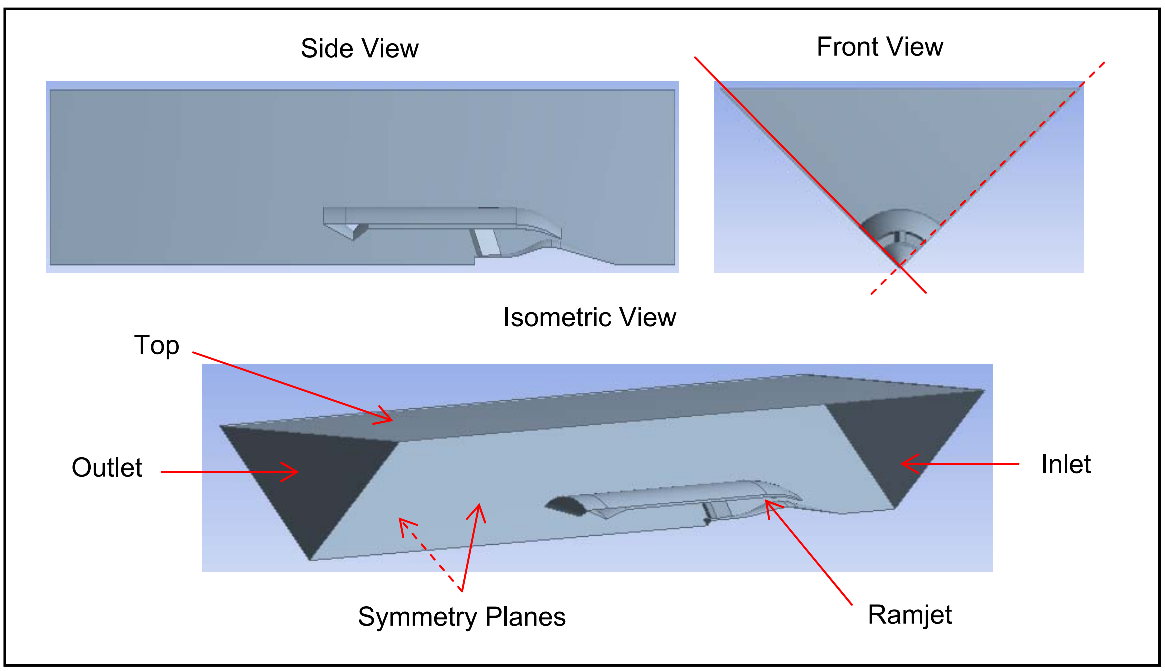

Figure 3. Three-dimensional computational model for cold-flow analysis, with boundary namespace

The 3-D grid of the computational model was generated with the ANSYS meshing utility. For the default model, a total of 2.69 million nodes and 14.99 million elements was generated. Figure 4 presents the mesh profile of the computational model, with a close-up view of the meshes at the inlet cowl, showing the inflation layers at the surface. Details of the meshing parameters can be found in Appendix A.

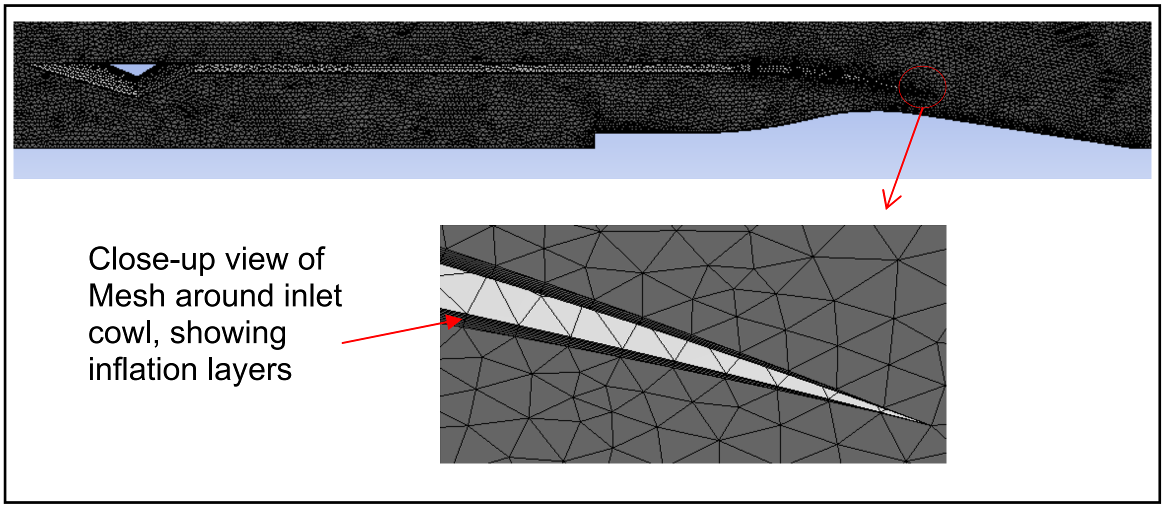

Figure 4. Mesh of computation model for cold-flow analysis

2. Boundary Conditions and Key Simulation-Setup Parameters

Boundary conditions and setup parameters for the computational model were defined in CFX-PRE. Table 1 presents a snapshot of these boundary conditions. Details for setup parameters are elaborated in Appendix A.

Table 1. Boundary conditions for cold-flow analysis.

Boundary	Type	Boundary Conditions
Inlet	Inlet	Supersonic; V = 661 m/s; P = 7378 Pa; T = 68 K
Outlet	Outlet	Supersonic
Ramjet	Wall	No-Slip Wall
Sym1 & Sym2	Symmetry	-
Top	Wall	Free Slip Wall

Table 2 provides a list of important parameters that must be set in CFX-PRE.

Table 2. Important setup parameters for CFX-PRE.

Parameter	**Location**	**Description**
High Speed Numerics	Solver Control → Advance Options → Compressibility Control	For better resolution of high-speed flows and shocks.
Max Continuity Loop	Expert Parameters →Convergence Control	Set to 3. Necessary for high-speed flows to aid convergence

C. RESULTS AND DISCUSSION

1. Flow-Profile Comparison

Figure 5 shows the Mach number distribution through the ramjet at Mach 4. Comparing Figure 5 with the shock profile in [1] and [2] in Figures 6 and 7, respectively, the similarity in the shock profiles can be seen. As in [1] and [2], the first shock, a conical shock sitting at the lip of the inlet cowl, was observed. Also, instead of a normal shock terminating at the inlet cowl and nose cone, the second shock was observed to be the coalescence of two oblique shocks sitting downstream of the inlet cowl.

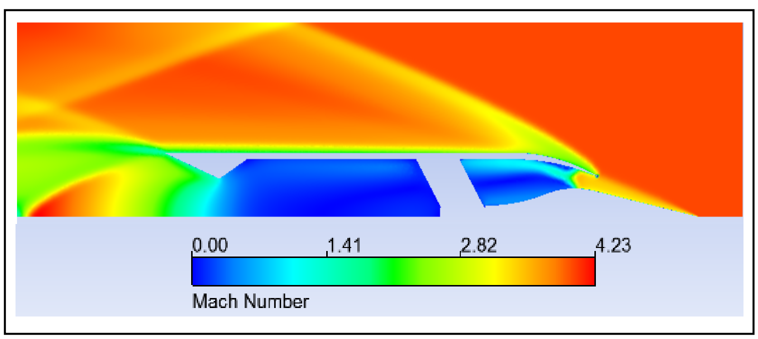

Figure 5. Mach number distribution with ANSYS-CFX

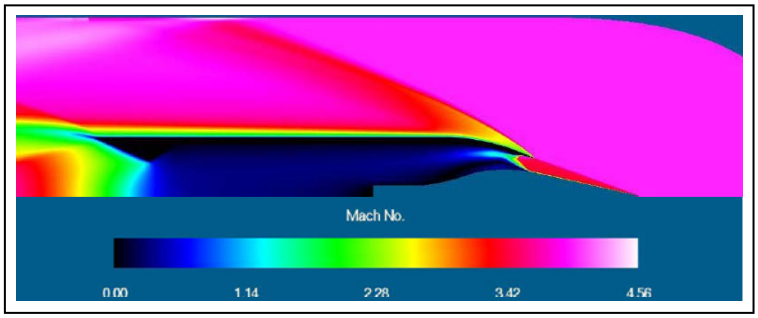

Figure 6. Mach number distribution with Overflow code [1]

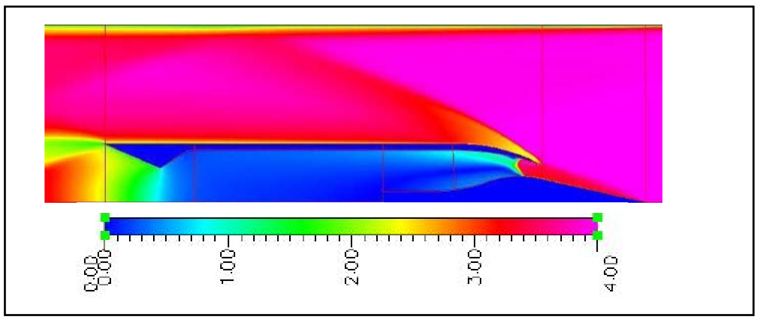

Figure 7. Mach number distribution with CFDRC-FASTRAN [2]

The density, pressure, and temperature distributions are shown in Figures 8 to 10, respectively. Comparing these with those in [1] and [2], a great level of congruency between the plots was also observed.

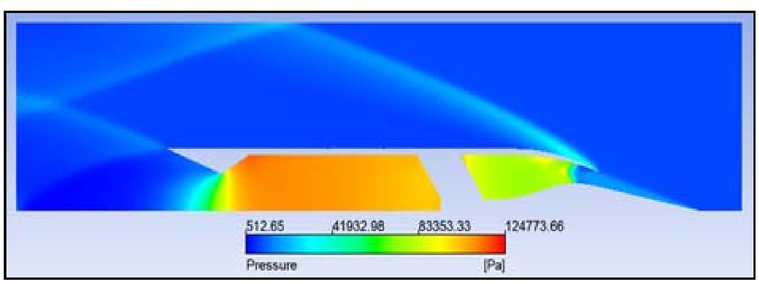

Figure 8. Pressure distribution with ANSYS-CFX

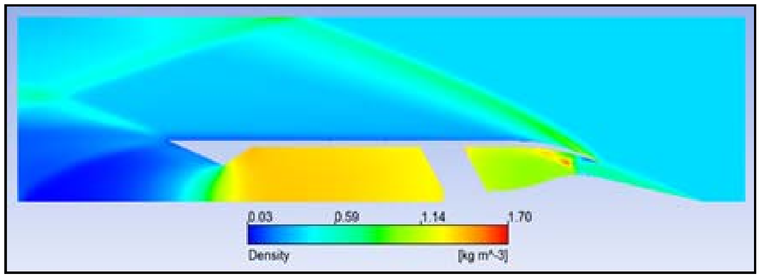

Figure 9. Density distribution with ANSYS-CFX

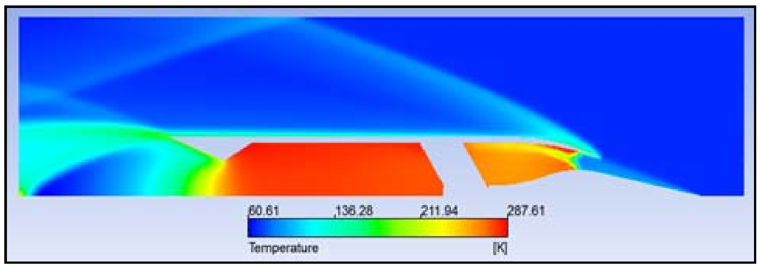

Figure 10. Temperature distribution with ANSYS-CFX

From Figure 11, it was observed that there are huge re-circulatory flow within the ramjet.

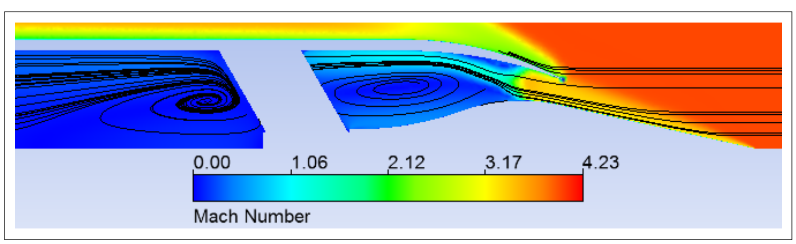

Figure 11. Streamline plot with ANSYS-CFX

With reference to figure 1, Table 3 presents a summary of the stagnation pressure recovery at the various stations of the ramjet.

Table 3. Summary of stagnation pressure recovery at various stations

Free Stream Stagnation Pressure ($P_{t\infty}$)		1,116.36 kPa	
Station Number (n)	**Theoretical Stagnation Pressure Recovery Ratio ($P'_{tn}/P_{t\infty}$) from [1]**	**Stagnation Pressure (P_{tn})**	**Stagnation Pressure Recovery Ratio ($P_{tn}/P_{t\infty}$)**
2	0.991	980.54 kPa	0.878
3	0.676	219.68 kPa	0.197
61	-	126.64 kPa	0.113
7	-	119.72 kPa	0.107

From Table 3, the stagnation pressure recovery ratios obtained from the CFD showed that the current ramjet design provides for poor pressure recovery. The biggest drop in pressure recovery ratio occurred at station 3 - after the second shock system. This indicated that the subsonic diffuser system of the inlet would need to be redesigned to improve the stagnation pressure recovery.

The drag on the ramjet was computed to be 26.838N, with a corresponding drag coefficient of 0.371. This compares favorably with the drag of 21.35 N computed in [1].

2. Results of Cold-Flow Analysis with Varied Nozzle-Throat Area

Figures 12 to 15 shows the Mach-number profile achieved with the corresponding reduced nozzle-throat area. Figure 16 shows the shock indicator plot for the reduced nozzle-throat areas.

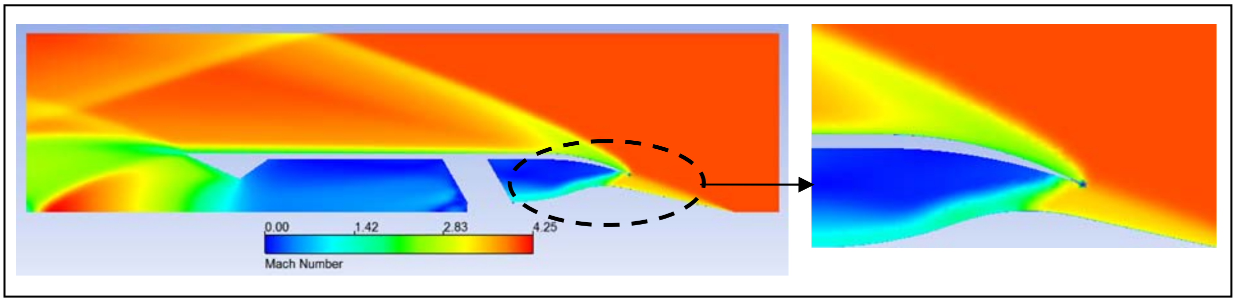

Figure 12. Cold-flow shock profile with 10% reduction in nozzle-throat area

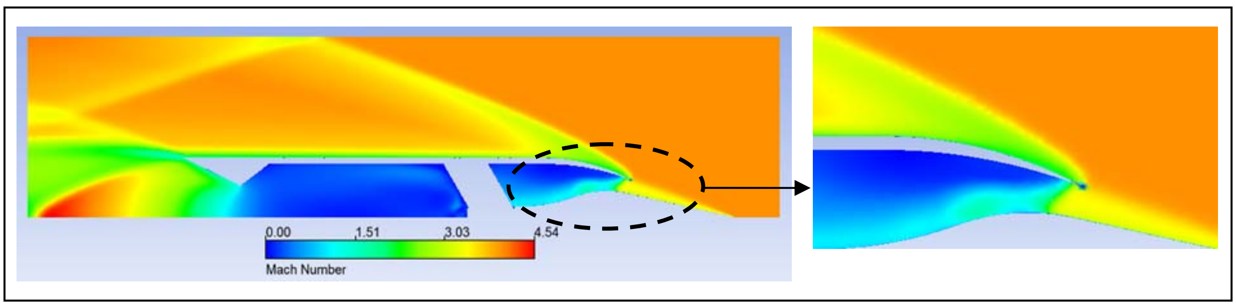

Figure 13. Cold-flow shock profile with 20% reduction in nozzle-throat area

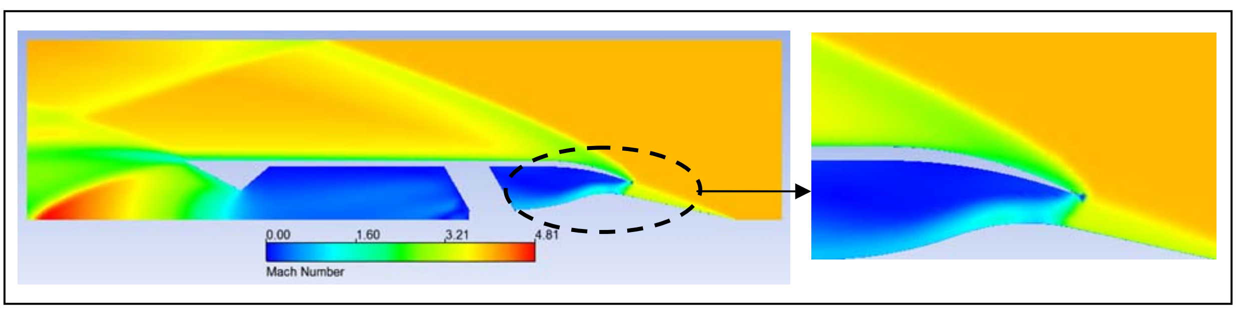

Figure 14. Cold-flow shock profile with 30% reduction in nozzle-throat area

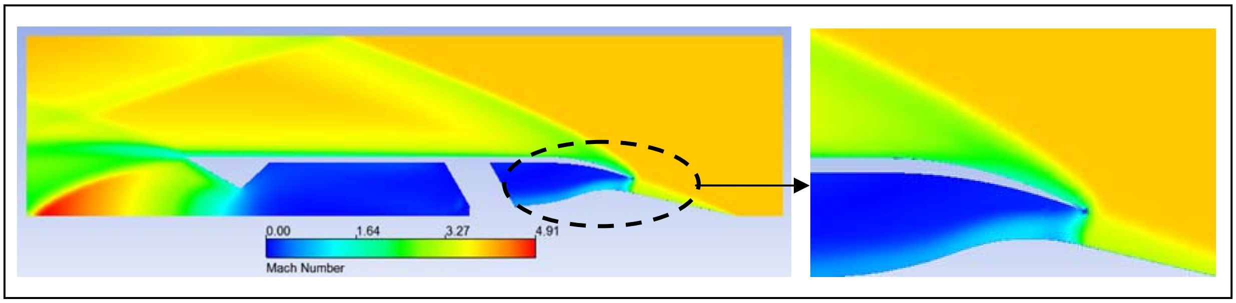

Figure 15. Cold-flow shock profile with 40% reduction in nozzle-throat area

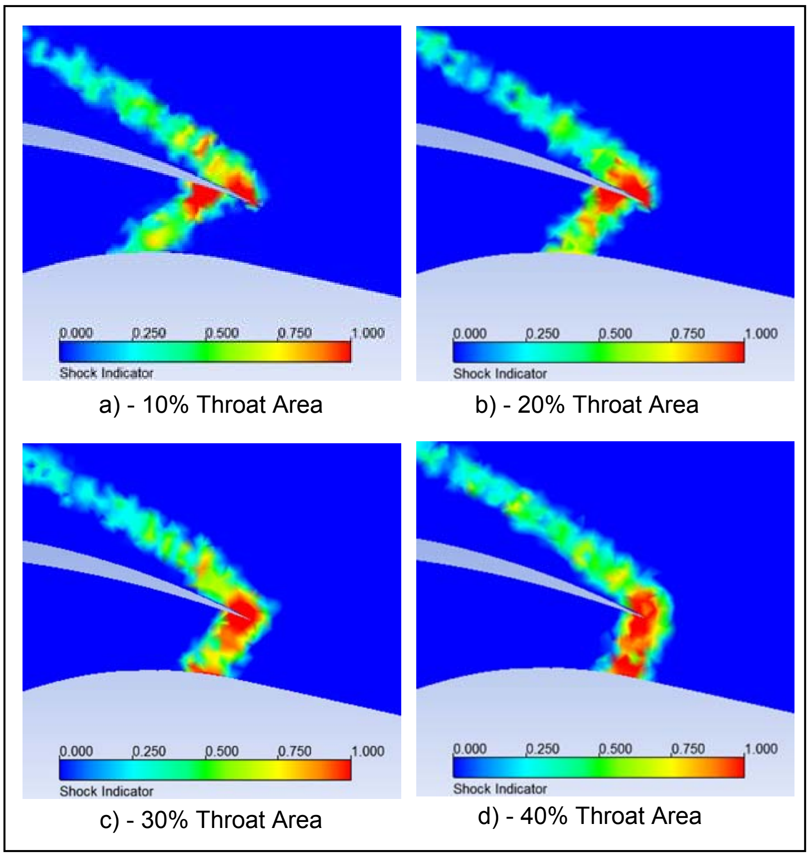

Figure 16. Shock indicator around inlet for
a) 10% b) 20%, c) 30%, d) 30% reduction in throat area

As seen in figures 15, 16 and Table 3, reducing the nozzle-throat area resulted in increased back pressure which pushed the coalesced oblique shocks upstream towards the inlet cowl.

a. At 10% and 20% reduction in nozzle-throat area, the two coalesced oblique shocks remained downstream the lip of the inlet cowl.

b. At 30% reduction in nozzle-throat area, a normal shock was formed at the lip of the inlet cowl. However, as shown in figures 15 and 16b, unlike theoretical predictions, this normal shock is not truly orthogonal to the flow.

c. At 40% reduction in nozzle-throat area, the coalesced oblique shocks were pushed into a normal shock which developed upstream the lip of the inlet cowl, resulting in flow spillage.

While the results showed that a reduction of 30% in the nozzle-throat area would site the normal shock at the lip of the inlet cowl, in reality, this may not be desirable. With the normal shock sitting on the lip of the inlet cowl, slight perturbations in the chamber conditions can push the normal shock upstream, causing the inlet to unstart. Hence, depending on the required performance buffer, the nozzle should be sized accordingly to site the shock at the desired position.

IV. CFD ANALYSIS FOR AIR INJECTION THROUGH THE TIP PORTS

A. BACKGROUND AND METHODOLOGY

In [1], from the SSWT experiment, it was reported that atmospheric air from outside the SSWT was seeping into the ramjet model through the open ports, resulting in the air ejecting from the tip ports of the ramjet's nose cone. It was suspected that this ejected air interacted wih the downstream shock structure.

To investigate the effect of this interaction, CFD analyses for injection of air through the tip ports were performed with total pressure settings of 1 atmosphere, 0.75 atmosphere and 0.5 atmosphere. The other boundary conditions were selected such that they replicate the SSWT experiment conditions. This allowed the results to be compared to the CFD cold-flow analysis results and will facilitate the conduct of any subsequent verification in the SSWT.

Parallel computing over four local processors was employed to allow for faster computation of each simulation. Typical run times of 7 to 8 hours were experienced.

B. COMPUTATIONAL MODEL SETUP

1. Three-Dimensional Model Setup

The 3-D computational model (Figure 17) used for the steady-state injection analysis was a quarter-cut model of the ramjet's nose cone.

The 3-D mesh of the computational model was generated with the ANSYS meshing utility. A total of 456k nodes and 2.17 million elements was generated. Figure 18 displays the mesh profile for the computational model, with a close-up view of the meshes at the tip ports of the ramjet's nose cone. The meshing parameters are detailed in Appendix C.

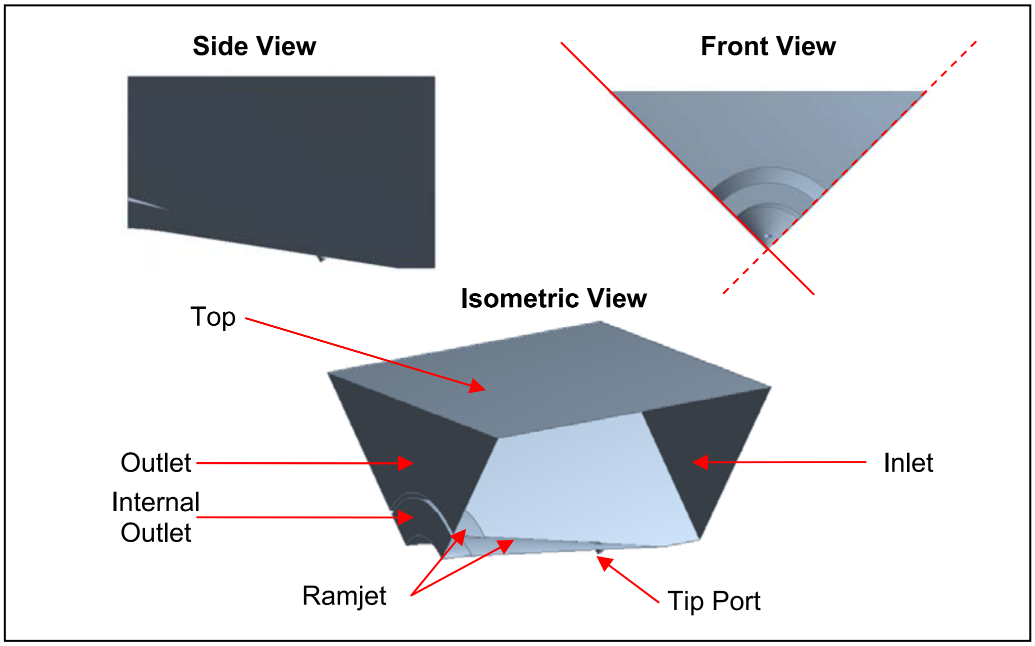

Figure 17. Three-dimensional geometry of computational model for air injection analysis, with boundary namespace

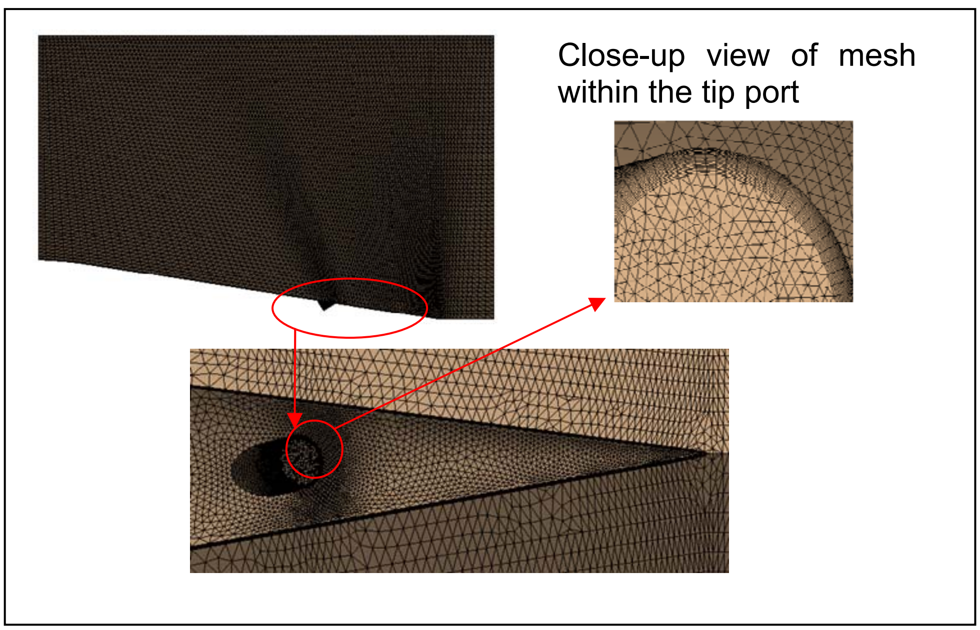

Figure 18. Mesh of computational model for air injection analysis

2. Boundary Conditions and Key Simulation-Setup Parameters

Table 4 shows a summary of the boundary conditions applied. Details for setup parameters are elaborated in Appendix C.

Table 4. Boundary conditions for air injection analysis

Boundary	**Type**	**Boundary Conditions**
Inlet	Inlet	Supersonic; V = 661 m/s; P = 7378 Pa; T = 68 K
Outlet	Outlet	Supersonic
Internal Outlet	Outlet	Supersonic[1]
Ramjet	Wall	No-Slip Wall
Tip Ports	Inlet	Subsonic; Total Pressure = 101325 Pa; T = 298.15 K
Top	Wall	Free-Slip Wall
Sym1 & Sym2	Symmetry	-

C. RESULTS AND DISCUSSION

Detailed results for the tip port air injection analysis can found in Appendix D. Figure 19 to 21 shows the Mach number distribution for the air injection at total pressure settings of 0.5 atm, 0.75 atm and 1 atm. From these figures, it is apparent that the injected air perturbed the conical shock, deflecting the conical shock away from the nose cone.

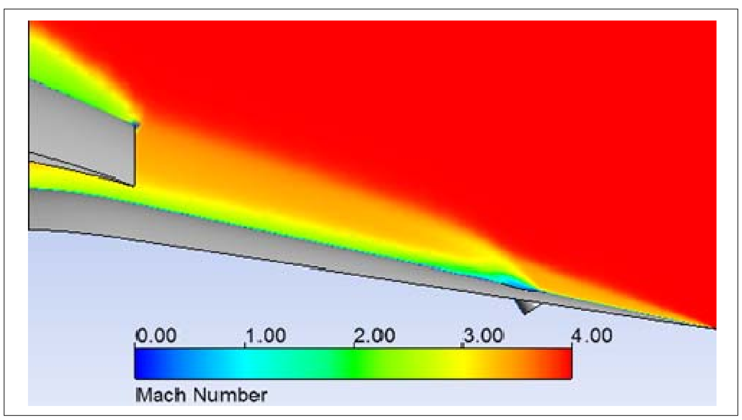

Figure 19. Mach number distribution for air injection through tip port with P_t = 0.5 atm

[1] The supersonic boundary condition for the "Internal Outlet" was determined from the default cold-flow solution.

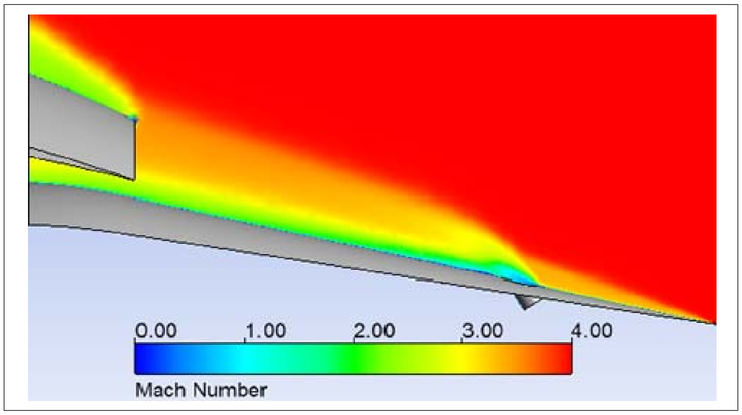

Figure 20. Mach number distribution for air injection through tip port with P_t = 0.75 atm

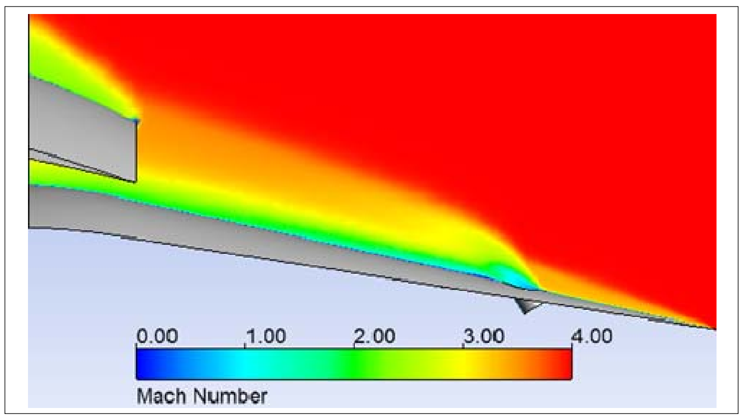

Figure 21. Mach number distribution for air injection through tip port with P_t = 1 atm

Upstream of the tip port, where the conical shock remained unperturbed, the Mach number at the fringe was computed to be 3.65. If unperturbed, this will be the Mach number for the conical shock incident on the lip of the ramjet's inlet cowl.

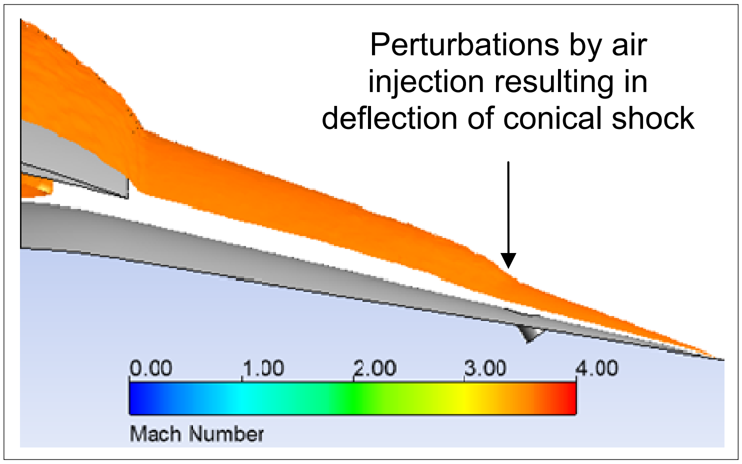

Figure 22. Iso-surface plot of Mach 3.65, for air injection through tip port with P_t = 0.5 atm

Figure 22 shows an iso-surface plot for Mach 3.65, with air injection at a total pressure setting of 0.5 atm. Beyond the indicated point of perturbation, the conical shock was deflected away from the nose cone. This observation was held for the air injection at the total pressure setting of 1 atm and 0.75 atm. The ramjet, which was previously analyzed to be operating on-design during the cold-flow analysis encountered flow spillage and operates at sub-critical condition.

The tip ports were initially planned to be placed on the nose cone to induce early fuel-air mixing. However, with the spillage occurring, any benefits brought about by the early fuel-air mixing will be negated.

One way to resolve the problem of flow spillage is to shift the tip ports further downstream of the cone. With proper position of the tip ports, vis-a-vis the expected fuel injection conditions, it may be possible to keep the perturbations within the inlet capture-area such that no flow spillage occur.

In the extreme case, the tip ports may even be shifted to a region within the inlet. However, this may affect the formation of the normal shock at the lip of the inlet cowl and further CFD analyses will need to be performed to ascertain its suitability.

THIS PAGE INTENTIONALLY LEFT BLANK

V. COMBUSTION CFD ANALYSIS

A. BACKGROUND AND METHODOLOGY

In [2], a mixture analysis of propane and air was performed on a 45-degree slice of the ramjet. However, due to the limitations in computing resources and the CFD code used, the combustion CFD analysis was performed on a 2-D computational model, with propane injected into the ramjet at low speeds.

In this thesis, a 3-D computational model was used for the steady-state combustion analysis in ANSYS-CFX. The combustion analysis was based upon a single-step hydrogen–oxygen (H_2–O_2) combustion model within air and with the “eddy dissipation combustion model”.

The stoichiometric combustion of hydrogen and air (with 23.3% oxygen) requires a hydrogen-air mass ratio of 1:30.94. With the ramjet operating at designed condition, the required mass-flow rate of the hydrogen fuel was calculated to be 4.07×10^{-4} kg/s (Appendix E) and this equated to an injection velocity of more than 1000 m/s.

With the high fuel injection velocity required, any combustion that developed will be highly unsteady may be blown out of the nozzle. With this consideration, a moderate approach was taken for the combustion analysis with fuel injection at 400m/s.

B. COMPUTATIONAL MODEL SETUP FOR MIXING-FLOW ANALYSIS

1. Three-Dimensional Model Setup

The 3-D computational model (Figure 23) used for the combustion analysis is a quarter-cut model of the ramjet. For simplicity in flow computation, only the rear fuel-injection ports on the struts were modeled. Since the interest in the combustion analysis is confined to the internal flow, to reduce the complexity and time required for simulation, irrelevant external-flow regions were excluded from the computational model.

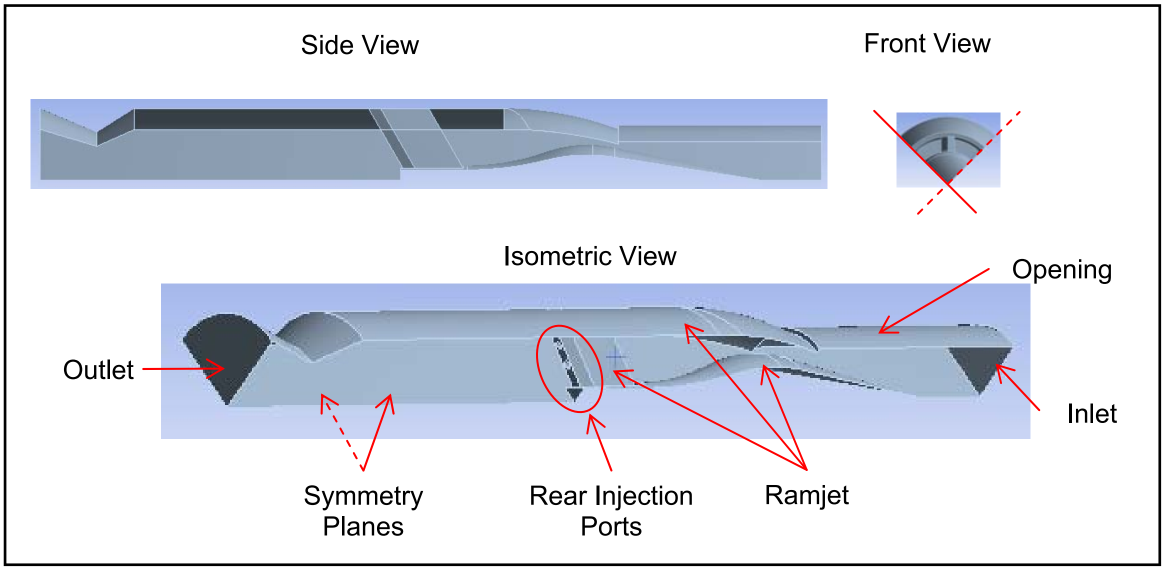

Figure 23. Three-dimensional geometry of computational model for combustion analysis, with boundary namespace

The 3-D mesh of the computational model was generated with the ANSYS meshing utility. A total of 1.82 million nodes and 6.57 million elements was generated. Figure 24 displays the mesh profile for the computational model, with a close-up view of the meshes at the rear fuel ports showing the inflation layers. The meshing parameters are detailed in Appendix F.

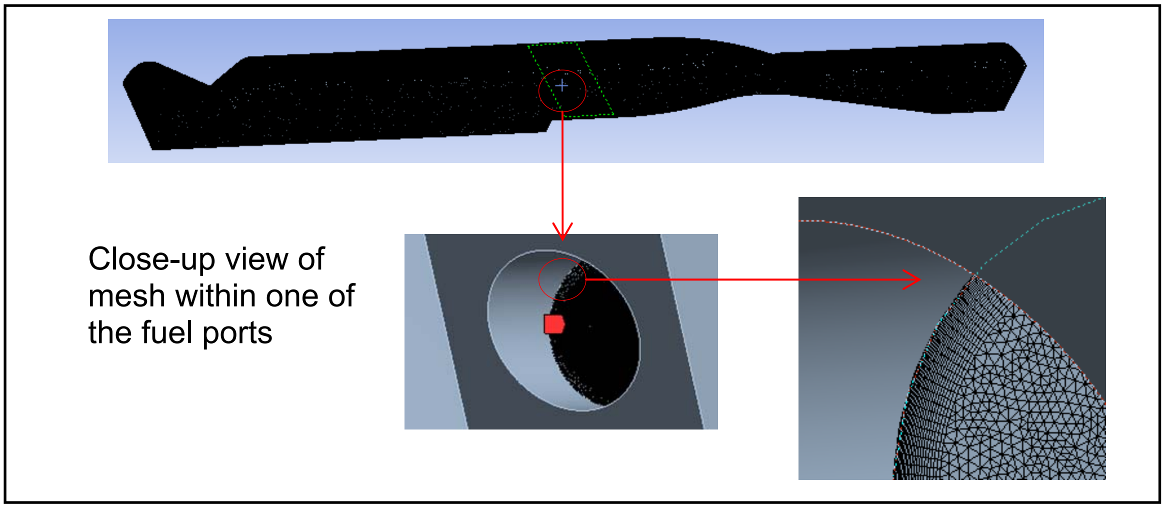

Figure 24. Mesh of computational model for mixing analysis

2. Boundary Conditions and Key Simulation-Setup Parameters

Table 5 shows a summary of the boundary conditions applied. Details for the setup parameters are elaborated in Appendix F.

Table 5. Boundary conditions for mixing analysis

Boundary	Type	Boundary Conditions
Inlet	Inlet	Supersonic; V = 1180.17 m/s; P = 7504.8 Pa; T = 216.65 K
Outlet	Outlet	Supersonic
Ramjet	Wall	No-Slip Wall
Rear Ports	Inlet	Subsonic; V = 50 m/s[2]; Total Temperature = 300 K
Opening	Opening	Subsonic; P = 7504.8 Pa; T = 216.65 K
Sym1 & Sym2	Symmetry	-

In ANSYS-CFX, for combustion to take place, it is necessary for the computational domain to contain a small fraction of the products. Hence, a 1% mass fraction of H_2O was set in the computational domain.

Due to the complex flow model, a solution with no combustion was first obtained. This pre-combustion solution was then used as the input for the actual combustion analysis.

C. RESULTS AND DISCUSSION

Figure 25 shows the RMS convergence history of the simulation run with the reference time step labeled.

[2] Injection velocity for hydrogen was ramped up gradually from 50 m/s to the required velocity of 400 m/s.

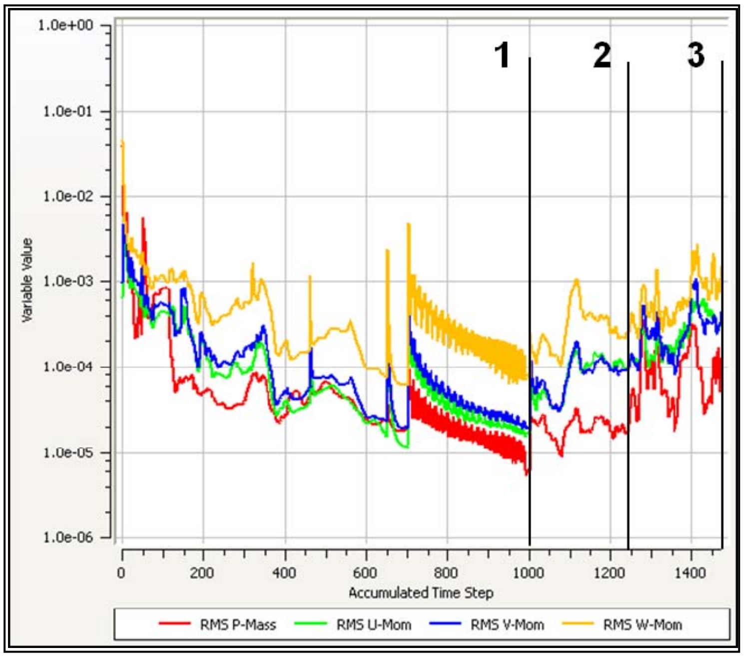

Figure 25. RMS convergence history with reference time step for hydrogen injection

Prior to and inclusive of reference time step 1, no combustion was simulated. After reference time step 1, combustion was activated. Beyond reference time step 3, the solution diverged and the simulation terminated prematurely.

Figures 25 shows the temperature distribution of the computational model, at the referenced time step.

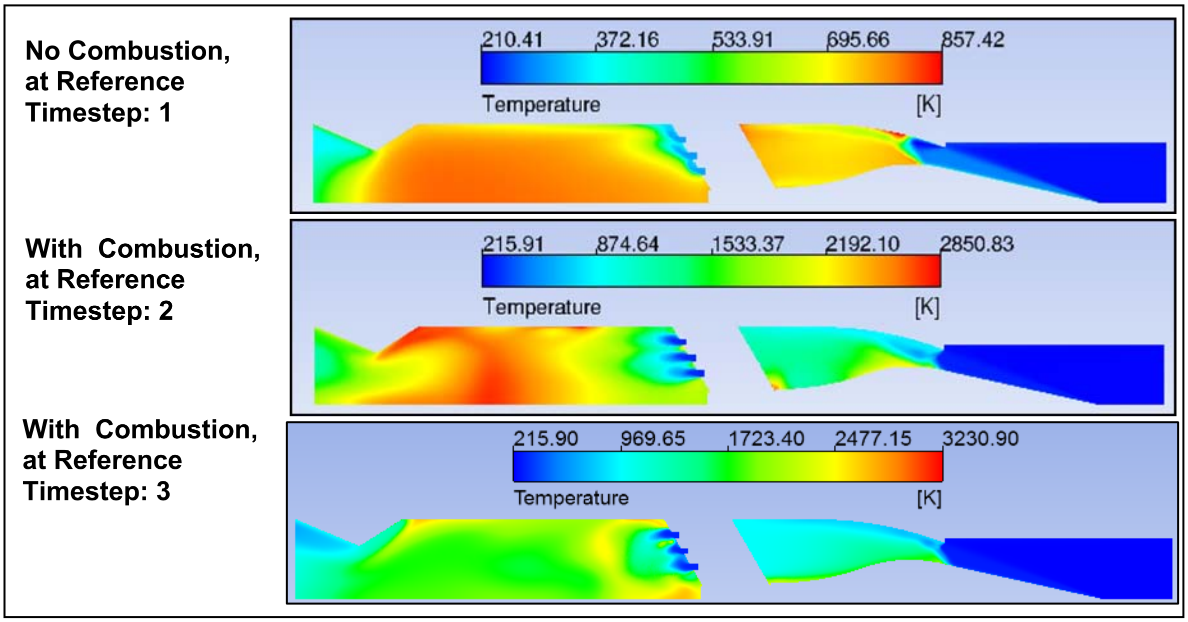

Figure 26. Temperature distribution for fuel injection at each reference location

From Figure 26, the following observations and deductions were made.

1. At reference time step 2, combustion was observed to be taking place at the middle of the combustion chamber. This combustion flame however seemed to be unsteady and at reference time step 3, broke into two zones – first zone immediately aft of the rear struts and the second zone at the entrance to the nozzle.

2. At reference time step 2 and 3, instead of a normal shock forming at the entrance of the inlet cowl, two oblique shocks were seen to coalesce near the lip of the inlet cowl. Also combustion seemed to be creeping up the center body, towards the inlet.

3. At reference time step 3, with the lower oblique shock at the entrance of the inlet sitting upstream of the inlet cowl, unstarting of the inlet was taking place. The eventual unstart of the inlet could have resulted in the divergence and permature termination of the simulation.

Table 6 presents a summary of the thrust or drag forces on the quarter-cut ramjet model. While the combustion was seen to be unsteady and the simulation did not converge to a steady state, thrust augmentation was nevertheless predicted.

Table 6. Summary of thrust and drag forces on ramjet for combustion analyses

Fuel Injection Velocity	**Analysis Type (Reference Time Step)**	**Thrust / Drag Forces**
400 m/s	No Combustion (1)	Drag: 3.304 N
	Combustion (2)	Thrust: 1.379 N
	Combustion (3)	Thrust: 2.253 N

From the results, before proceeding further, it is recommended that the problem of the unstable combustion be resolved first. With the fuel injection velocity at 400m/s, this may still be too fast for the combustion to develop properly. Reducing the fuel injection velocity will allow more time for the fuel-air mixing to take place, thereby allowing the combustion to develop properly. To reduce the fuel injection velocity, the current fuel injection ports may be widened and more fuel injection ports may be added to the struts and the center body. In addition, flame holders may be introduced into the ramjet, aft of the struts to stabilize the flame.

V. SUPERSONIC WIND-TUNNEL EXPERIMENT AND COMPARISON WITH CFD

A. BACKGROUND AND METHODOLOGY

The SSWT experiment was first ran in [1] and due to the imperfections of the physical ramjet model, the schlieren image showed a lopsided conical shock angle attached to the tip of the nose cone.

With the NASA Overflow code, the drag on the ramjet was predicted in [1] to be 21.351 N. In [2], based on a 2-D double wedge profile, the drag on each load flexure was calculated to be 20.177N. Overall, the drag for the ramjet model in the SSWT was predicted to be 61.71N. Wind tunnel tests however, showed the drag to be 57.85N (13 lbf). The over-prediction in drag was previously hypothesized to be the result of using a simple 2-D model for the load flexure, which did not account for sweep effects that would reduce the load prediction.

The temperature of the test section in the SSWT while running is 68K, and the strain gauges used in [2] were operating outside their performance envelope. It was believed that these were more likely to cause the observed disparity in drag measurement and prediction.

Figure 27 shows a top-down schematic of the ramjet mounted within the SSWT. With the air on in the wind tunnel, the drag induced on the ramjet and inner flexure will cause axial deflection of the flexure beams, changing the resistance of the strain gauges. Measuring the voltage difference from this change allows the determination of the drag induced on the ramjet and inner flexures.

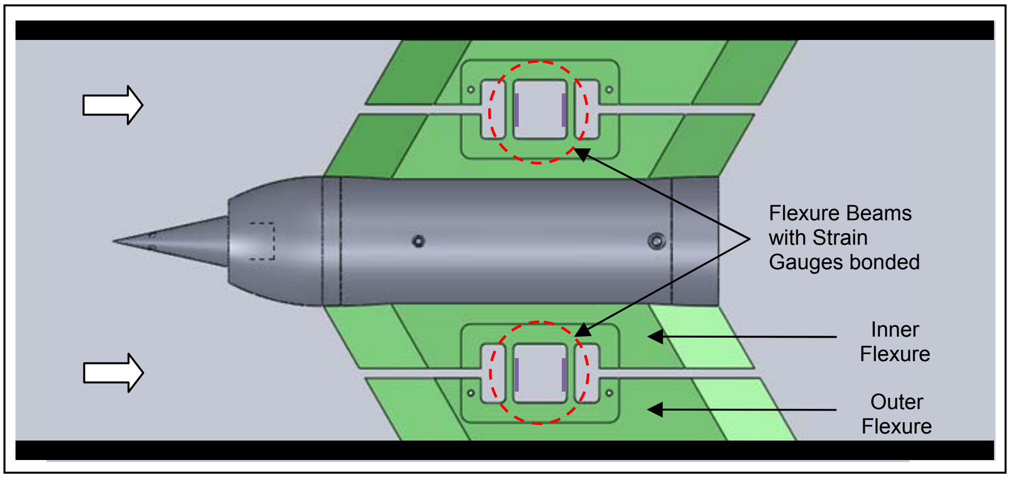

Figure 27. Top-down schematic of ramjet in SSWT

B. EXPERIMENTAL SETUP

1. New Ramjet Model with Shortened Flexures

In this thesis, the drag measurement in the SSWT was conducted with a new physical model of the ramjet.

In Figure 28, the cylinder aft of the ramjet's center-body was leveled off in the new model for easier machining. Correspondingly, the struts that are in contact with the center-body and cylinder body were resized to maintain the integrity of the model. Aside from these, the new model had the same overall dimensions as the ramjet designed in [1]. Engineering drawings for the new model are included in Appendix G.

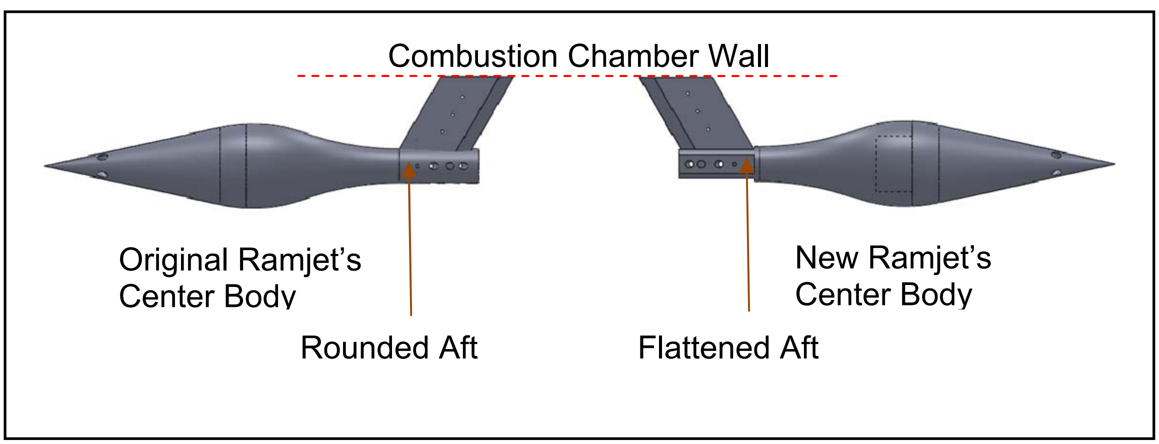

Figure 28. Comparison of center-body (partial) and strut dimensioning

While the dimensions of the ramjet remain relatively unchanged, the chord length of the flexures was reduced. Like the originals, the new flexures are swept back at a 30-degree angle, but only measure 10.16cm along the wall-mount side.

An assembled model of the new ramjet is shown in Figure 29 and Figure 30 shows the new model mounted in the SSWT.

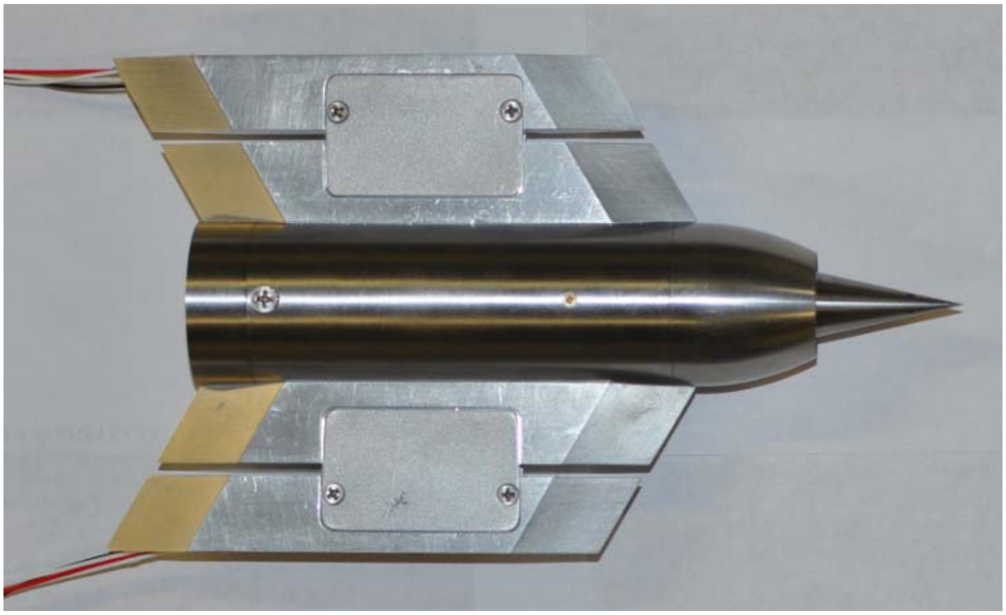

Figure 29. Assembled new ramjet model

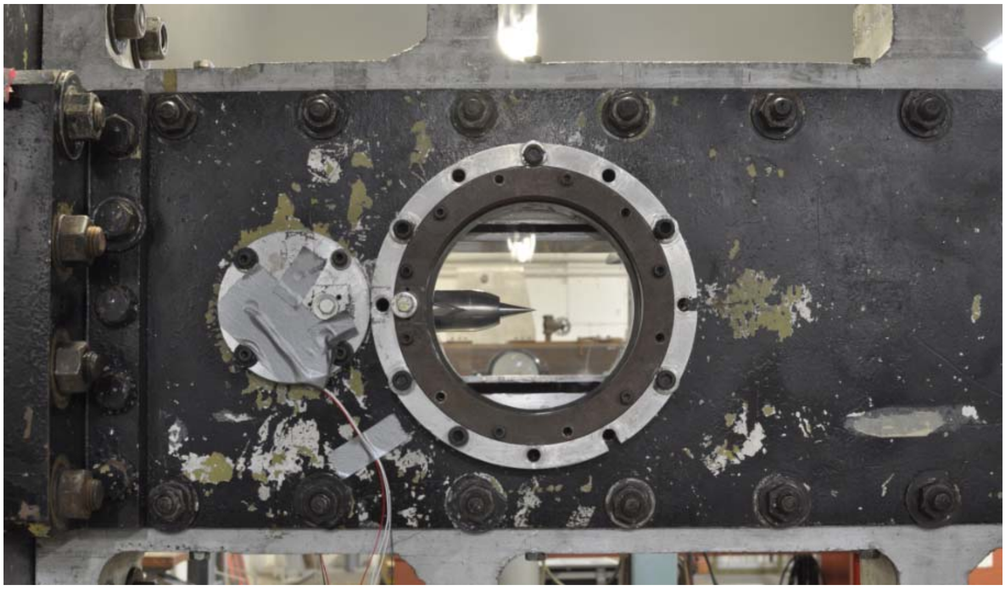

Figure 30. Assembled ramjet model mounted in the SSWT

2. Strain Gauges and Wiring

With a static temperature of 68K expected in the SSWT, cryogenic strain gauges were used. The strain gauges used were model WK-13062AP-350 from Micro-Measurements. Details for the strain gauges can be found in Appendix H. The strain gauges were bonded to the flexure beams at the mid-span using an epoxy-based glue – EP29LPSP from Micro-Measurements, which retains sufficient "flexibility" under extreme temperatures. The strain gauges were wired in a Wheatstone bridge (Figure 31) for maximum potential difference measurements. In the full bridge configurations, where all four arms of the bridge are used in the measurement, temperature compensation is a default feature of the setup.

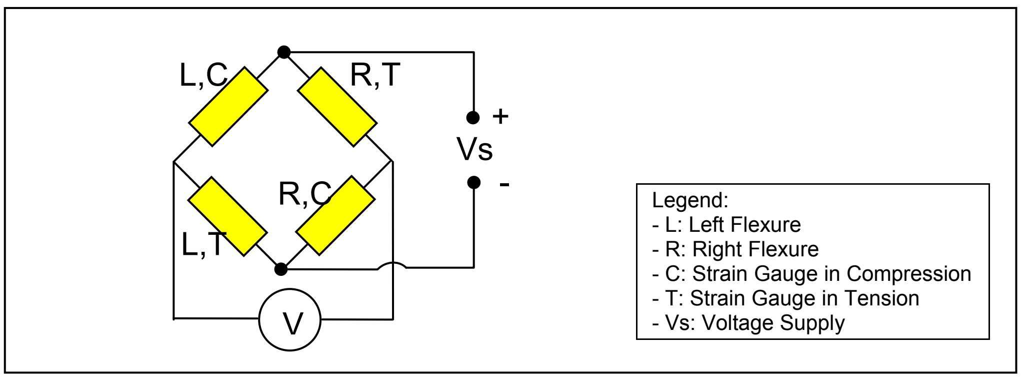

Figure 31. Wheatstone bridge for potential difference measurements

4. Signals Conditioning System

To facilitate data acquisition, signal measurements from the Wheatstone bridge was passed through a signals-conditioning system – the CALEX model 163MK Bridgesensor, mounted on a CALEX model 8610 Backplane mounting board.

Key features of the CALEX Model 163MK Bridgesensor include the following:

a. A low-noise bridge supply to power the Wheatstone bridge.

b. An instrumentation amplifier with adjustable gain for amplification of the small output signal from the Wheatstone bridge.

c. An active low-pass filter for cleaning up the output signal before it enters the data acquisition hardware.

The CALEX Model 8610 Backplane supports the mounting of up to eight signals-conditioning cards. Figure 32 shows the Bridgesensor mounted on the CALEX Model 8610 Backplane.

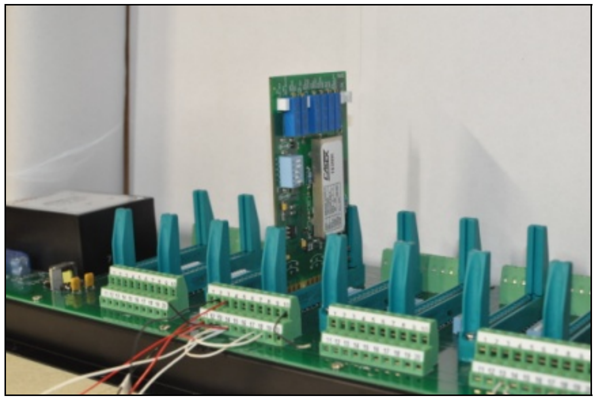

Figure 32. Signals-conditioning system

5. Data Acquisition System

The hardware for the data-acquisition system was the USB-1698FS-Plus – a data-acquisition (DAQ) module from Measurement Computing (Figure 33) – and a 32-bit PC. The analog output signal from the Bridgesensor was piped into the DAQ, which digitized the signals and sends it to the data-acquisition PC via the USB port.

Figure 33. Measurement Computing USB-1698FS-Plus data acquisition (DAQ) module

The TracerDAQ software that was supplied with the hardware was used to display and log the input signals.

C. PROCEDURES

The following procedures were performed sequentially. The details for these procedures are presented in Appendix I.

1. Calibration of the signal conditioning system to obtain the correct input-to-output response required.

2. Calibration of the flexure arms to determine the expected range of output response.

3. SSWT experiment to measure the drag induced on the ramjet and flexures using the collected output signal response.

D. CFD DRAG PREDICTION

For CFD drag prediction, an equivalent of the experimental ramjet model is shown in Figure 34.

Physically, adding the pair of flexures onto the ramjet breaks the two-plane symmetrical model into a single-plane symmetrical model. In the drag-prediction model, the computational model still assumes a two-plane symmetrical model. The ramjet and the flexure, however, were defined as separate entities so that the drag on the ramjet and flexures can be obtained separately. The final drag for the ramjet and flexures will be four times and twice the drag computed in ANSYS-CFX, respectively. Details for setting up the computational domain for CFD drag prediction are shown in Appendix J.

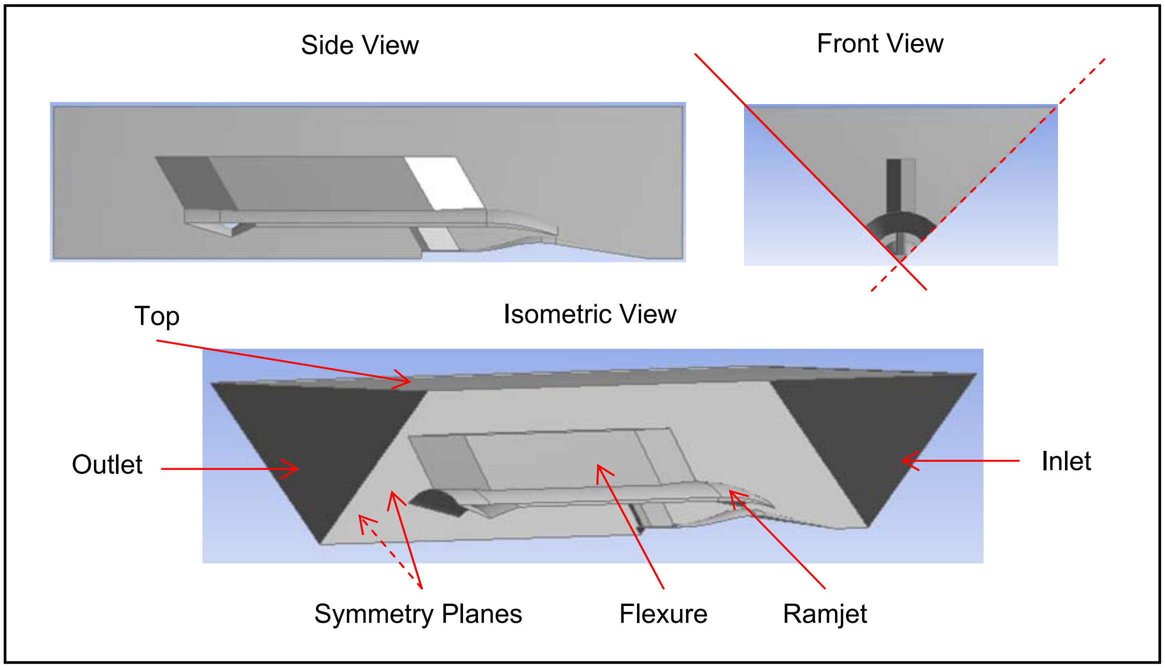

Figure 34. 3-D computational model for cold-flow drag analysis, with boundary namespace

Figure 35 shows a comparison of the physical and computational model of the flexure used. In the SSWT experiment, drag is determined from the deflections of the flexure beams, and the outer flexure is merely an extension of the wall to attach the flexure beams to the inner flexure. Unlike the experiment requirements, we do not need the flexure beams for drag calculations in CFD. Hence, the simplified and equivalent model of the inner flexure shown in Figure 35b was used.

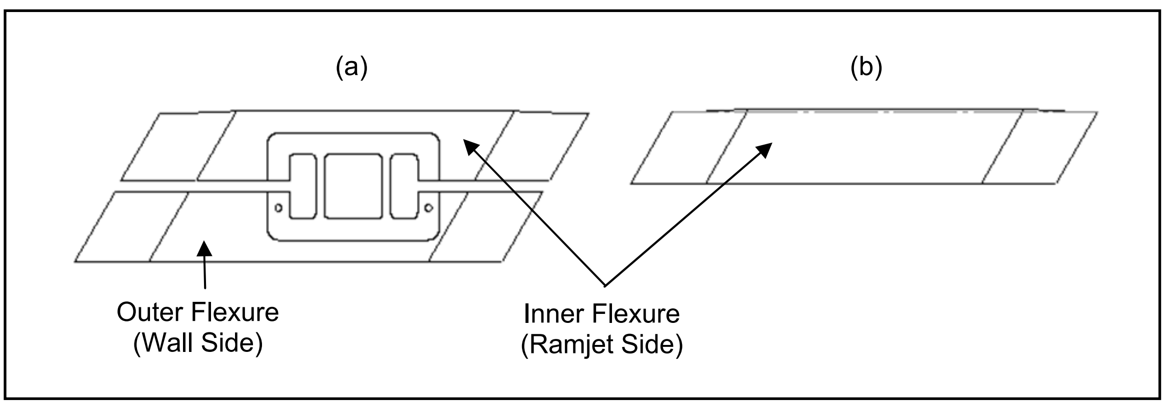

Figure 35. Comparison of (a) Physical flexure model and (b) Equivalent CFD flexure model

E. RESULTS AND DISCUSSION

1. SSWT Experiment

Two runs were conducted in the SSWT. A representative schlieren image for the experiments is shown in Figure 36. With the ramjet mounted at zero angle of attack, the attached symmetrical conical shock from the nose cone to the inlet cowl can be seen.

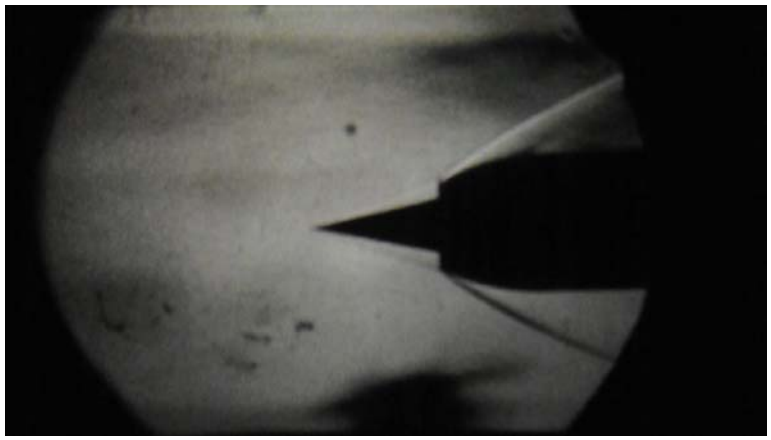

Figure 36. Schlieren image of ramjet in SSWT at Mach 4 conditions

In both experiments, the Wheatstone bridge was re-balanced at the start of the run. In the first run, the load across the input arms of the Wheatstone bridge was observed to be -0.503 mV, equating to a drag force of 54.8 N.

In the second run, logging of the output signal from the signals condition card began two seconds after the formation and attachment of the shock on the nose cone and inlet cowling, for a period of five seconds. The average drag force was determined to be 55.54 N.

2. CFD Drag Prediction

The CFD drag prediction is presented in Table 7. The total drag force predicted on the ramjet with the flexures mounted in the wind tunnel was 36.99N.

Table 7. CFD drag prediction

	Predicted Drag	**Remarks**
Ramjet	26.67 N	-
Flexure	5.16 N	For each Flexure
Total	36.99 N	-

3. Discussion

A summary of the various CFD predicted results and SSWT result is presented in Table 8.

Table 8. Summary of predicted and measured drag forces

<table>
<tr><th>Parts</th><th>Ramjet</th><th>Flexures</th><th>Total</th><th>Remarks</th></tr>
<tr><td>Predicted in ANSYS CFX</td><td>26.67 N</td><td>10.32 N</td><td>36.99 N</td><td>-</td></tr>
<tr><td>Predicted in [1]</td><td>21.35 N</td><td>-</td><td rowspan="2">61.71 N</td><td rowspan="2">Combined prediction</td></tr>
<tr><td>Predicted in [2]</td><td>-</td><td>40.36 N</td></tr>
<tr><td>Current Experimental Results</td><td>-</td><td>-</td><td>55.17 N</td><td>-</td></tr>
<tr><td>Experimental Results in [2]</td><td>-</td><td>-</td><td>57.83 N</td><td>-</td></tr>
</table>

While the experimental drag forces were seen to be very similar, the CFD drag force prediction by ANYS CFX was very different from that predicted by [2]. ANSYS CFX predicted a very low drag for the flexures.

With the large difference in drag predicted in ANSYS-CFX, a check was performed on the drag predictions. The drag force induced on a body is correlated to the "obstruction" seen by the flow. The ratios of the cross-section projected frontal area of the ramjet and flexures seen by the flow and the ANSYS-CFX predicted drag forces were computed to be 2.56:1 and 2.58:1, indicating that the results from ANSYS-CFX may not be erroneous.

With the two experimental results agreeing, there is no reason to suspect the results. However, in the conduct of the experiment, the following observations and recommendations are made for better experimental accuracies.

1. While the model fitted into the test section, when the windows were closed, the bridge was unbalanced, indicating an inward compressing force on the model. While these were subsequently neutralized before the run, this compressing force may affect the axially measured drag force. The flexures should be redesigned to reduce the impact of any compressive or tensile forces acting on the ramjet body, as this could affect the drag measurements.

2. Figure 37 shows the setup for strain gauge calibration. The jackscrew was tightened to vary the applied force on the ramjet and the potential difference is measured across the Wheatstone bridge. Despite measurements taken to ensure that the load cell was properly wedged between the jackscrew and the thrust fixture, the applied load could not be stabilized. It is suspected that this was due to the creep of the wooden reaction block and the thrust fixture. Eventually, over a hundred readings at varying loads were taken to averaged out the potential errors from the measurements. To reduce errors in calibration due to the creep, the thrust fixture should be lengthened such that it rests on the inner flexures instead of the diffuser.

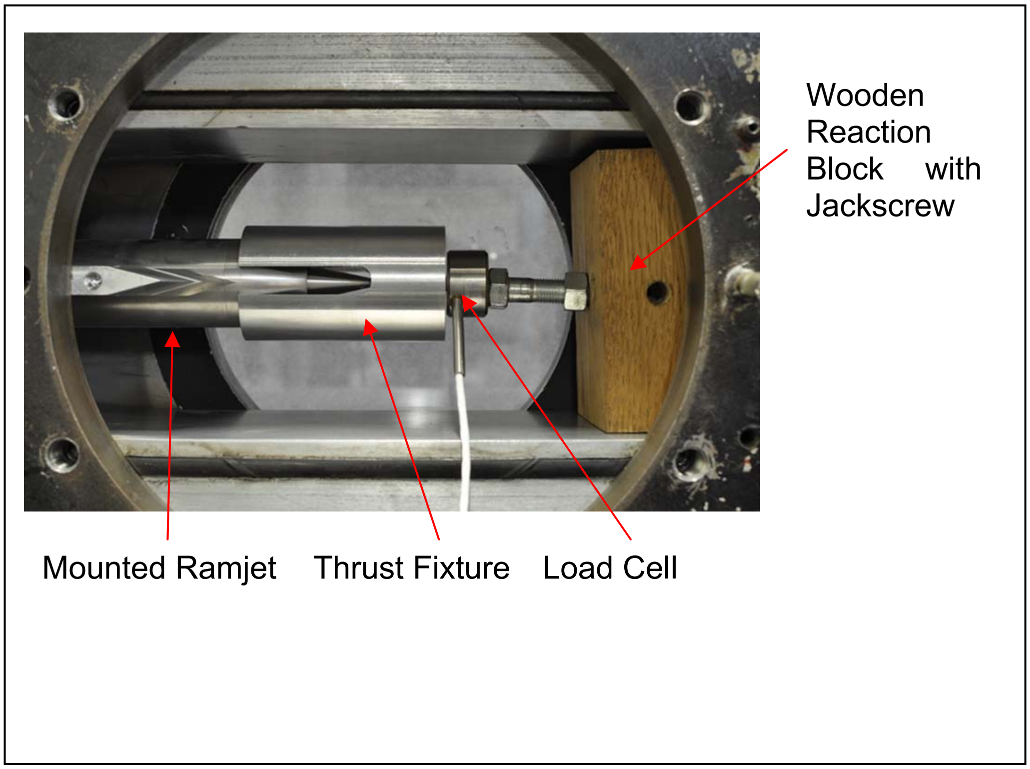

Figure 37. Calibration setup of load cell and thrust fixture in SSWT

The following recommendations are made for better CFD drag prediction modeling.

1. CFD should be performed on a model of the flexure. This result can be put together with the CFD ramjet drag prediction and verified against the experimental results.

2. For completeness, the full flexure may be modeled with the ramjet to determine the drag force induced on it. This can then be verified with the experimental results.

THIS PAGE INTENTIONALLY LEFT BLANK

VII. CONCLUSIONS AND RECOMMENDATIONS

A successful cold-flow model was developed in ANSYS-CFX. On the current ramjet design, the diffuser of the inlet would need to be redesigned to improve its total pressure recovery. This model can be used as a baseline model for comparison with subsequent CFD analysis.

The effects of fluid injection through the existing tip ports were investigated. It was determined that fluid injection through the current tip ports at total pressure settings of 0.5 atm and higher would perturb the conical shock, resulting in flow spillage at the inlet region.

An initial combustion model was developed in ANSYS-CFX using hydrogen gas injected aft of the struts. Results suggest that fuel combustion with the current design would result in thrust augmentation. However, for combustion and thrust to be sustained, the model will need to be modified. Computationally, with further improvement, it is likely that a suitable combustion model can be developed.

A SSWT experimentation was performed, and the measured drag force of 55.17N was within 5% of the drag measurements in [2]. The current CFD model was determined to under predict the drag force induced on the ramjet and flexures.

Results from the CFD analysis showed the flow field to be very complex. As such, a mesh-sensitivity study should be performed to determine the sufficiency of the current mesh resolution in capturing the complex flow field.

THIS PAGE INTENTIONALLY LEFT BLANK

APPENDIX A – DETAIL SETUP FOR COLD-FLOW ANALYSIS

A1. MESH SETUP

Table 9. Details of mesh setup for cold-flow analysis

Defaults	
Physics Preference	CFD
Solver Preference	CFX
Relevance	50
Sizing	
Use Advance Size Function	On: Proximity and Curvature
Relevance Centre	Fine
Initial Size Seed	Active Assembly
Smoothing	High
Transition	Slow
Span Angle Centre	Fine
- Curvature Normal Angle	15 deg
- Proximity Accuracy	0.6
- Num Cells Across Gap	Default (3)
- Min Size	0.0001 m
- Proximity Min Size	0.0001 m
- Max Face Size	0.0008 m
- Max Size	0.0008 m
- Growth Rate	1.1
Inflation	
Use Automatic Inflation	None
Patch Conforming Option	
Triangle Surface Mesher	Program Controlled
Advance	
Shape Checking	CFD
Element Midside Nodes	Dropped
Extra Retries for Assembly	Yes
Mesh Morphing	Disabled

Table 10. Details of mesh inflation settings for cold-flow analysis

Scope	
Scoping Method	Geometry Selection
Geometry	1 body
Definition	
Suppressed	No
Boundary Scoping Method	Named Selections
Boundary	Ramjet
Inflation Option	Total Thickness
- Number of Layers	20
- Growth Rate	1.05
- Maximum Thickness	1e-4m
Inflation Algorithm	Pre

A2. CFX-PRE SETUP PARAMETERS

Table 11. Default domain for cold-analysis

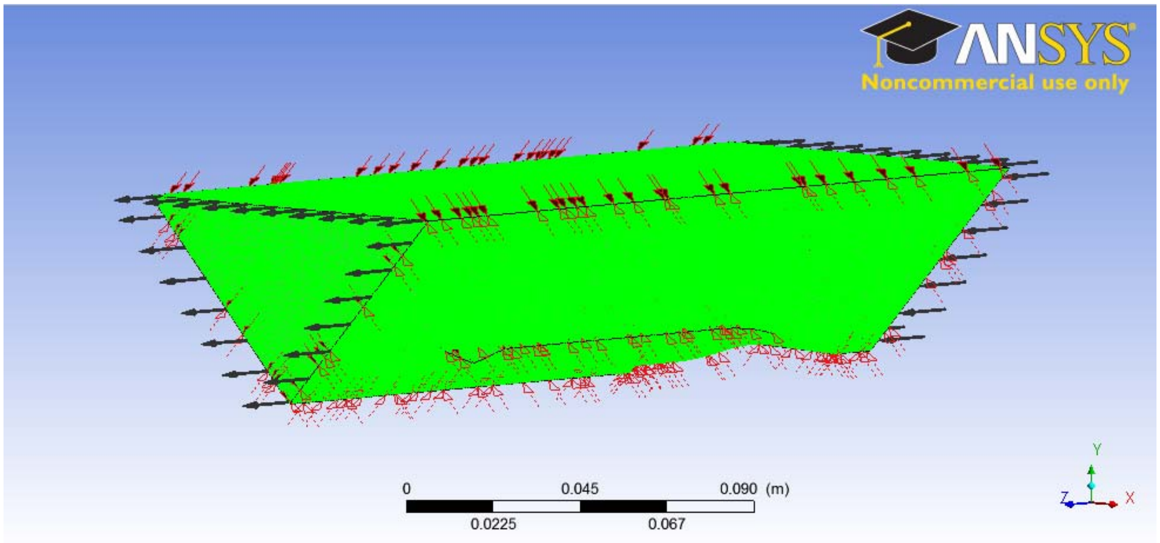

BASIC SETTINGS	
Location and Type - Location - Domain Type - Coordinate Frame	 <use default> Fluid Domain Coord 0
Fluid and Particles Definition for Fluid 1 - Option: - Material - Morphology	 Material Library Air Ideal Gas Continuous Fluid
Domain Models - Pressure → Reference Pressure - Buoyancy Model → Option - Domain Motion → Option - Mesh Deformation → Option	 0 Pa Non-Buoyant Stationary None
FLUID MODELS	
Heat Transfer → Option	Total Energy
Turbulence - Option - Transitional Turbulence	 Shear Stress Transport Gamma Theta Model
Combustion → Option	None
Thermal Radiation → Option	None

Table 12. Boundary: Inlet – for cold-flow analysis

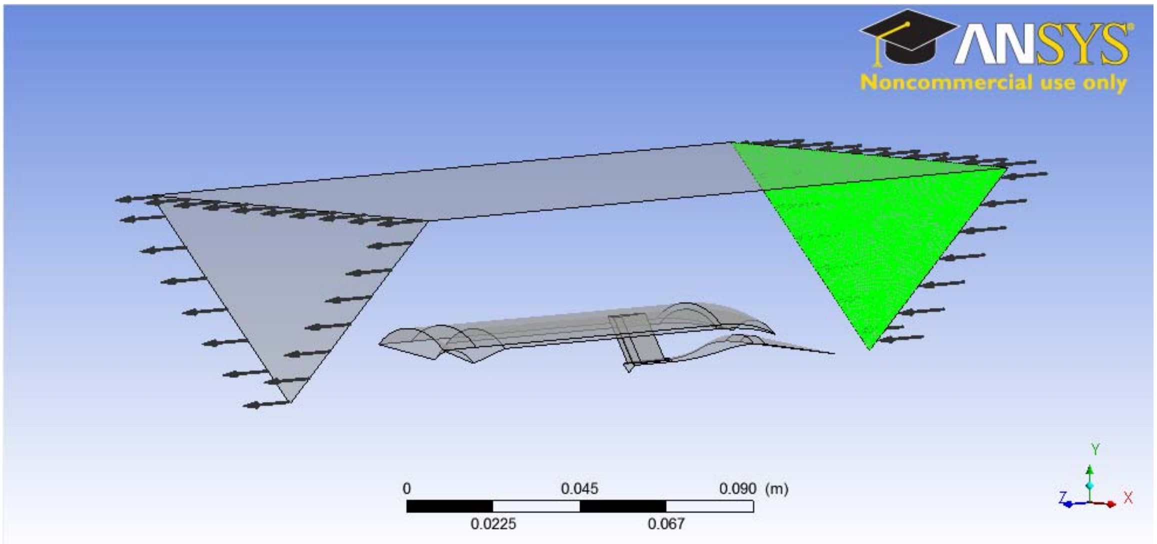

BASIC SETTINGS	
Boundary Type Location	Inlet Inlet
BOUNDARY DETAILS	
Flow Regime → Option	Supersonic
Mass and Momentum - Option - Rel. Static Pressure - Normal Speed	 Normal Speed & Pressure 7378 Pa 661 m/s
Turbulence → Option	Medium (Intensity = 5%)
Heat Transfer - Option - Static Temperature	 Static Temperature 68K

Table 13. Boundary: Outlet – for cold-flow analysis

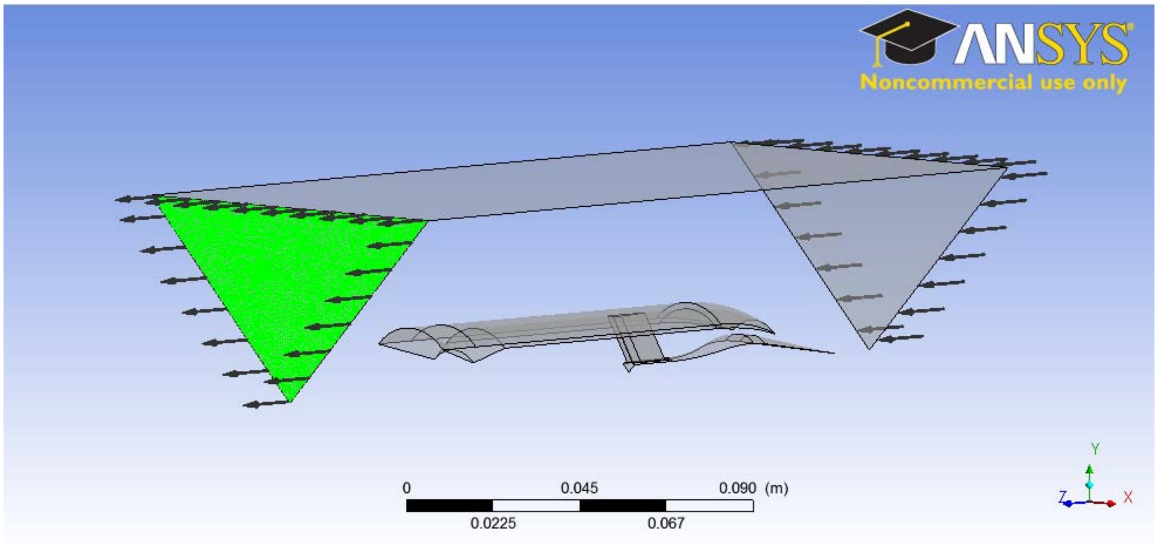

BASIC SETTINGS	
Boundary Type Location	Outlet Outlet
BOUNDARY DETAILS	
Flow Regime → Option	Supersonic

Table 14. Boundary: Sym1 – for cold-flow analysis

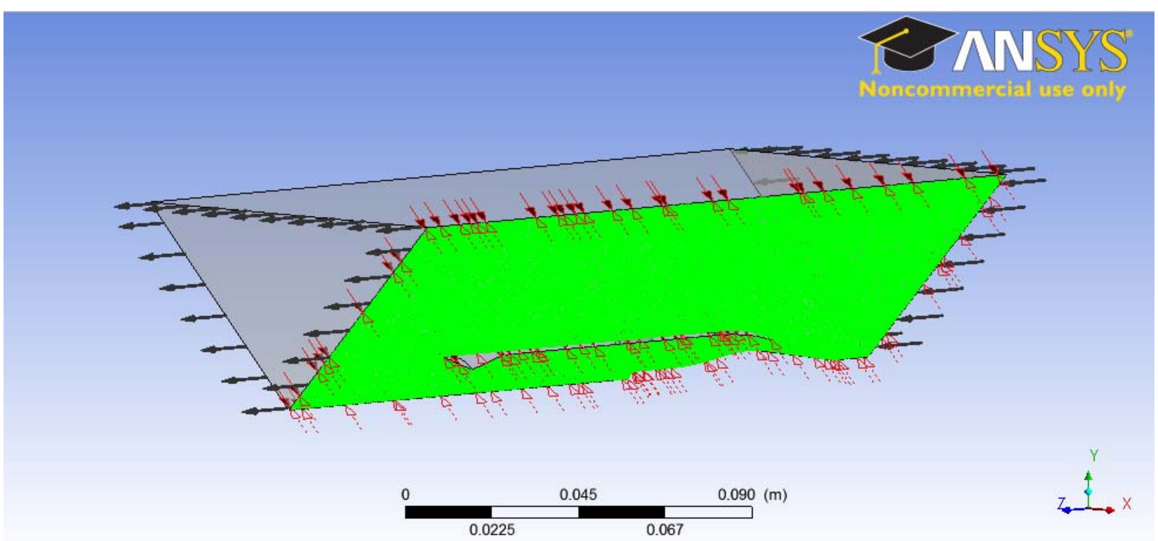

BASIC SETTINGS	
Boundary Type Location	Symmetry Sym1

Table 15. Boundary: Sym2 – for cold-flow analysis

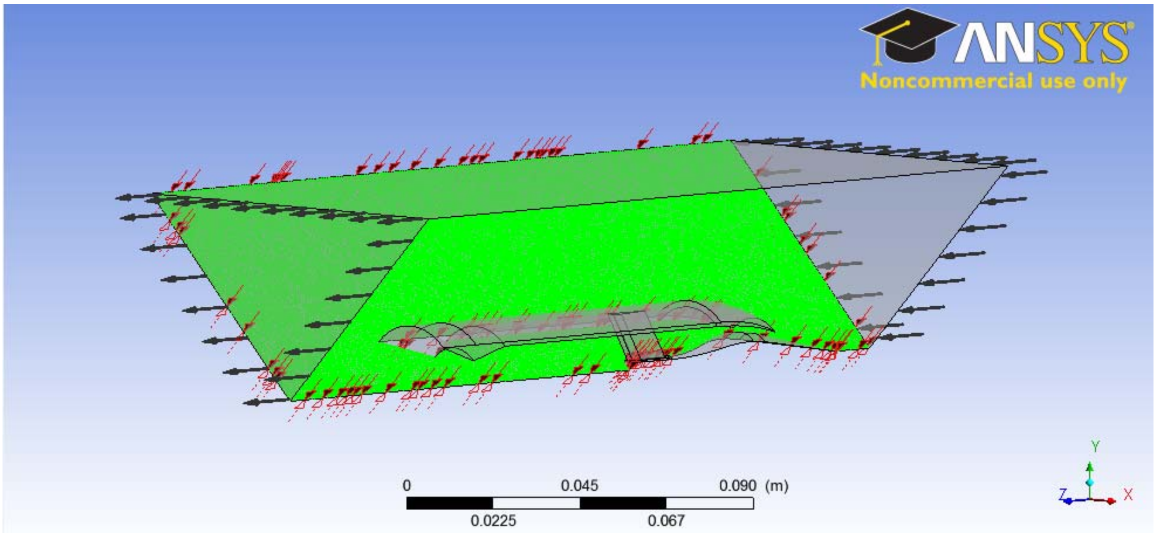

BASIC SETTINGS	
Boundary Type	Symmetry
Location	Sym2

Table 16. Boundary: Top – for cold-flow analysis

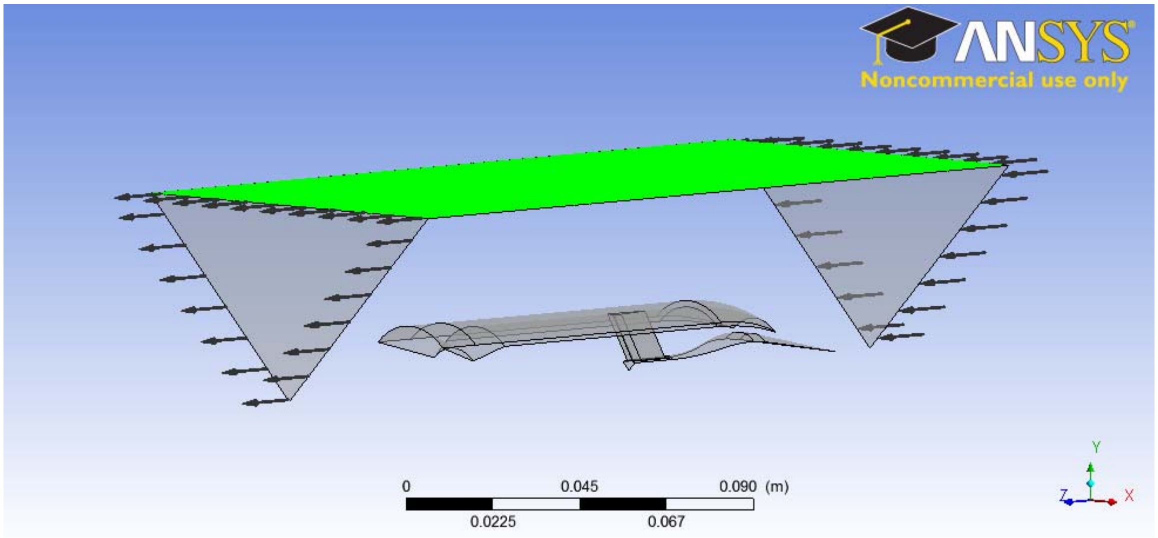

BASIC SETTINGS	
Boundary Type	Wall
Location	Top
BOUNDARY DETAILS	
Mass and Momentum → Option	No Slip Wall
Heat Transfer → Option	Adiabatic

Table 17. Boundary: Ramjet – for cold-flow analysis

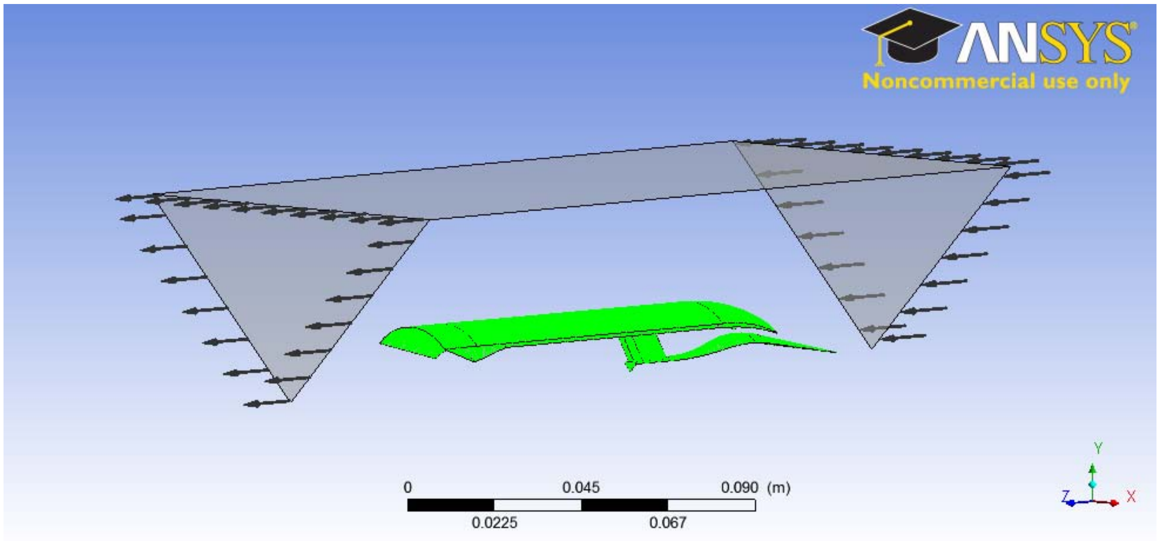

BASIC SETTINGS	
Boundary Type	Wall
Location	Ramjet
BOUNDARY DETAILS	
Mass and Momentum → Option	No Slip Wall
Wall Roughness → Option	Smooth Wall
Heat Transfer → Option	Adiabatic

Table 18. Expert parameters for cold-flow analysis

CONVERGENCE CONTROL	
Memory Control	
- Topology Estimate Factor	Checked
+ Value	1.2
High Speed Numerics	
- Max Continuity Loops	Checked
+ Value	3

Table 19. Solver control settings for cold-flow analysis

BASIC SETTINGS	
Advection Scheme --> Option	High Resolution
Turbulence Numerics --> Option	High Resolution
Convergence Control	
- Min. Iterations	1
- Max. Iterations	1000
- Fluid Timescale Control	
+ Timescale Control	Local Timescale Factor
+ Local Timescale Factor	3
Convergence Criteria	
- Residual Type	RMS
- Residual Target	1.00E-06
ADVANCE OPTIONS	
Compressibility Control	Checked
- High Speed Numerics	Checked

A3. OTHER NOTES

1. Time-stepping

As seen in the CFX-PRE setup section, a local timescale control with a factor of 3 was used to start the simulation. As the simulation stabilizes, the timescale control was switched to automatic timescale control with a timescale factor of 1. Subsequently, the timescale factor was also ramped progressively to a factor of 3 to reduce the time taken for the results to converge. These changes in time scaling can be performed on the fly with the "Edit Run in Progress" function in CFX-POST.

APPENDIX B – RESULTS FOR COLD-FLOW CFD ANALYSES

B1. MACH NUMBER PROFILE

Nozzle Throat Area	Mach Number Profile Plot
Default Sizing	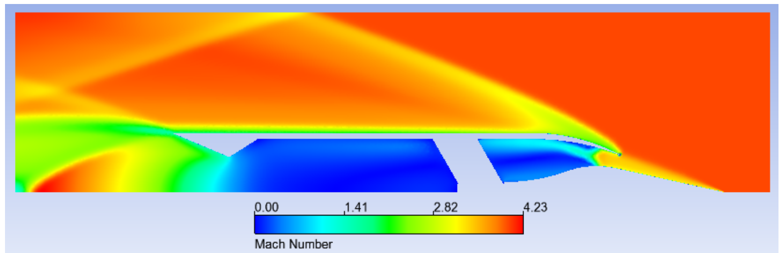
10% Reduction	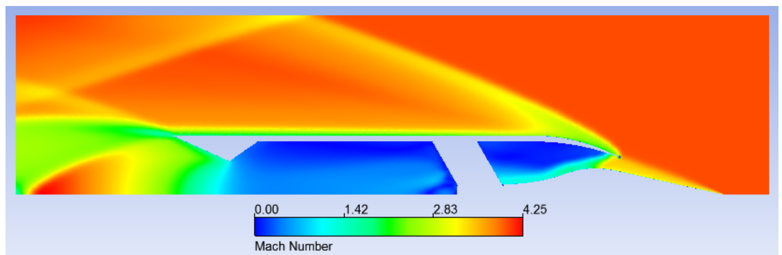
20% Reduction	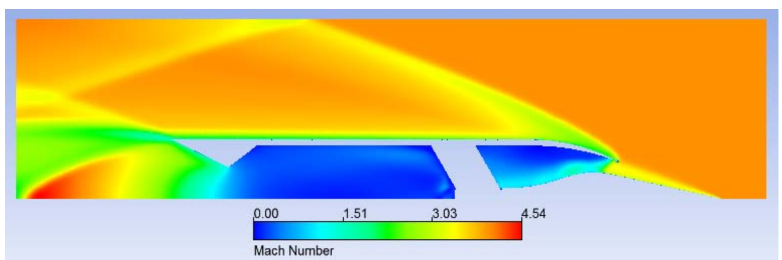
30% Reduction	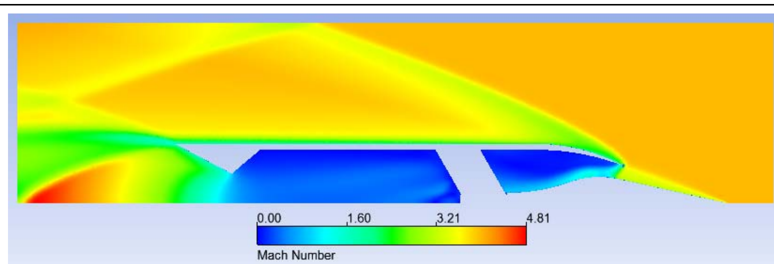
40% Reduction	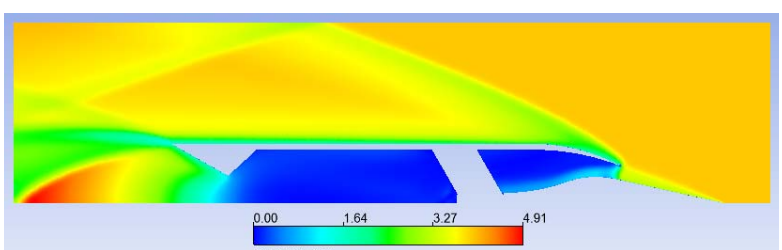

B2. PRESSURE PROFILE

<table>
<tr><th>Nozzle Throat Area</th><th>Mach Number Profile Plot</th></tr>
<tr><td>Default Sizing</td><td>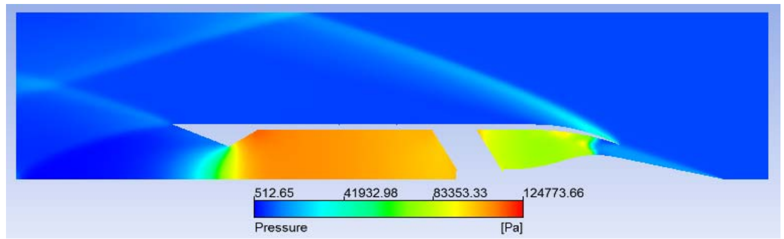
</td></tr>
<tr><td>10% Reduction</td><td>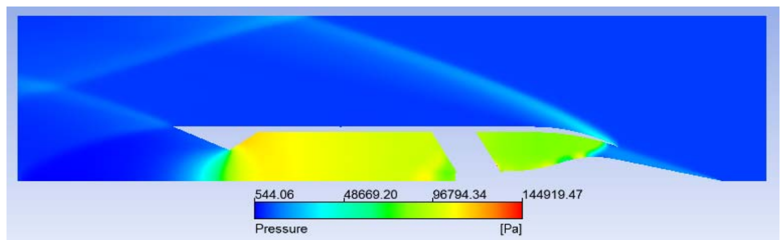
</td></tr>
<tr><td>20% Reduction</td><td>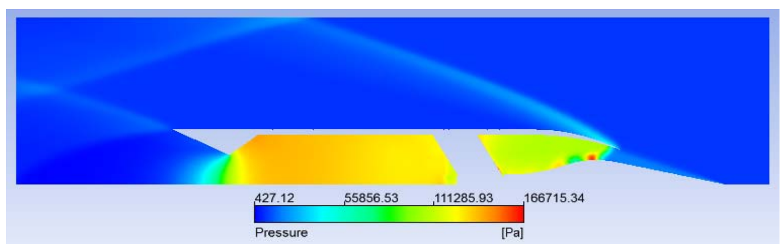
</td></tr>
<tr><td>30% Reduction</td><td>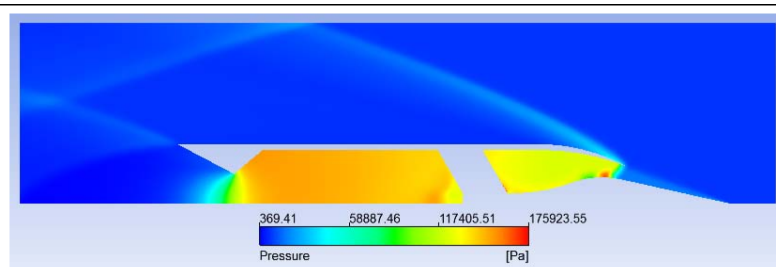
</td></tr>
<tr><td>40% Reduction</td><td>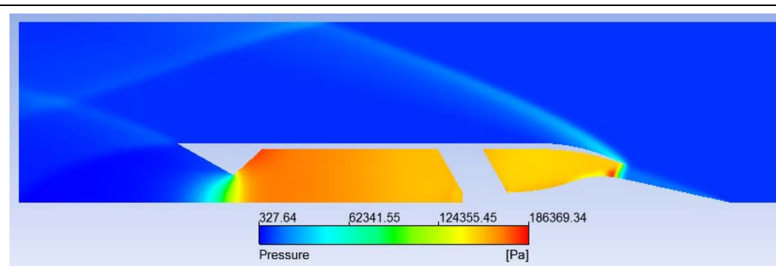
</td></tr>
</table>

B3. DENSITY PROFILE

Nozzle Throat Area	Density Profile Plot
Default Sizing	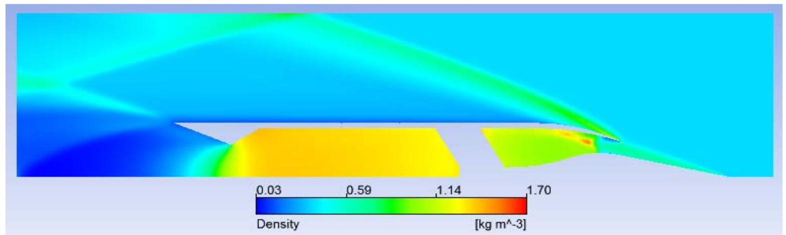
10% Reduction	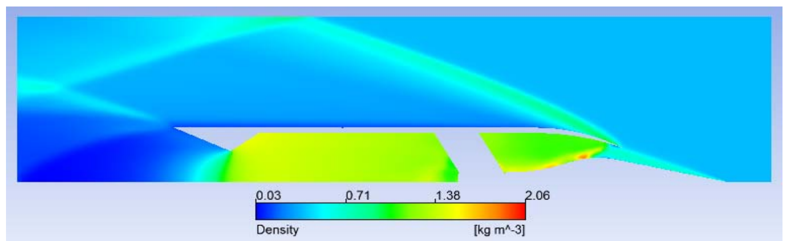
20% Reduction	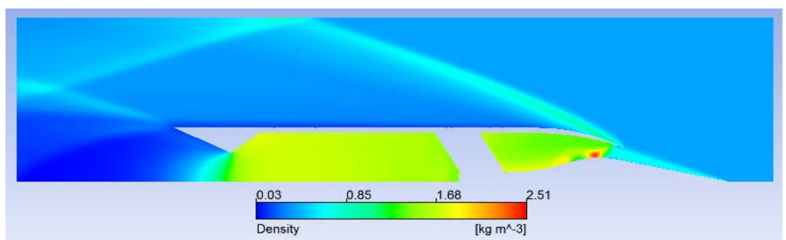
30% Reduction	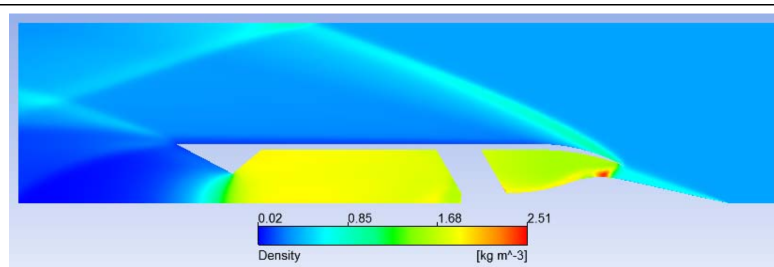
40% Reduction	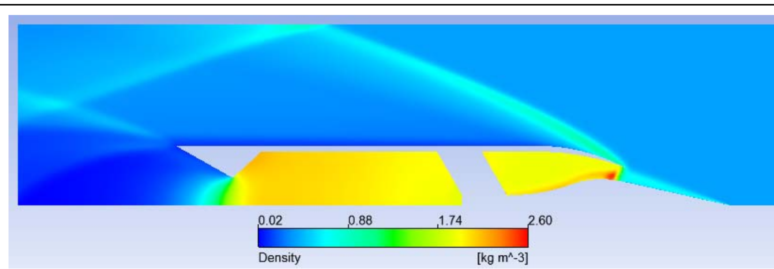

B4. STREAMLINE PLOT

<table>
<tr><th>Nozzle Throat Area</th><th>Streamline Plot</th></tr>
<tr><td>Default Sizing</td><td>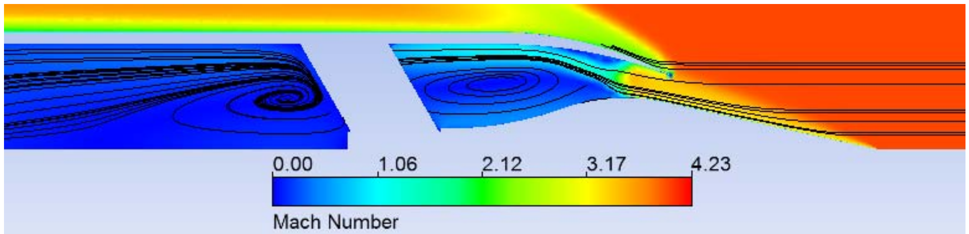
</td></tr>
<tr><td>10% Reduction</td><td>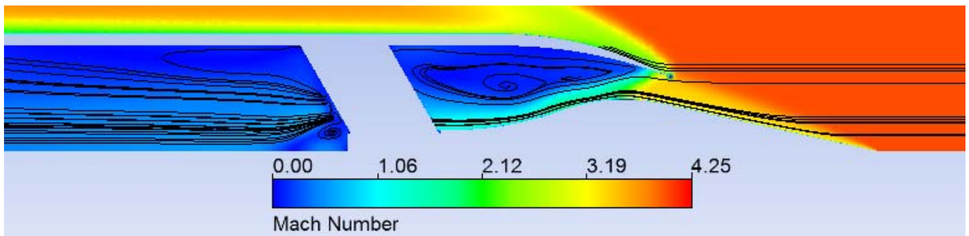
</td></tr>
<tr><td>20% Reduction</td><td>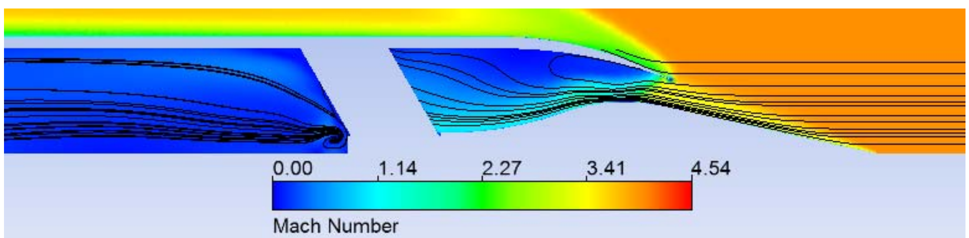
</td></tr>
<tr><td>30% Reduction</td><td>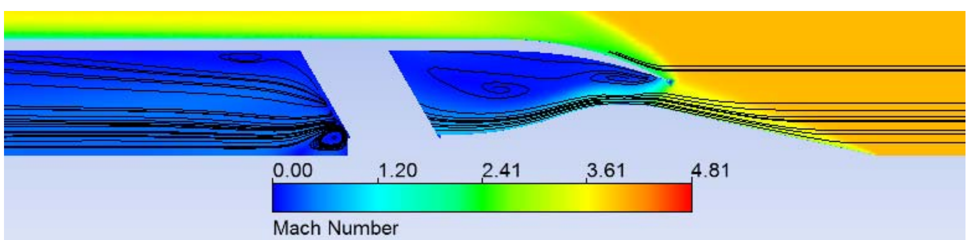
</td></tr>
<tr><td>40% Reduction</td><td>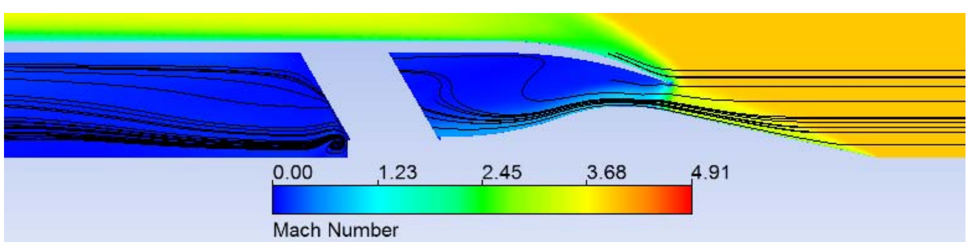
</td></tr>
</table>

B5. SHOCK INDICATOR PLOT

Nozzle Throat Area	Shock Indicator Plot	Remarks
Default Sizing	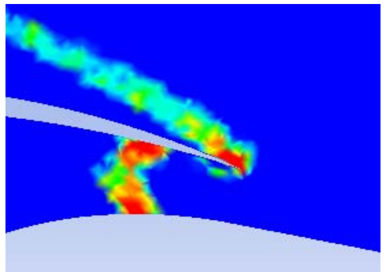	Oblique shock downstream the lip of the inlet cowl.
10% Reduction	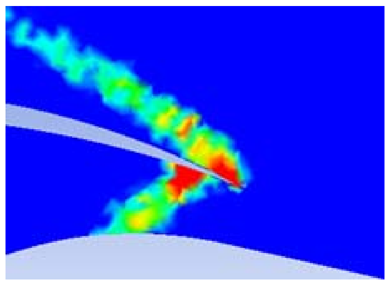	Oblique shock downstream the lip of the inlet cowl.
20% Reduction	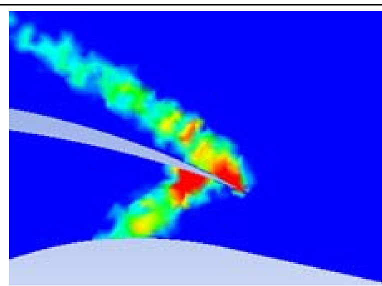	Oblique shock downstream the lip of the inlet cowl.
30% Reduction	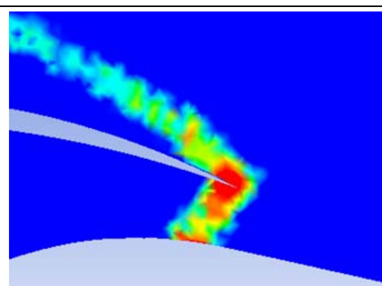	Shock on lip of inlet cowl. Flow downstream of shock is subsonic. However, shock is not truly normal to flow.
40% Reduction	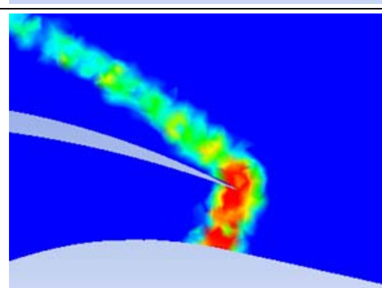	Normal shock formed upstream the lip of the inlet cowl. Flow spillage. Sub-critical operation.
Legend:	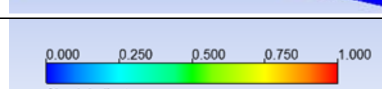	

B6. DRAG COEFFICIENT COMPUTATION

Drag induced on quarter - cut ramjet model = 6.70959 N

Total drag on full ramjet model (D) = 6.70959 × 4 = 26.838 N

$$\text{Cross-section radius of ramjet} = \frac{0.03340}{2}\ \text{m}$$

$$\text{Cross-section area of ramjet (A)} = \pi R^2 = \pi\left(\frac{0.03340}{2}\right)^2 = 8.762\times10^{-4}\ \text{m}^2$$

Free stream velocity (V) = 661 m/s

Free stream air density(ρ) = 0.377915 kg/m^3

$$\text{Drag coefficient} = \frac{D}{\frac{1}{2}\rho V^2 A} = 0.371$$

APPENDIX C – DETAIL SETUP FOR CFD analysis on AIR INJECTION THROUGH THE TIP PORTS

C1. MESH SETUP

Table 20. Details of mesh setup for CFD analysis on air injection through tip ports

Defaults	
Physics Preference	CFD
Solver Preference	CFX
Relevance	50
Sizing	
Use Advance Size Function	On: Proximity and Curvature
Relevance Centre	Fine
Initial Size Seed	Active Assembly
Smoothing	High
Transition	Slow
Span Angle Centre	Fine
- Curvature Normal Angle	18 deg
- Proximity Accuracy	0.5
- Num Cells Across Gap	Default (3)
- Min Size	0.00005 m
- Proximity Min Size	0.00005 m
- Max Face Size	0.0005 m
- Max Size	0.0005 m
- Growth Rate	1.1
Inflation	
Use Automatic Inflation	None
Patch Conforming Option	
Triangle Surface Mesher	Program Controlled
Advance	
Shape Checking	CFD
Element Midside Nodes	Dropped
Extra Retries for Assembly	Yes
Mesh Morphing	Disabled

Table 21. Details of mesh inflation settings for CFD analysis on air injection through tip ports

Scope	
Scoping Method	Geometry Selection
Geometry	1 body
Definition	
Suppressed	No
Boundary Scoping Method	Named Selections
Boundary	Ramjet
Inflation Option	Total Thickness
- Number of Layers	20
- Growth Rate	1.05
- Maximum Thickness	1e-4m
Inflation Algorithm	Pre

Table 22. Details of face sizing settings for CFD analysis on air injection through tip ports

Scope	
Scoping Method	Named Selection
Named Selection	Port
Definition	
Suppressed	No
Type	Element Size
- Element Size	0.000001
Behavior	Soft
- Curvature Normal Angle	Default
- Growth Rate	Default

C2. CFX-PRE SETUP PARAMETERS

1. Domain: Default domain

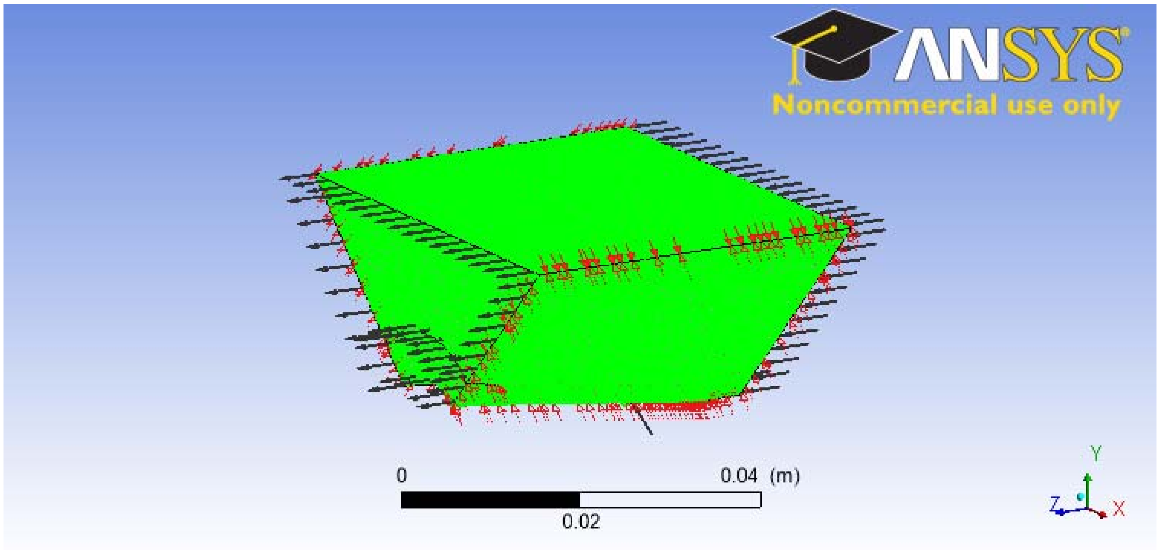

BASIC SETTINGS	
Location and Type	
- Location	<use default>
- Domain Type	Fluid Domain
- Coordinate Frame	Coord 0
Fluid and Particles Definition for Fluid 1	
- Option:	Material Library
- Material	Air Ideal Gas
- Morphology	Continuous Fluid
Domain Models	
- Pressure → Reference Pressure	0 Pa
- Buoyancy Model → Option	Non-Buoyant
- Domain Motion → Option	Stationary
- Mesh Deformation → Option	None
FLUID MODELS	
Heat Transfer → Option	Total Energy
Turbulence	
- Option	Shear Stress Transport
- Transitional Turbulence	Gamma Theta Model
Combustion → Option	None
Thermal Radiation → Option	None

Table 23. Boundary: Inlet – for CFD analysis on air injection through tip ports

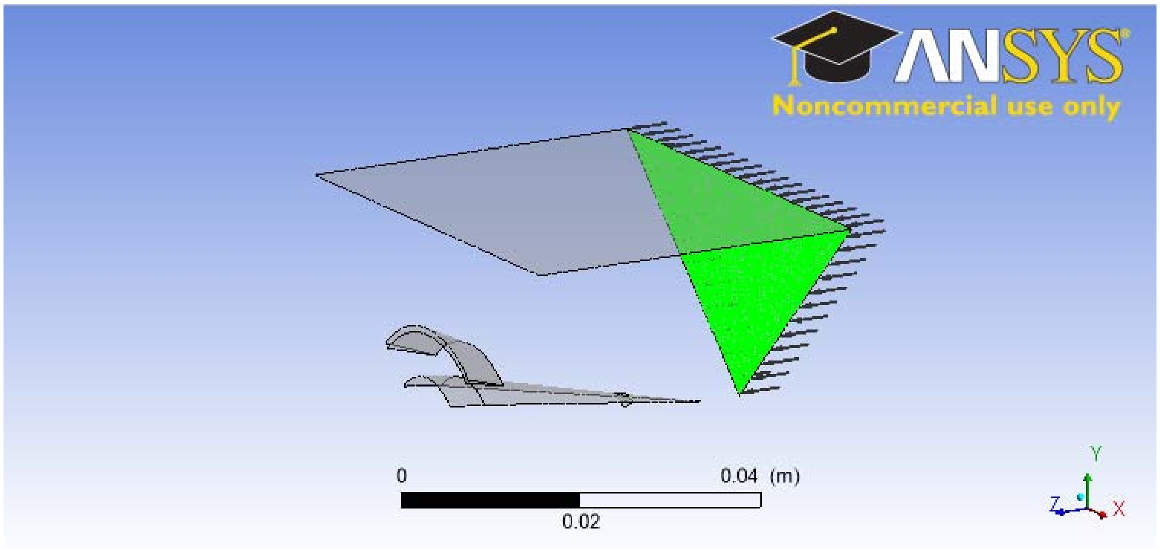

BASIC SETTINGS	
Boundary Type Location	Inlet Inlet
BOUNDARY DETAILS	
Flow Regime → Option	Supersonic
Mass and Momentum - Option - Rel. Static Pressure - Normal Speed	 Normal Speed & Pressure 7378 Pa 661 m/s
Turbulence → Option	Medium (Intensity = 5%)
Heat Transfer - Option - Static Temperature	 Static Temperature 68K

Table 24. Boundary: Outlet – for CFD analysis on air injection through tip ports

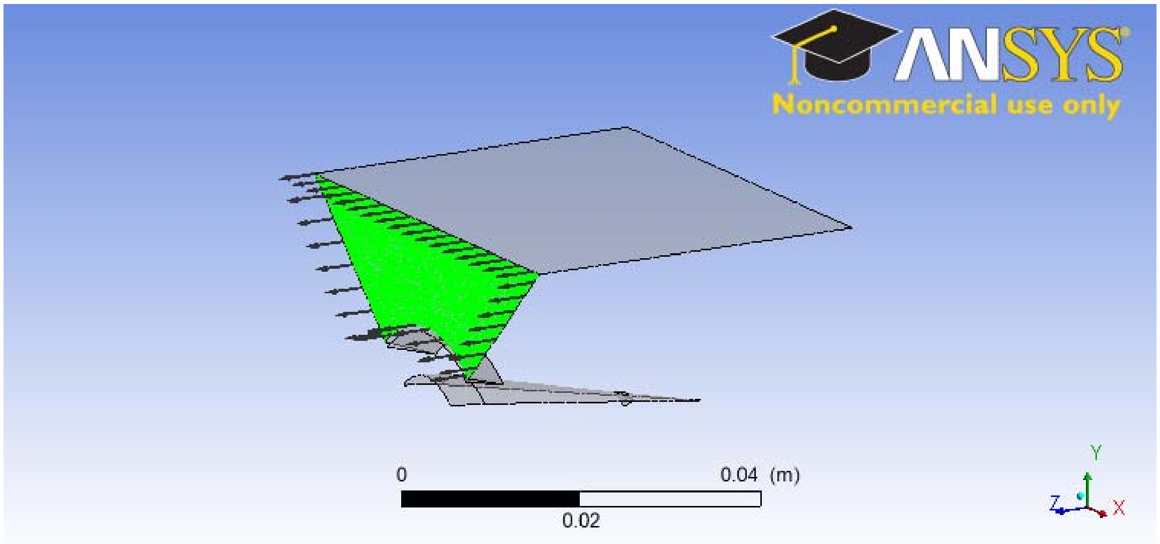

BASIC SETTINGS	
Boundary Type	Outlet
Location	Outlet
BOUNDARY DETAILS	
Flow Regime → Option	Supersonic

Table 25. Boundary: Sym1 – for CFD analysis on air injection through tip ports

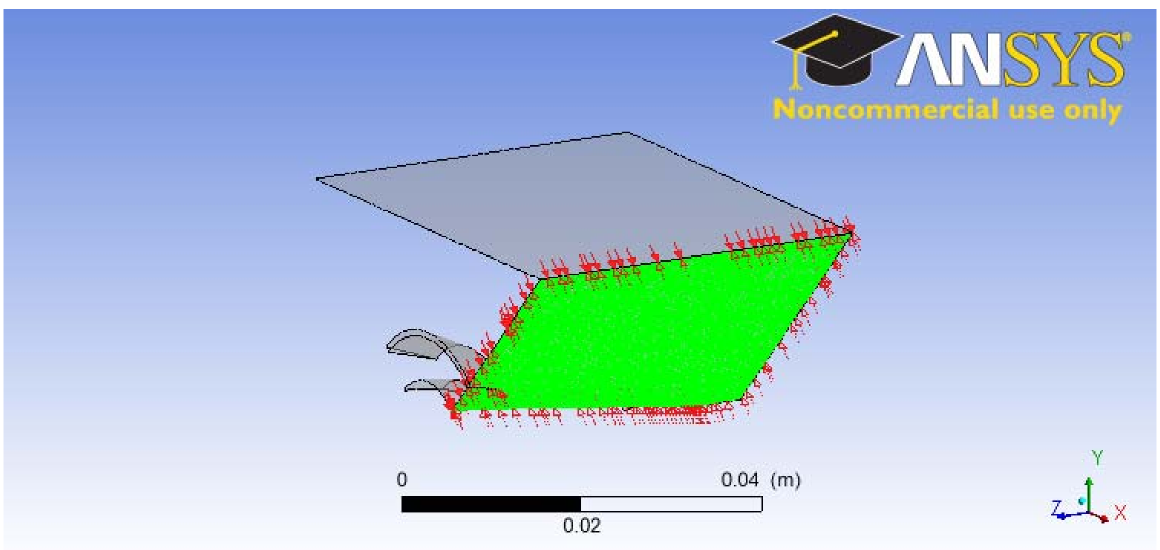

BASIC SETTINGS	
Boundary Type	Symmetry
Location	Sym1

Table 26. Boundary: Sym2 – for CFD analysis on air injection through tip ports

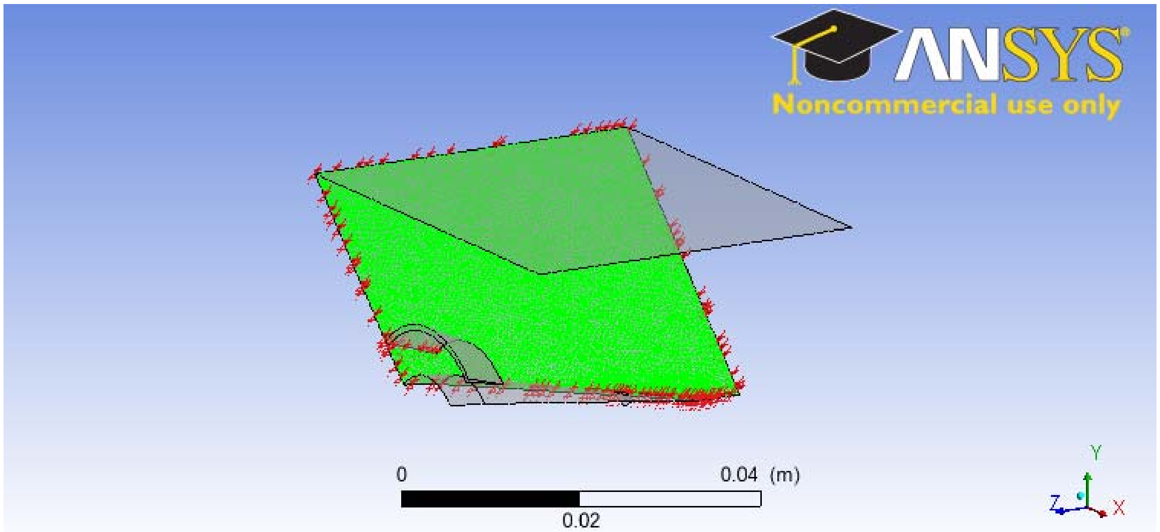

BASIC SETTINGS	
Boundary Type	Symmetry
Location	Sym2

Table 27. Boundary: Top – for CFD analysis on air injection through tip ports

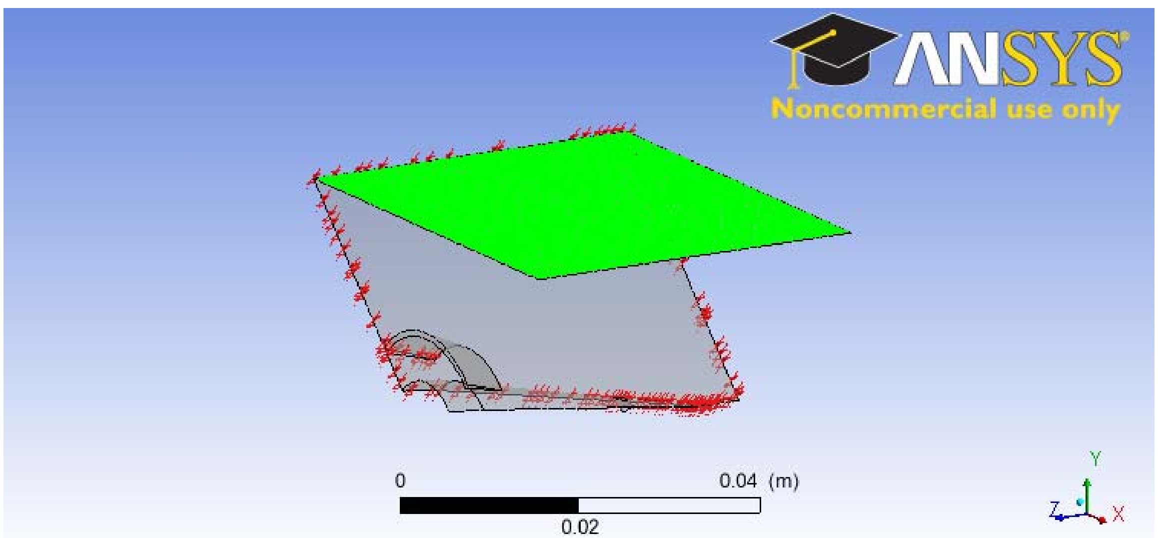

BASIC SETTINGS	
Boundary Type	Wall
Location	Top
BOUNDARY DETAILS	
Mass and Momentum → Option	No Slip Wall
Heat Transfer → Option	Adiabatic

Table 28. Boundary: Ramjet – for CFD analysis on air injection through tip ports

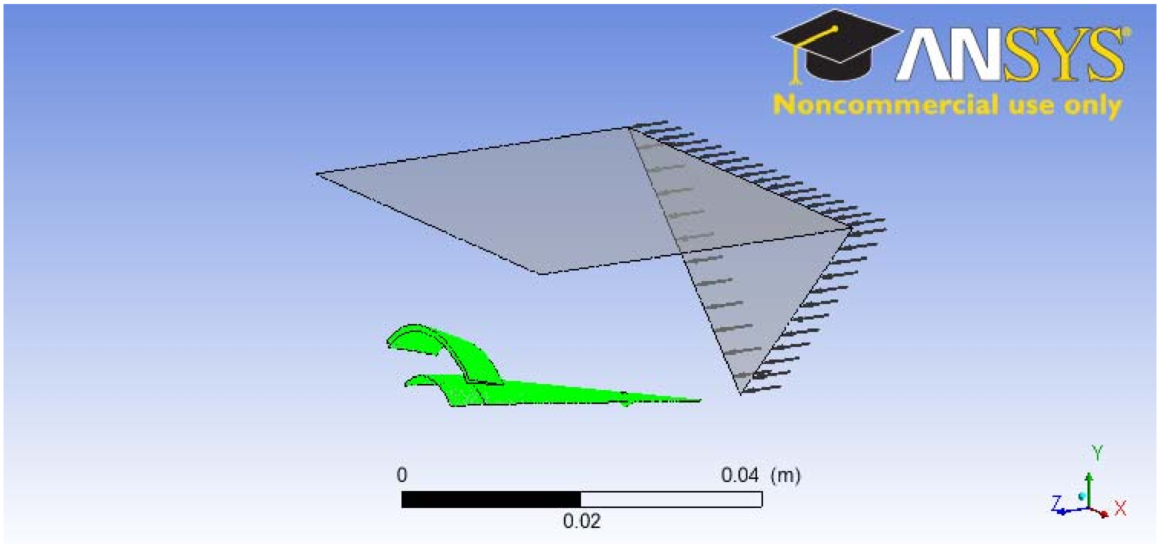

BASIC SETTINGS	
Boundary Type	Wall
Location	Ramjet
BOUNDARY DETAILS	
Mass and Momentum → Option	No Slip Wall
Wall Roughness → Option	Smooth Wall
Heat Transfer → Option	Adiabatic

Table 29. Boundary: Internal Outlet – for CFD analysis on air injection through tip ports

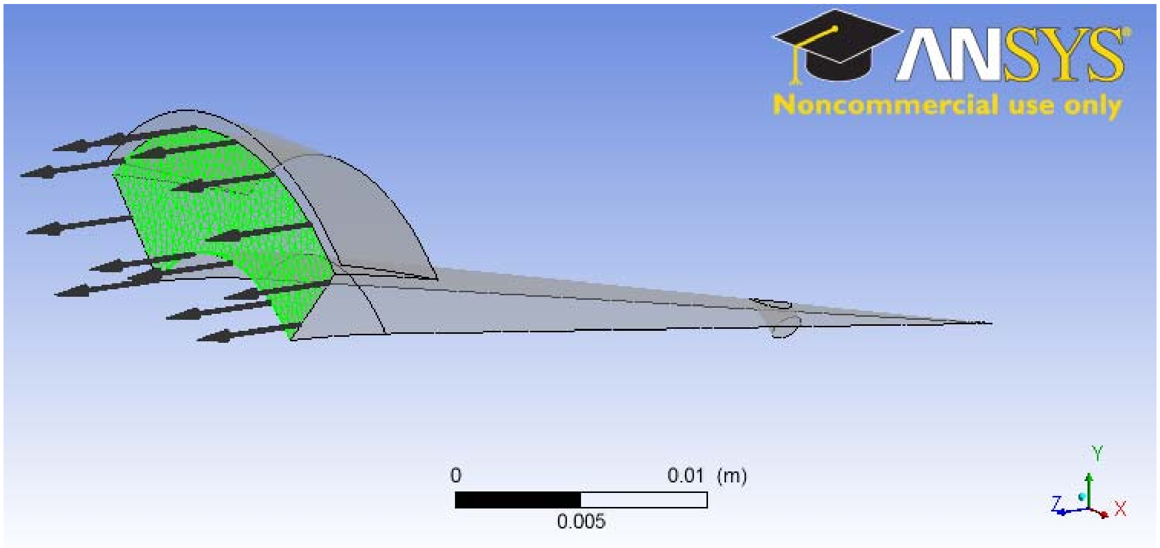

BASIC SETTINGS	
Boundary Type	Outlet
Location	Outlet
BOUNDARY DETAILS	
Flow Regime → Option	Supersonic

Table 30. Boundary: Port – for CFD analysis on air injection through tip ports

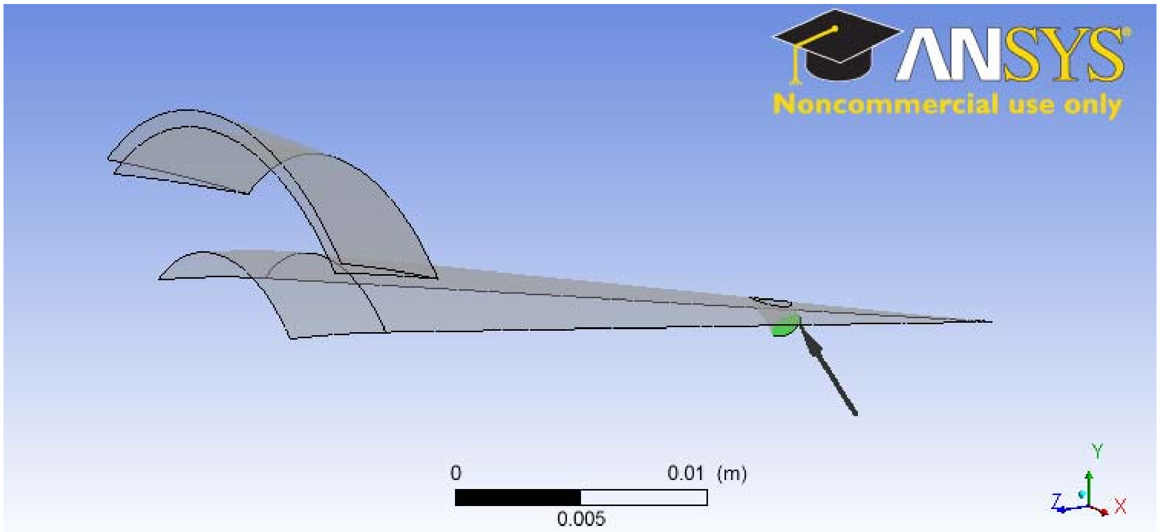

BASIC SETTINGS	
Boundary Type Location	Inlet Inlet
BOUNDARY DETAILS	
Flow Regime → Option	Supersonic
Mass and Momentum - Option - Rel. Static Pressure - Normal Speed	 Normal Speed & Pressure 7378 Pa 661 m/s
Turbulence → Option	Medium (Intensity = 5%)
Heat Transfer - Option - Static Temperature	 Static Temperature 68K

Table 31. Expert parameters for CFD analysis on air injection through tip ports

CONVERGENCE CONTROL	
Memory Control - Topology Estimate Factor + Value	 Checked 1.2
High Speed Numerics - Max Continuity Loops + Value	 Checked 3

Table 32. Solver control settings for CFD analysis on air injection through tip ports

BASIC SETTINGS	
Advection Scheme --> Option	High Resolution
Turbulence Numerics --> Option	High Resolution
Convergence Control - Min. Iterations - Max. Iterations - Fluid Timescale Control + Timescale Control + Local Timescale Factor Convergence Criteria - Residual Type - Residual Target	 1 1000 Local Timescale Factor 1 RMS 1.00E-06
ADVANCE OPTIONS	
Compressibility Control - High Speed Numerics	Checked Checked

C3. OTHER NOTES

1. Time-stepping

As seen in the CFX-PRE setup section, a local timescale control with a factor of 1 was used to start the simulation. As the simulation stabilizes, the timescale control was switched to automatic timescale control with a timescale factor of 1. This change in time scaling can be performed on the fly with the "Edit run in progress" function in CFX-POST.

APPENDIX D – RESULTS FOR CFD analysis on AIR INJECTION THROUGH THE TIP PORTS

D1. VELOCITY STREAMLINES

Total Pressure Setting	Velocity Streamline Plot
1 atm	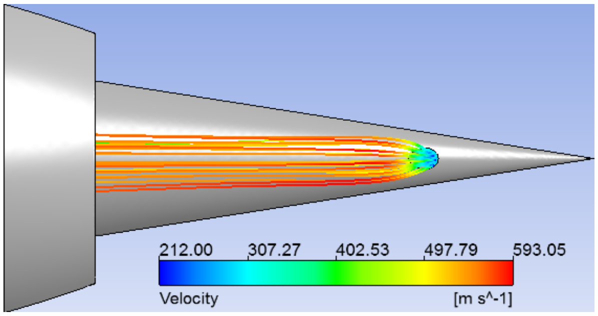
0.75 atm	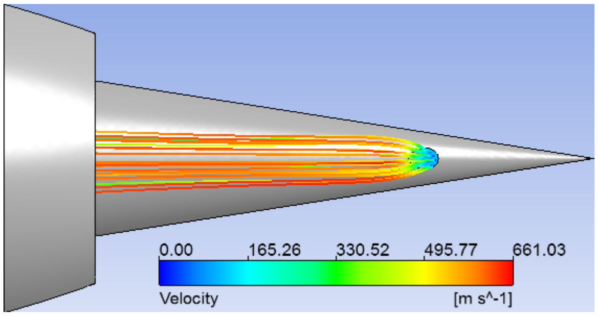
0.5 atm	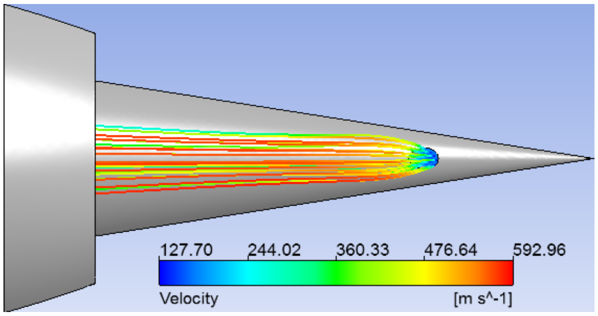

D2. MACH NUMBER PROFILE

Total Pressure Setting	Mach Number Profile Plot
1 atm	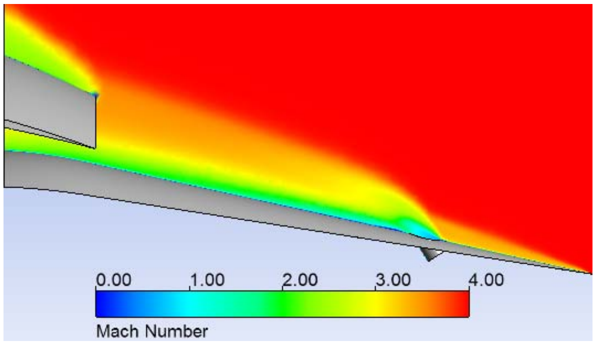
0.75 atm	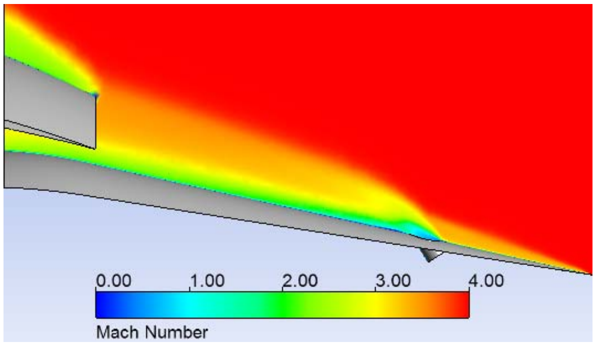
0.5 atm	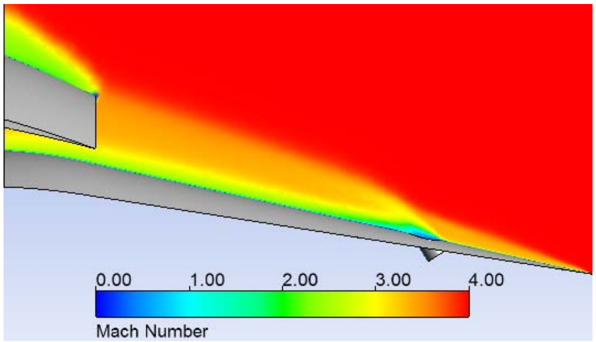

D3. ISO-SURFACE PLOT FOR MACH 3.65

Total Pressure Setting	Iso-Surface Plot for Mach 3.65
1 atm	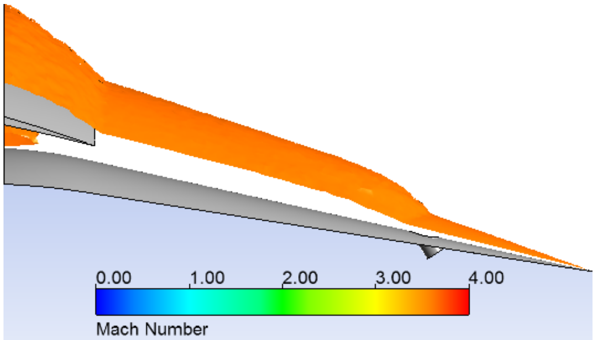
0.75 atm	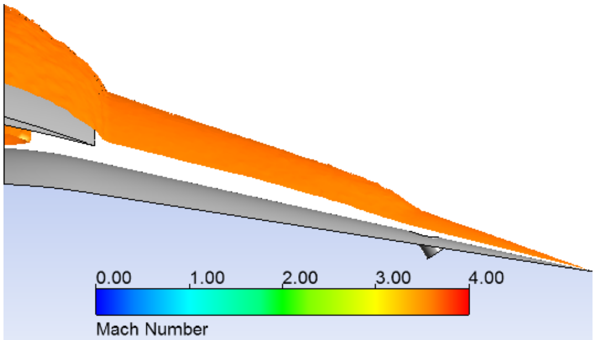
0.5 atm	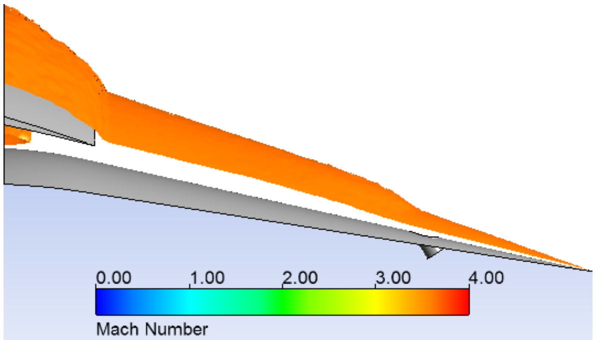

THIS PAGE INTENTIONALLY LEFT BLANK

APPENDIX E – STOICHIOMETRIC CALCULATION

E1. STOICHIOMETRIC FUEL-AIR RATIO

Assumed Composition of Air:

23.2% Oxygen, 76.8% Nitrogen

$\Rightarrow$ 1 Mole of Oxygen, 3.31 Mole of Nitrogen

Basic Equation for Stoichiometric Hydrogen – Air Combustion:

$H_2 + (3.31\ N_2 + O_2) \rightarrow 2\ H_2O + 3.31\ N_2$

Molar Mass of H_2 = 2.016 x 2 = 4.032

Molar Mass of O_2 = 31.99 x 1 = 31.99

Molar Mass of N_2 = 28.01 x 3.31 = 92.7131

Stoichiometric Fuel-Air Ratio

$\Rightarrow$ 4.032 : (92.7131+31.99)

$\Rightarrow$ 4.031 : 124.7031

$\Rightarrow$ 1: 30.94

E2. REQUIRED MASS FLOW FOR HYDROGEN

Based on International Standard Atmosphere conditions at altitude of 18000m:

- $\Rightarrow$ Temperature = T_∞ = 216.65 K
- $\Rightarrow$ Pressure = P_∞ = 7504.8 Pa

$$\text{Velocity at Mach 4} = 4 \times \sqrt{\gamma RT} = 4 \times \sqrt{1.4 \times 287 \times 216.65} = 1180.17\,\text{m/s}$$

$$\begin{aligned}
\dot{m}_{air} &= \rho_{air} A_{captured} V_{air} \\
&= \left(\frac{P_{air}}{R_{air} T_{air}}\right)(3.536 \times 10^{-4})(1180.17) \\
&= \left(\frac{7504.8}{287 \times 216.65}\right)(3.536 \times 10^{-4})(1180.17) \\
&= 0.05037\,\text{kg/s}
\end{aligned}$$

$$\frac{\dot{m}_{fuel}}{\dot{m}_{air}} = \frac{1}{30.94} \Rightarrow \frac{\dot{m}_{fuel}}{0.05037} = \frac{1}{30.94}$$

$$\Rightarrow \dot{m}_{fuel} = 1.628 \times 10^{-3}\,\text{kg/s}$$

APPENDIX F – DETAIL SETUP FOR COMBUSTION CFD ANALYSIS

F1. MESH SETUP

Table 33. Details of mesh setup for combustion analysis

Defaults	
Physics Preference	CFD
Solver Preference	CFX
Relevance	50
Sizing	
Use Advance Size Function	On: Proximity and Curvature
Relevance Center	Fine
Initial Size Seed	Active Assembly
Smoothing	High
Transition	Slow
Span Angle Center	Fine
- Curvature Normal Angle	Default
- Proximity Accuracy	0.5
- Num Cells Across Gap	Default (3)
- Min Size	0.00002 m
- Proximity Min Size	0.00002 m
- Max Face Size	0.0004 m
- Max Size	0.0004 m
- Growth Rate	1.1
Inflation	
Use Automatic Inflation	None
Patch Conforming Option	
Triangle Surface Mesher	Program Controlled
Advance	
Shape Checking	CFD
Element Midside Nodes	Dropped
Extra Retries for Assembly	Yes
Mesh Morphing	Disabled

Table 34. Details of mesh “Face Sizing” settings for combustion analysis

Scope	
Scoping Method	Named Selections
Geometry	Rear_Ports
Definition	
Suppressed	No
Type	Element Size
Element Size	1e-5 m
Behaviour	Soft
Curvature Normal Angle	Default
Growth Rate	Default

Table 35. Details of mesh inflation settings for combustion analysis

Scope	
Scoping Method	Geometry Selection
Geometry	1 body
Definition	
Suppressed	No
Boundary Scoping Method	Named Selections
Boundary	Ramjet
Inflation Option	Total Thickness
- Number of Layers	20
- Growth Rate	1.05
- Maximum Thickness	1e-4m
Inflation Algorithm	Pre

F2. CFX-PRE SETUP PARAMETERS

Table 36. Default domain for combustion analysis

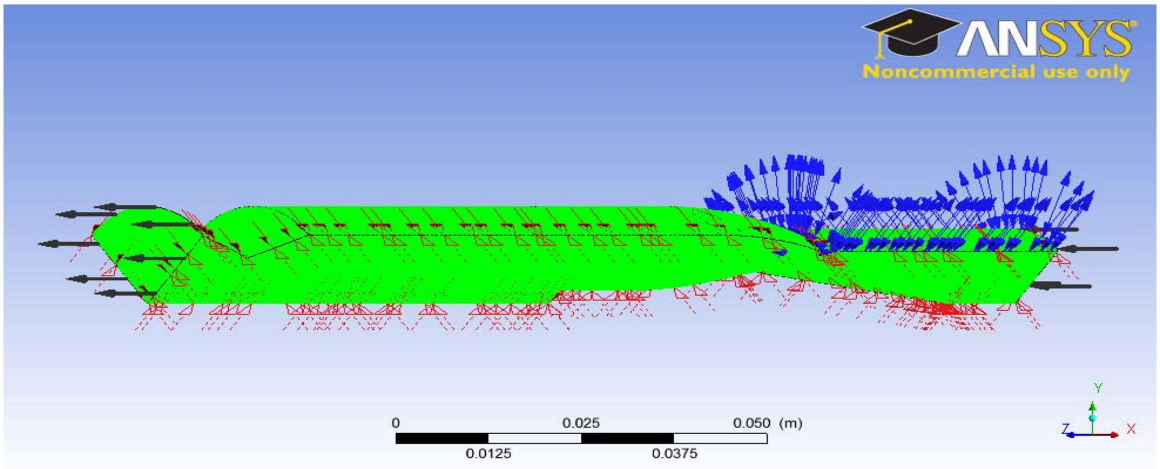

BASIC SETTINGS	
Location and Type - Domain Type - Coordinate Frame	 Fluid Domain Coord 0
Fluid and Particles Definition for Fluid 1 - Option: - Material - Morphology	 Material Library Hydrogen Air Mixture Continuous Fluid
Domain Models - Pressure → Reference Pressure - Buoyancy Model → Option - Domain Motion → Option	 0 Pa Non-Buoyant Stationary
FLUID MODELS	
Heat Transfer → Option	Total Energy
Turbulence - Option - Transitional Turbulence	 Shear Stress Transport Gamma Theta Model
Combustion → Option	None
Thermal Radiation → Option	None
Components Model → Component - H2 Option - H2O Option - N2 Option - O2 Option	 Transport Equation Transport Equation Constraint Transport Equation

Table 37. Boundary: Inlet – for combustion analysis

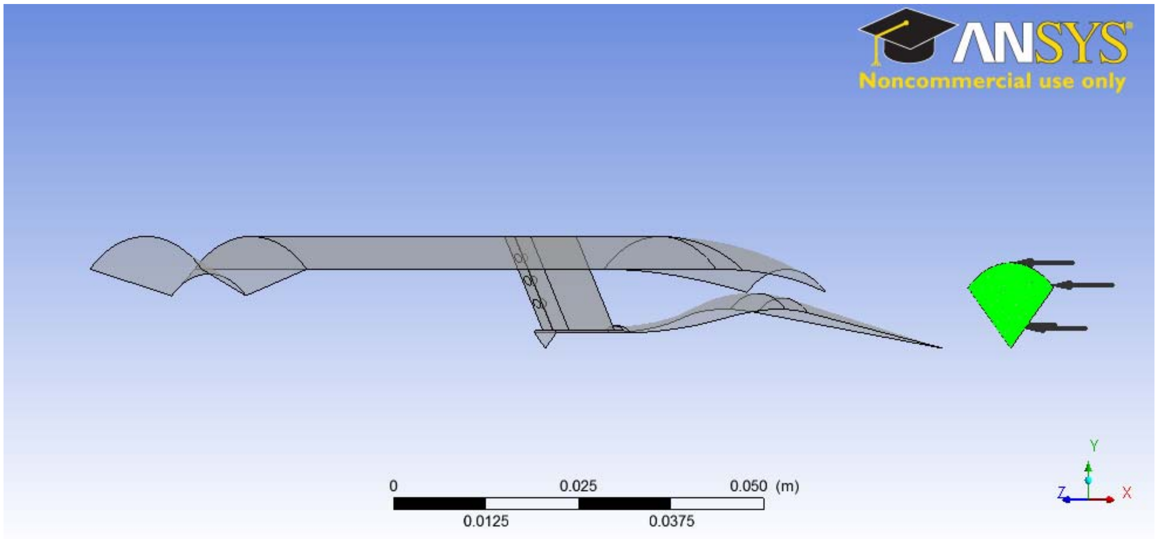

BASIC SETTINGS	
Boundary Type Location	Inlet Inlet
BOUNDARY DETAILS	
Flow Regime → Option	Supersonic
Mass and Momentum - Option - Rel. Static Pressure - Normal Speed	 Normal Speed & Pressure 7504.8 Pa 1180.17 m/s
Turbulence → Option	Medium (Intensity = 5%)
Heat Transfer - Option - Static Temperature	 Static Temperature 216.65K
Components Model → Component - H2 → Option + Mass Fraction - H2O → Option + Mass Fraction - O2 → Option + Mass Fraction	 Mass Fraction 0 Mass Fraction 0 Mass Fraction 0.232

Table 38. Boundary: Outlet – for combustion analysis

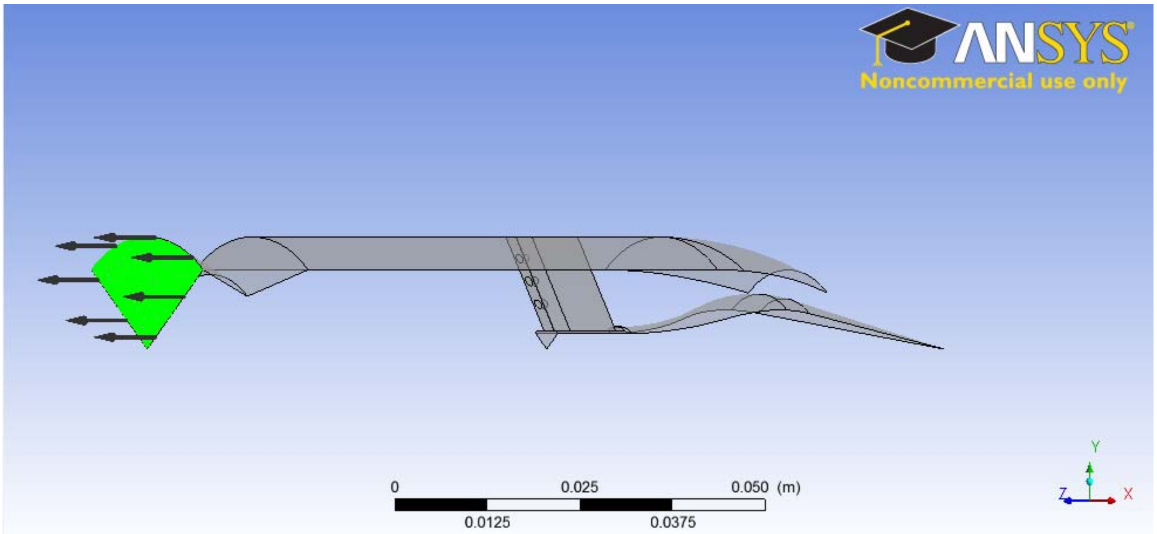

BASIC SETTINGS	
Boundary Type	Outlet
Location	Outlet
BOUNDARY DETAILS	
Flow Regime → Option	Supersonic

Table 39. Boundary: Sym1 – for combustion analysis

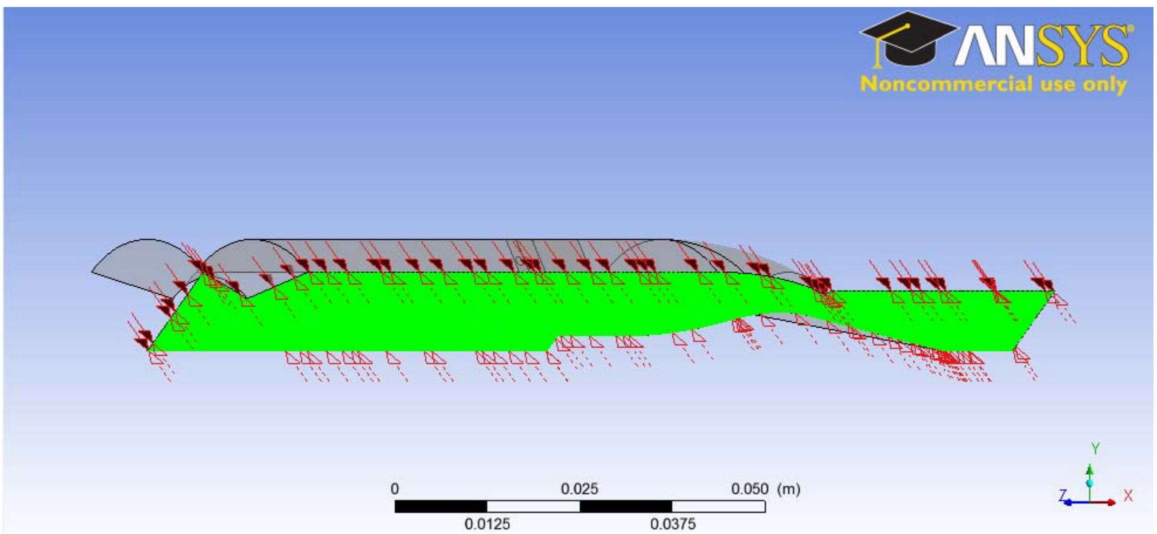

BASIC SETTINGS	
Boundary Type	Symmetry
Location	Sym1

Table 40. Boundary: Sym2 – for combustion analysis

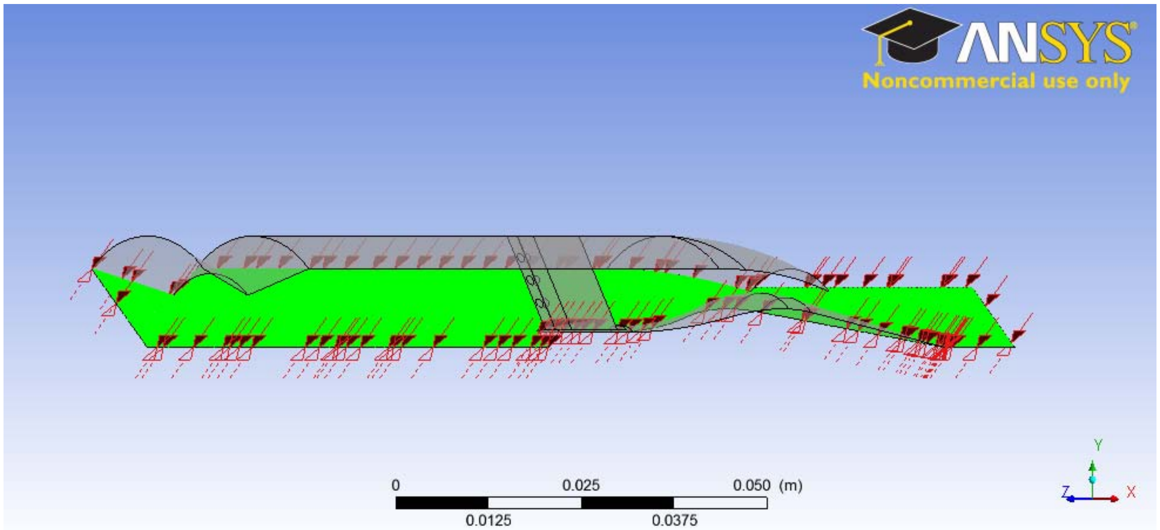

BASIC SETTINGS	
Boundary Type	Symmetry
Location	Sym2

Table 41. Boundary: Ramjet – for combustion analysis

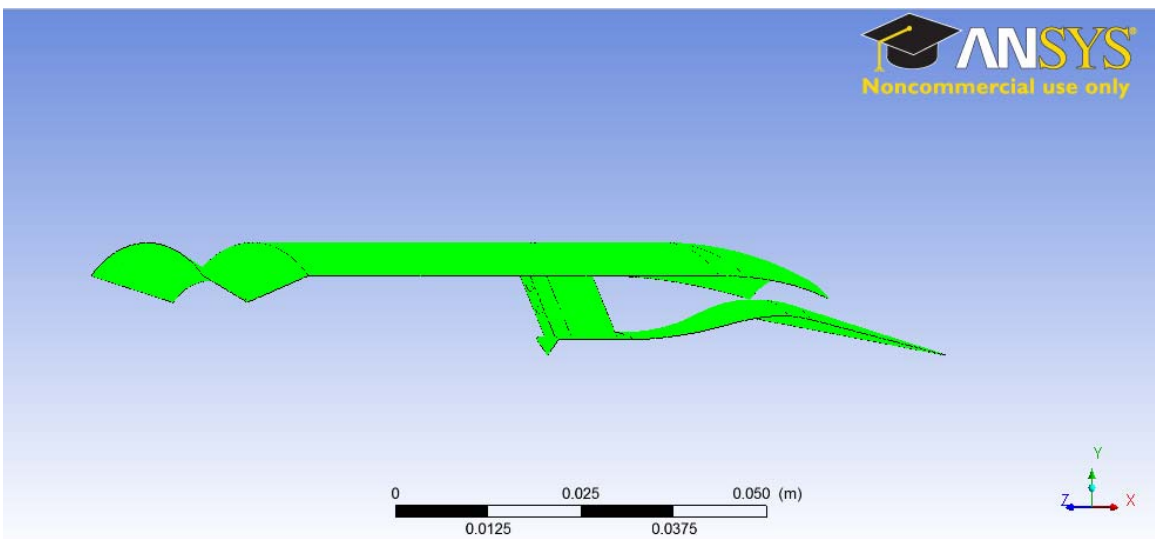

BASIC SETTINGS	
Boundary Type	Wall
Location	Ramjet
BOUNDARY DETAILS	
Mass and Momentum → Option	No Slip Wall
Wall Roughness → Option	Smooth Wall
Heat Transfer → Option	Adiabatic

Table 42. Boundary: Opening – for combustion analysis

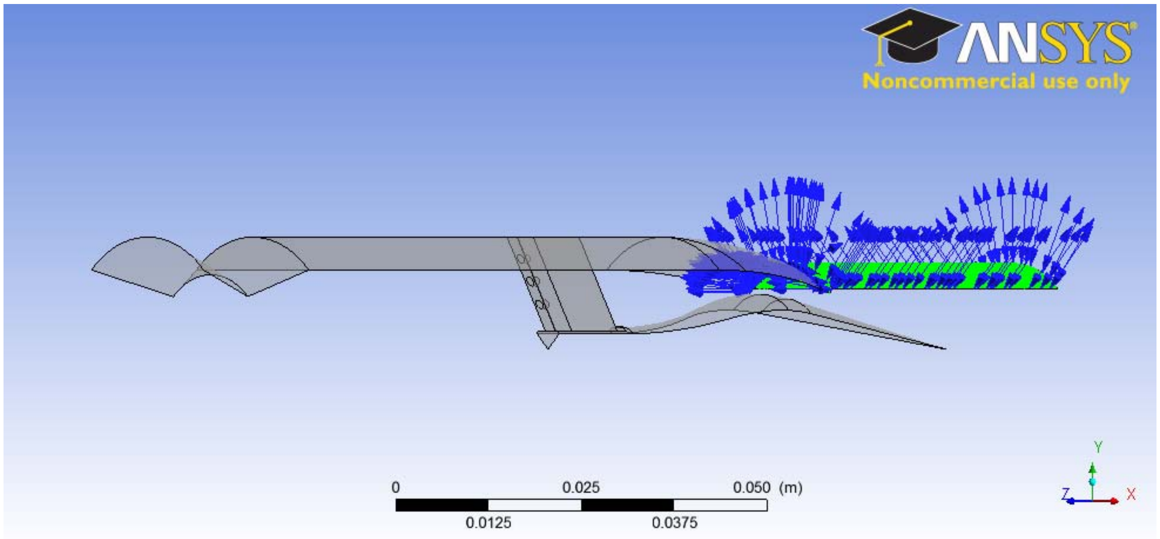

BASIC SETTINGS	
Boundary Type Location	Opening Opening
BOUNDARY DETAILS	
Flow Regime → Option	Subsonic
Mass and Momentum - Option - Relative Pressure	 Opening Pres. And Dirn 7504.8 Pa
Flow Direction → Option	Normal to Boundary Conditions
Turbulence → Option	Medium (Intensity = 5%)
Heat Transfer - Option - Static Temperature	 Static Temperature 216.65K
Components Model → Component - H2 Option + Mass Fraction - H2O Option + Mass Fraction - O2 Option + Mass Fraction	 Mass Fraction 0 Mass Fraction 0 Mass Fraction 0.232

Table 43. Boundary: Rear_Ports – for combustion analysis

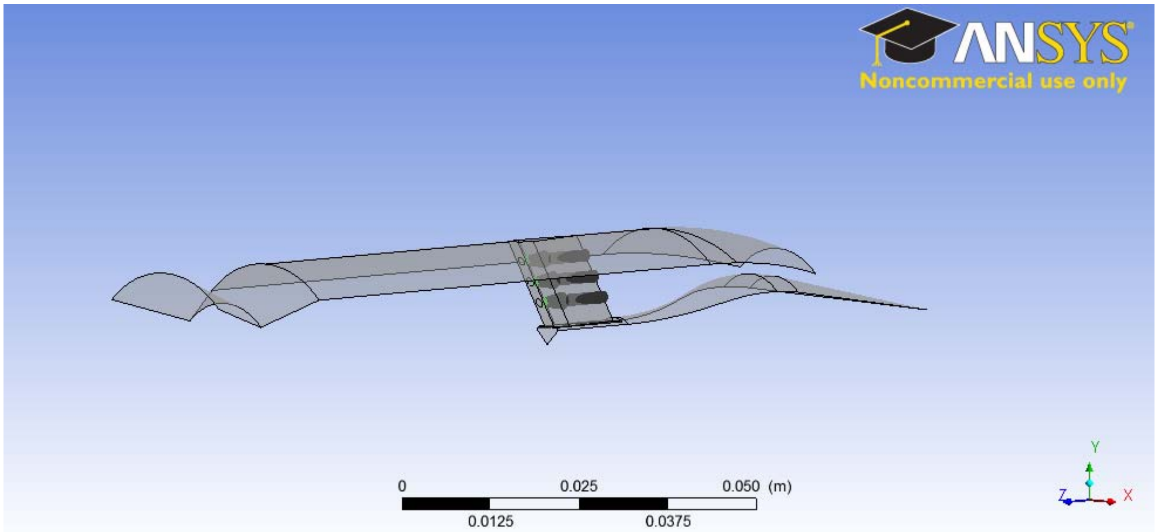

BASIC SETTINGS	
Boundary Type Location	Inlet Rear_Ports
BOUNDARY DETAILS	
Flow Regime → Option	Subsonic
Mass and Momentum - Option - Normal Speed	 Normal Speed 50 m/s
Turbulence → Option	Medium (Intensity = 5%)
Heat Transfer - Option - Total Temperature	 Static Temperature 300K
Components Model → Component - H2 Option + Mass Fraction - H2O Option + Mass Fraction - O2 Option + Mass Fraction	 Mass Fraction 1 Mass Fraction 0 Mass Fraction 0

Table 44. Materials settings: Hydrogen-Air Mixture – for combustion analysis

BASIC SETTINGS	
Option	Reacting Mixture
Material Group	Gas Phase Combustion
Reaction List	Hydrogen Air

Table 45. Expert parameters – for combustion analysis

CONVERGENCE CONTROL	
Memory Control	
- Topology Estimate Factor	Checked
+ Value	1.2
High Speed Numerics	
- Max Continuity Loops	Checked
+ Value	3

Table 46. Solver control settings for combustion analysis

BASIC SETTINGS	
Advection Scheme →Option	High Resolution
Turbulence Numerics →Option	High Resolution
Convergence Control	
- Min. Iterations	1
- Max. Iterations	1000
- Fluid Timescale Control	
+ Timescale Control	Local Timescale Factor
+ Local Timescale Factor	2
Convergence Criteria	
- Residual Type	RMS
- Residual Target	1.00E-06
ADVANCE OPTIONS	
Compressibility Control	Checked
- High Speed Numerics	Checked

Table 47. Global initialization for combustion analysis

GLOBAL SETTINGS	
Initial Conditions	
Velocity Type	Cartesian
Cartesian Velocity Components →Option	Automatic
Static Pressure →Option	Automatic
Temperature →Option	Automatic
Turbulence →Option	Medium (Intensity =5%)
Component Details - H2 Option - H2O Option + Mass Fraction - O2 Option + Mass Fraction	 Automatic Automatic with Value 0.01 Automatic with Value 0.232

Table 48. Activating combustion in domain for combustion analysis

FLUID MODELS	
Combustion - Option - Eddy Dissipation Model Coefficient B	 Eddy Dissipation 0.5
Thermal Radiation → Option	None

F3. OTHER NOTES

1. Mass-flow injection of Hydrogen fuel

A low hydrogen injection velocity of 50 m/s was used to start the simulation. This velocity was ramped up incrementally to 400 m/s. After the computation stabilized at 400 m/s, the combustion settings in the domain setup was activated.

2. Time-stepping

As seen in the CFX-PRE setup section, a local timescale control with a factor of 2 was used to start the simulation. As the simulation stabilizes, the timescale control was switched to automatic timescale control with a timescale factor of 1. Subsequently, the timescale factor was ramped progressively to a factor of 3 to reduce the time taken for the results to converge. These changes in time scaling can be performed on the fly with the “Edit run in progress” function in CFX-POST.

APPENDIX G – ENGINEERING DRAWINGS FOR RAMJET MODEL

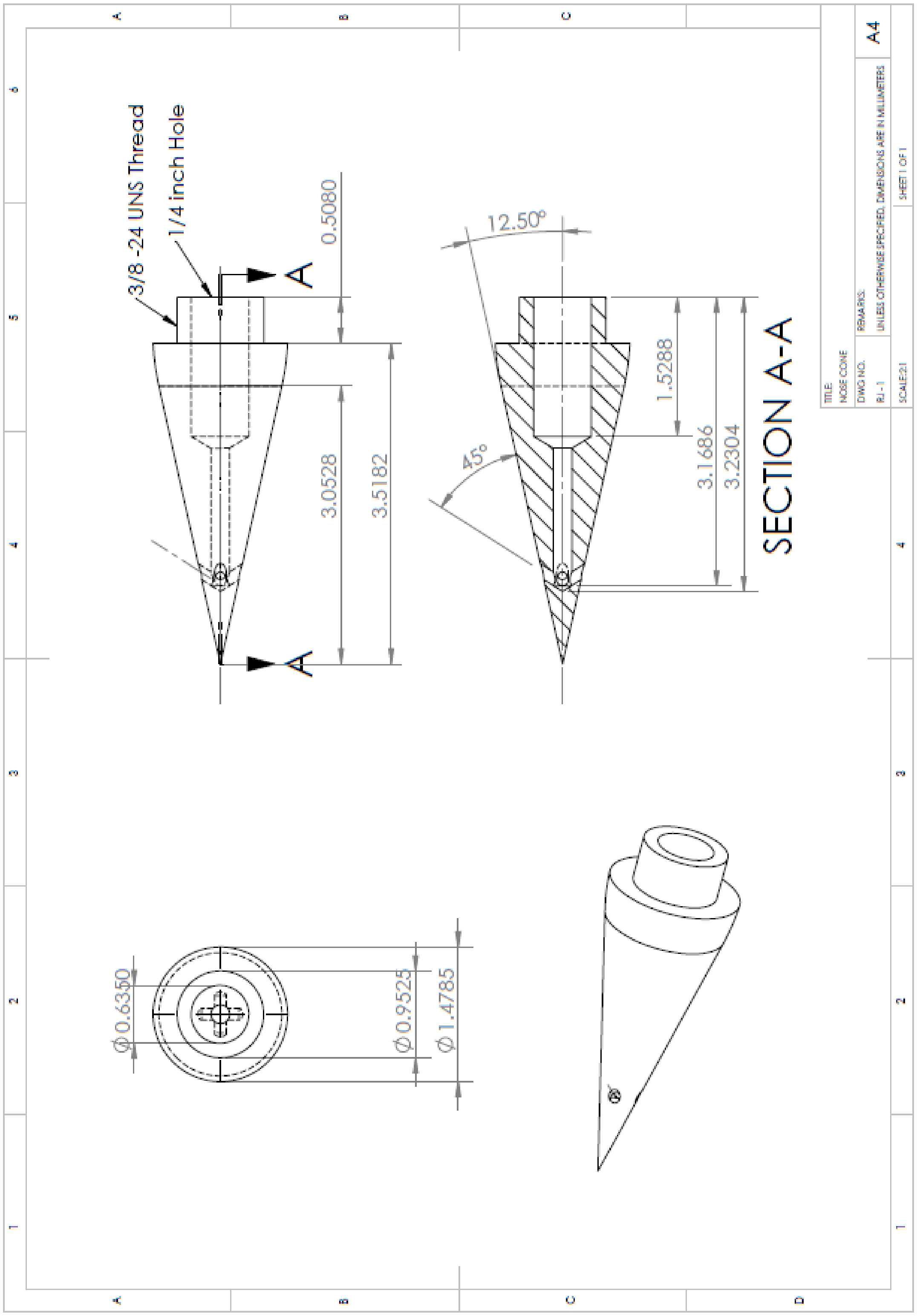

Figure 38. Part drawing: Ramjet inlet nose cone (RJ – 1)

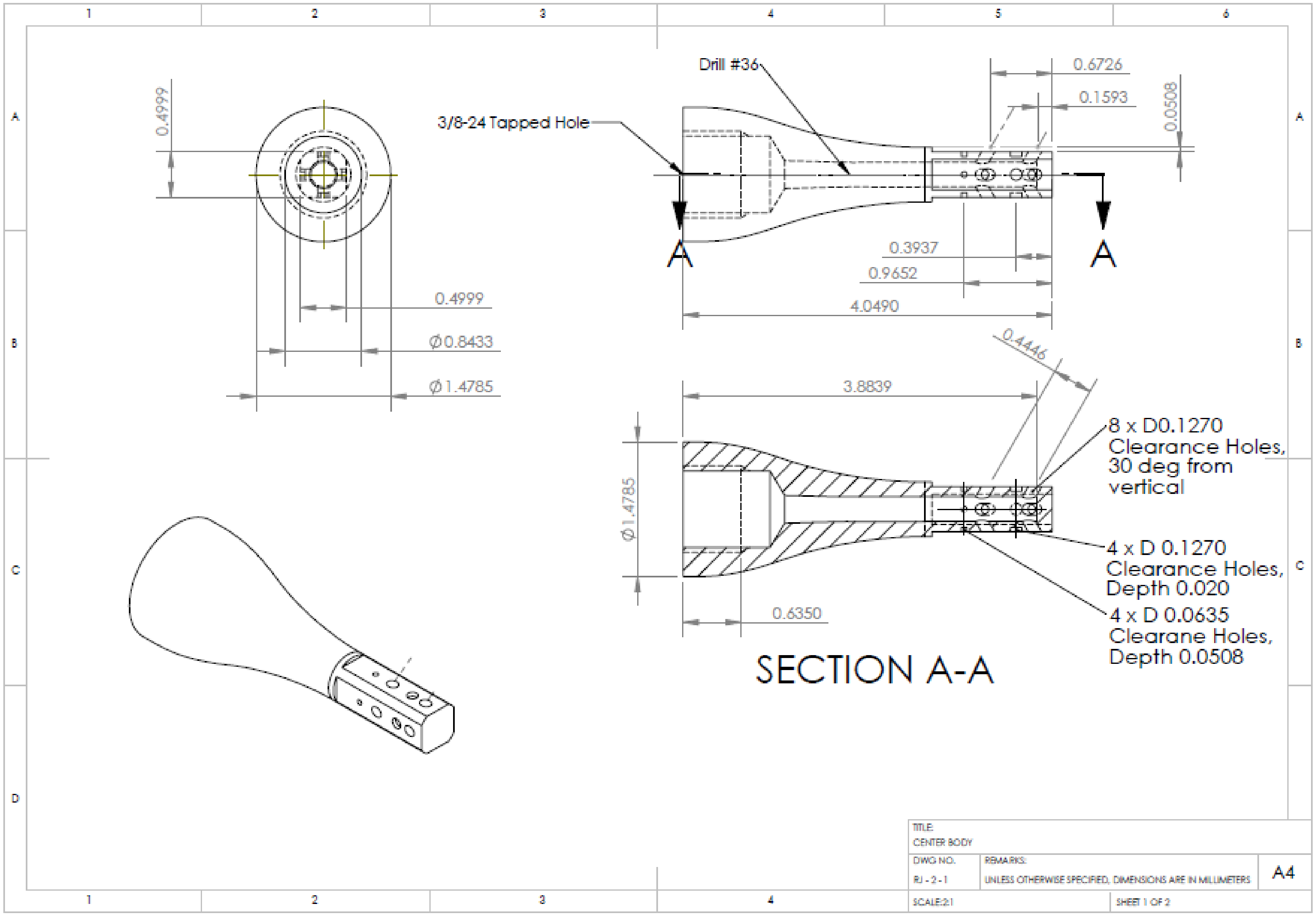

Figure 39. Part drawing: Ramjet center body (RJ – 2 – 1)

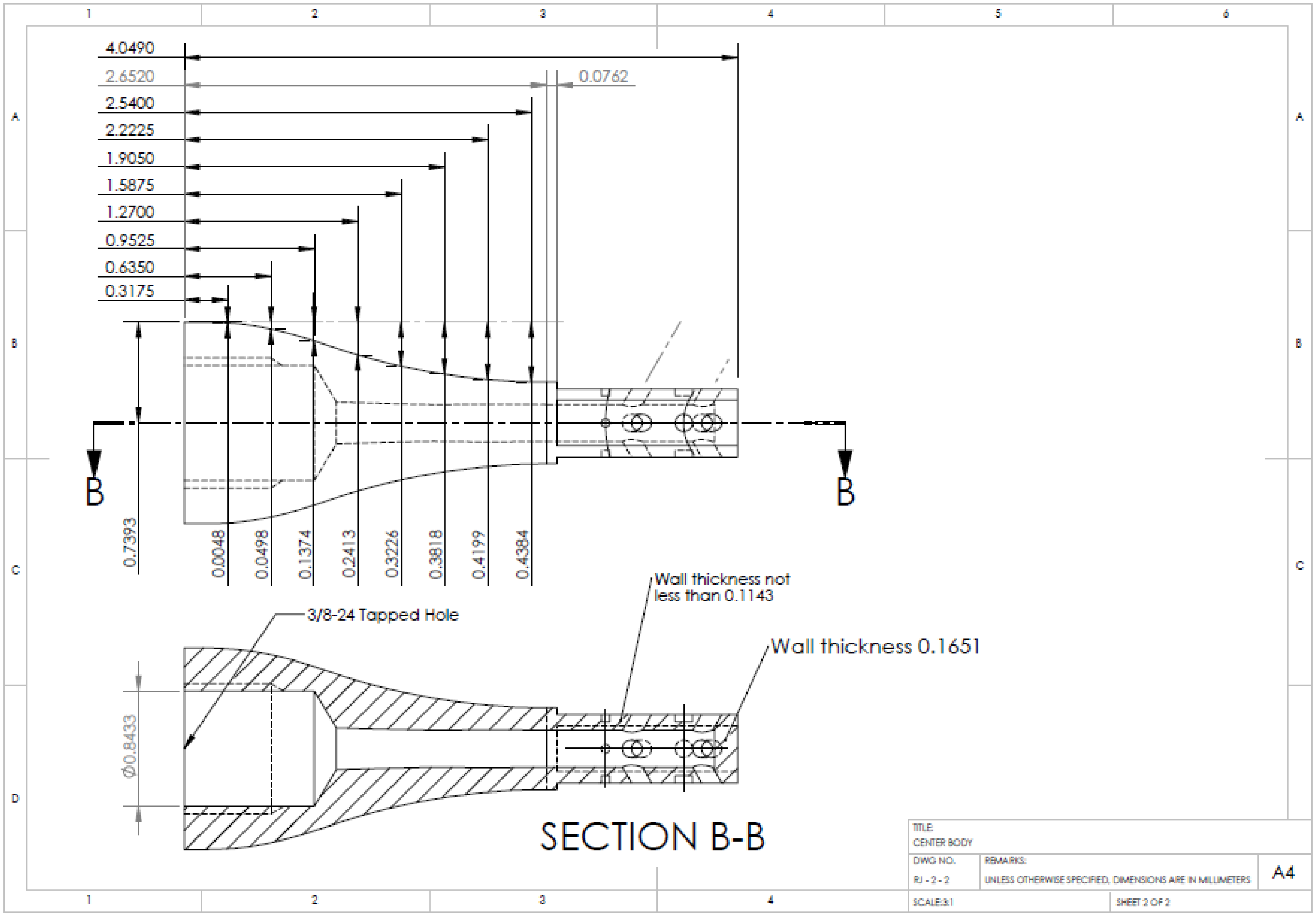

Figure 40. Part drawing: Contour of ramjet center body (RJ – 2 – 2)

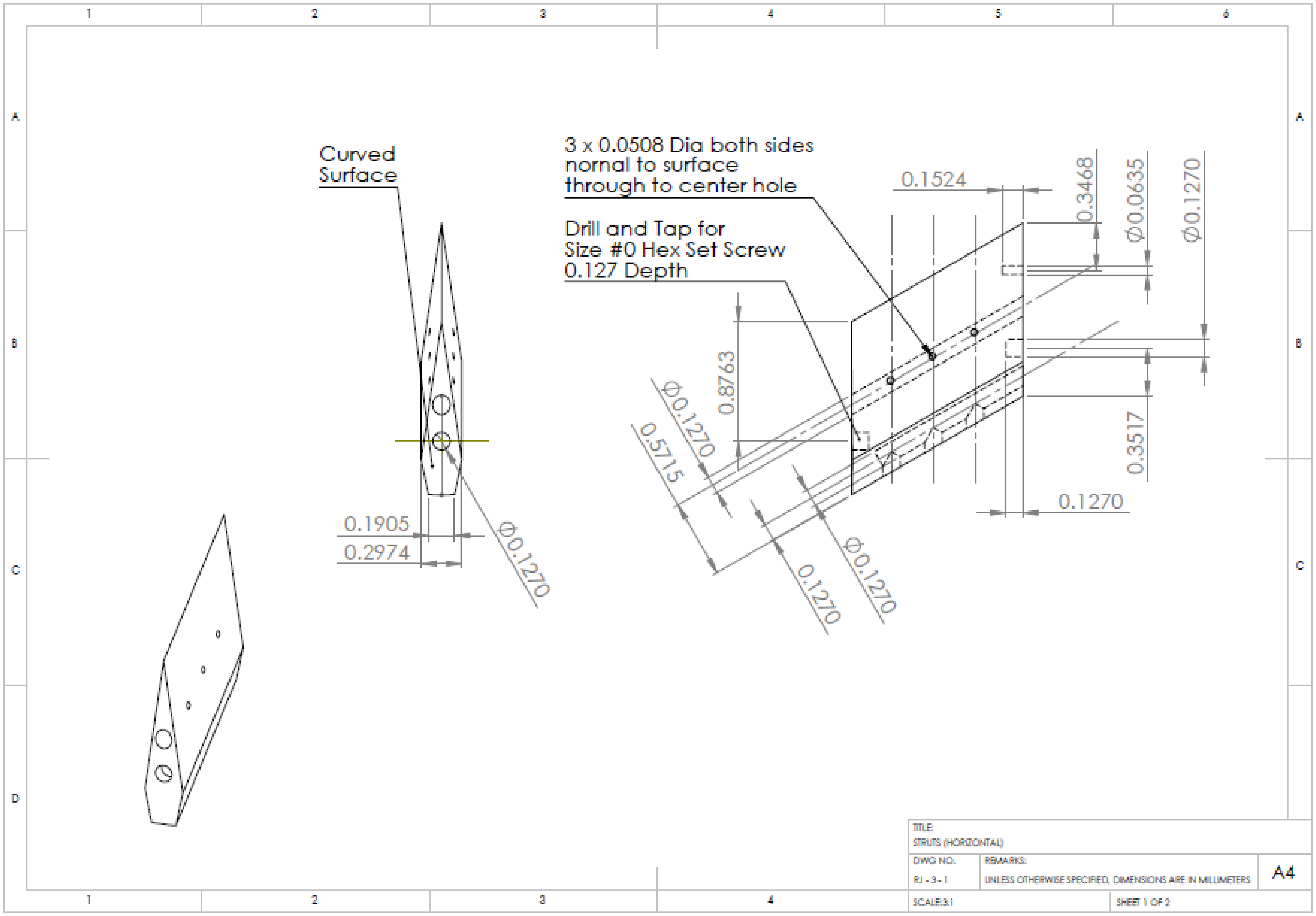

Figure 41. Part drawing: Ramjet horizontal struts (RJ – 3 – 1)

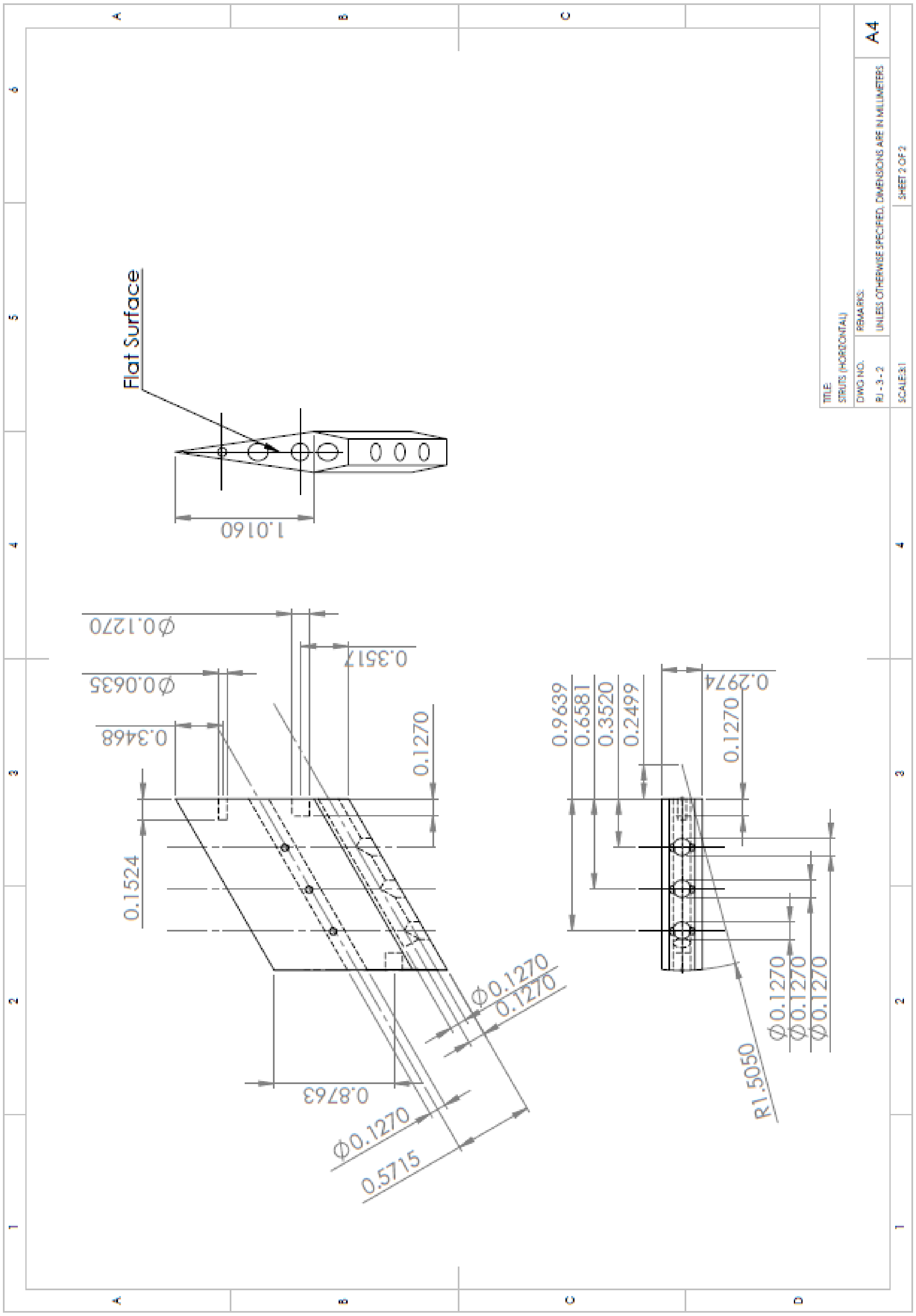

Figure 42. Part drawing: Ramjet horizontal struts (RJ – 3 – 2)

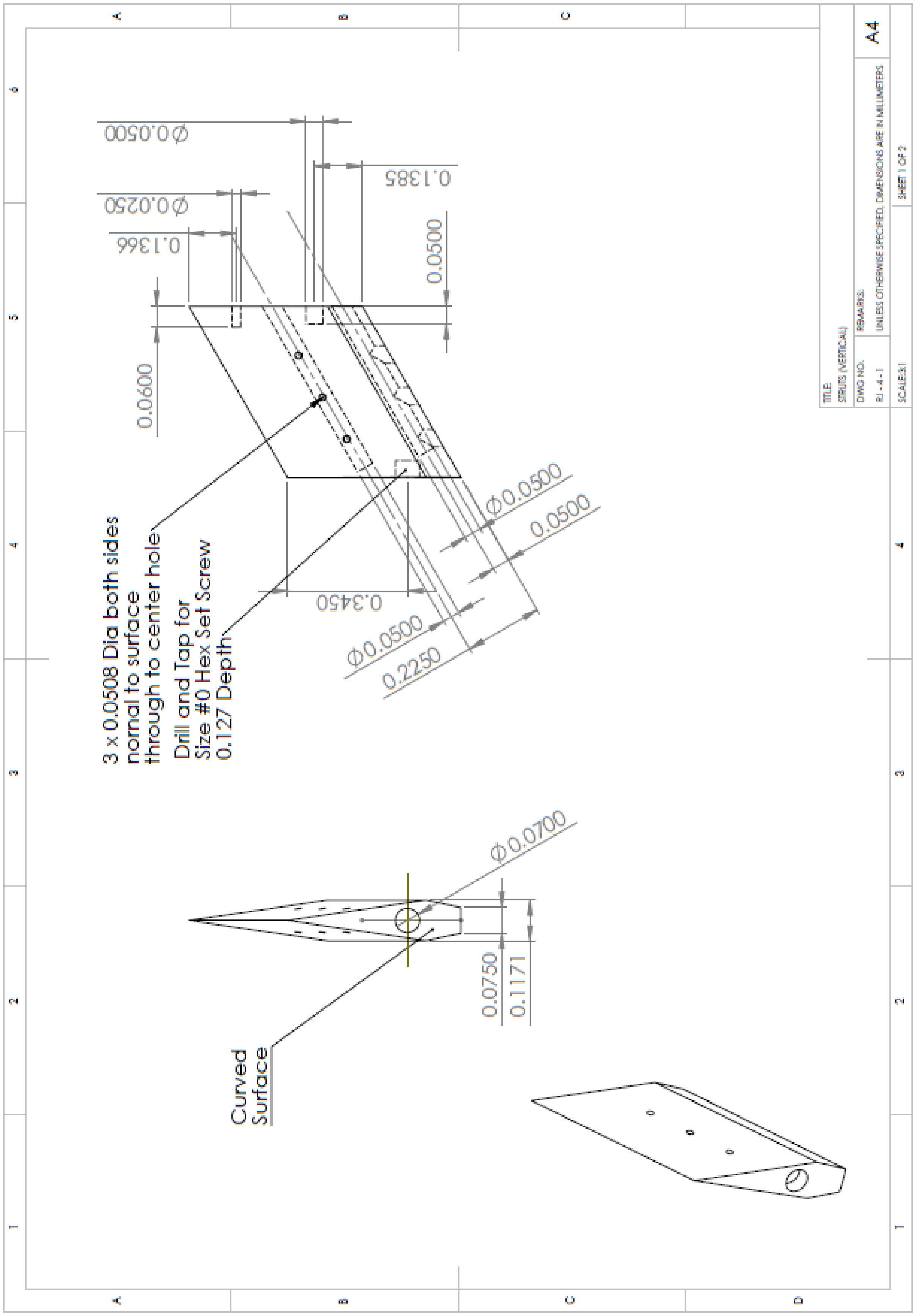

Figure 43. Part drawing: Ramjet vertical struts (RJ – 4 – 1)

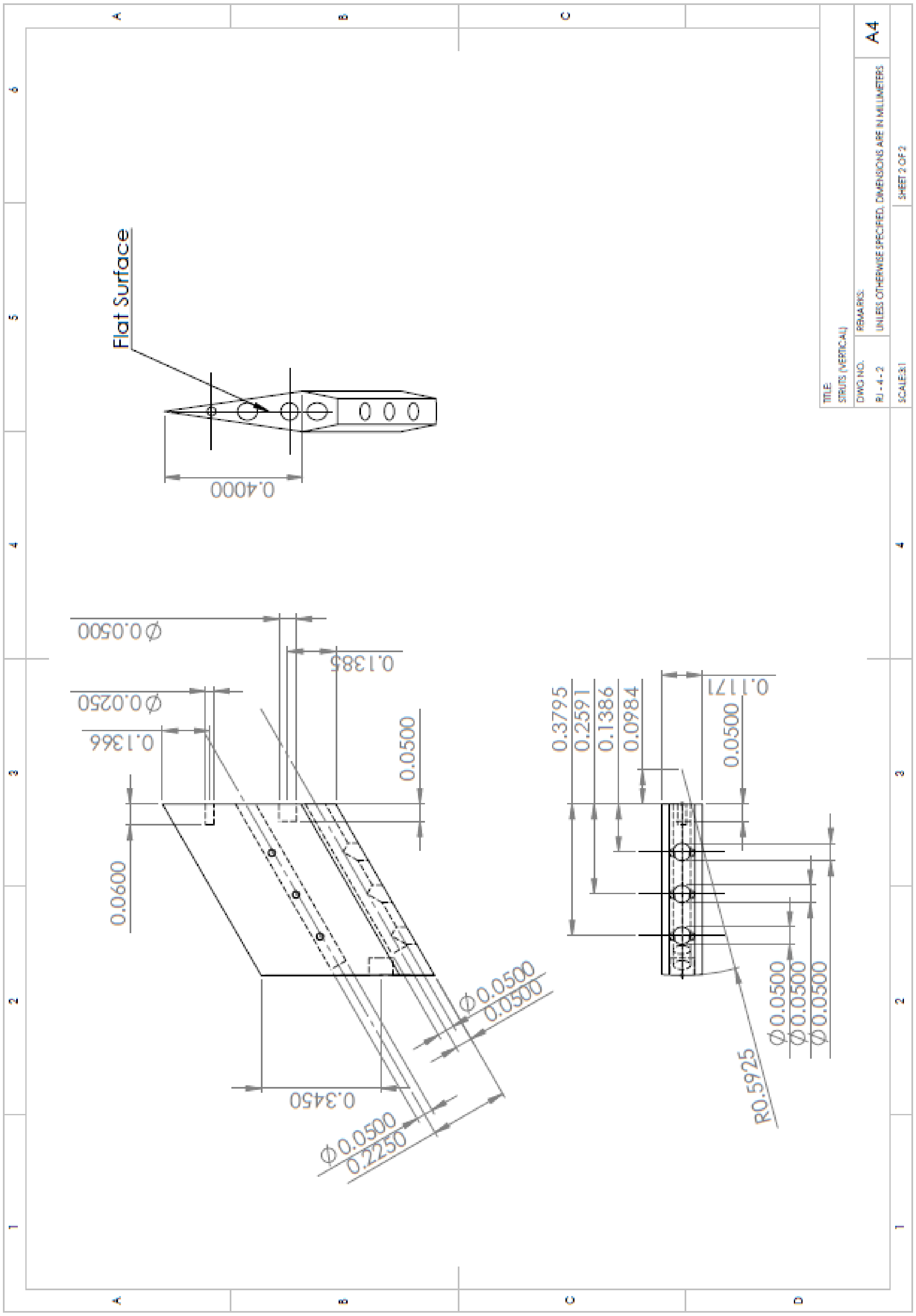

Figure 44. Part drawing: Ramjet vertical struts (RJ – 4 – 2)

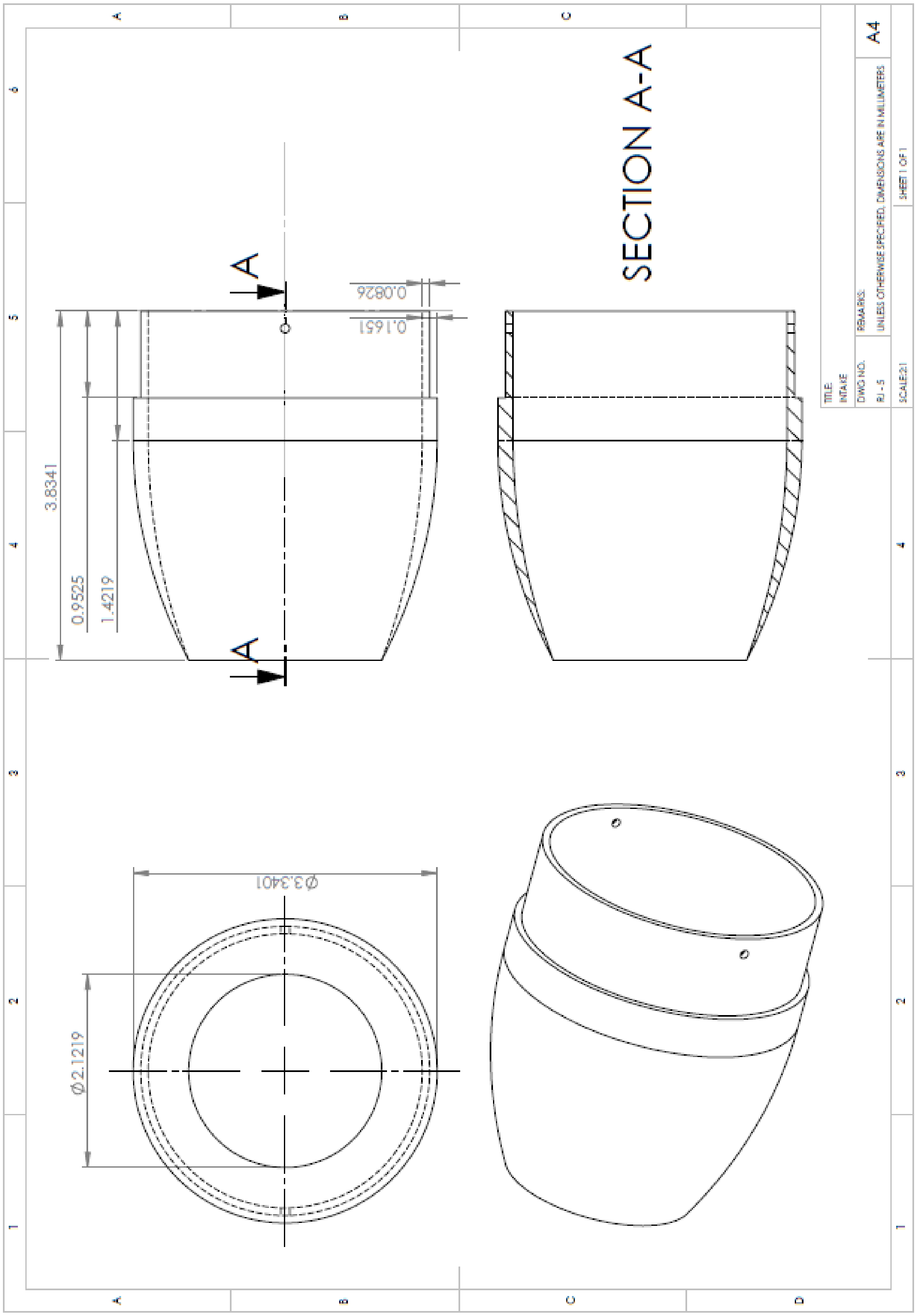

Figure 45. Part drawing: Ramjet intake (RJ – 5)

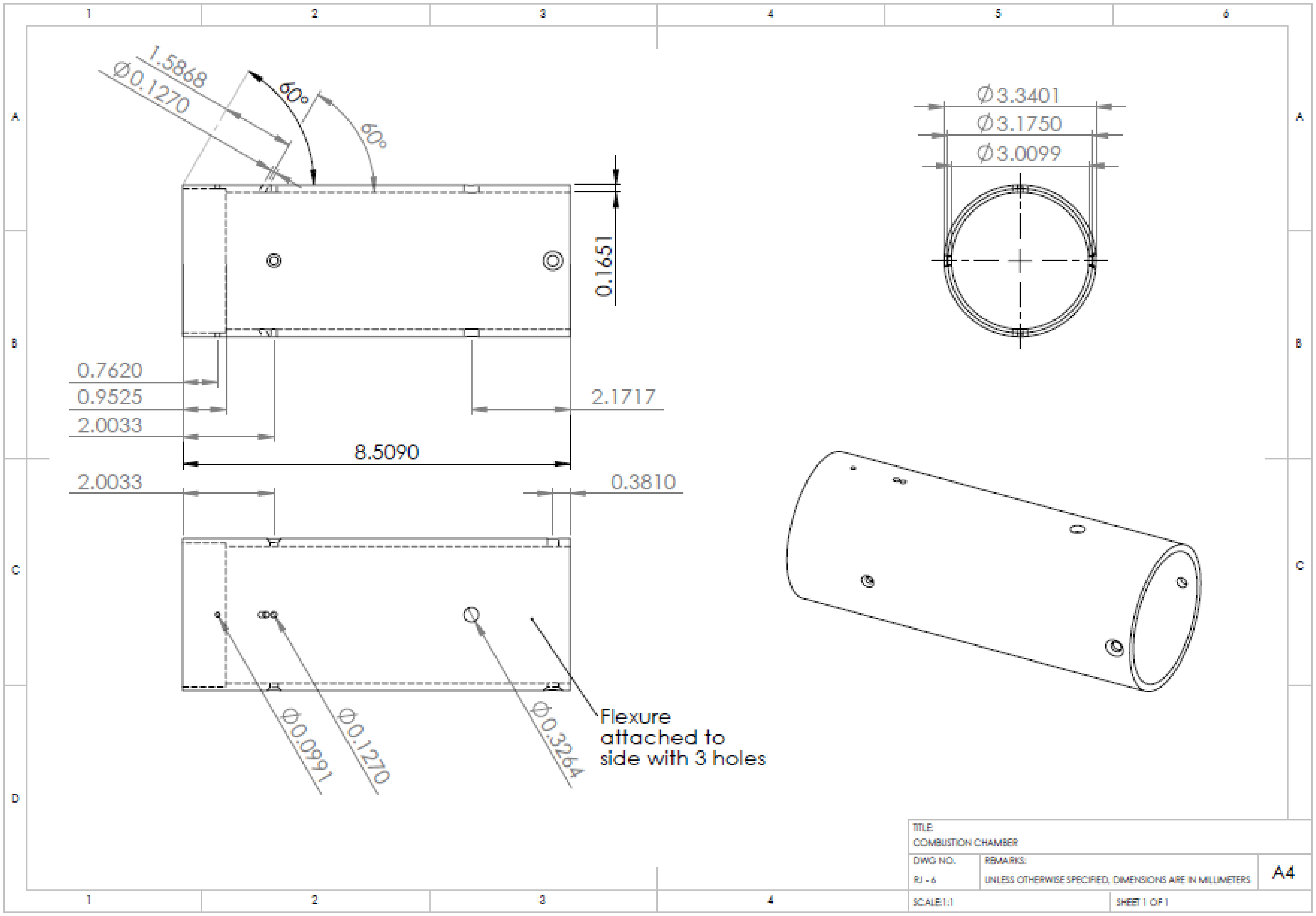

Figure 46. Part drawing: Ramjet combustion chamber (RJ – 6)

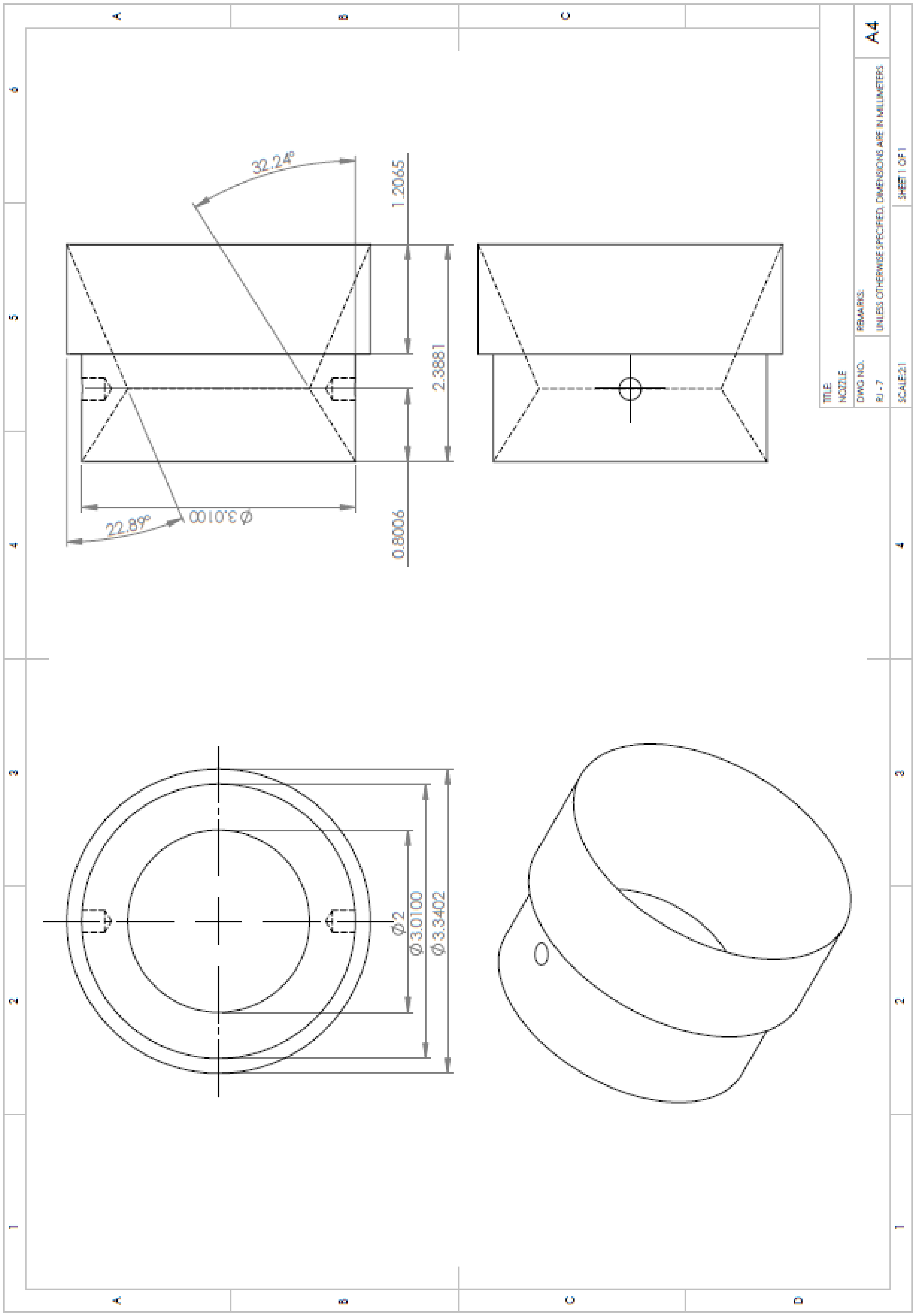

Figure 47. Part drawing: Ramjet nozzle (RJ – 7)

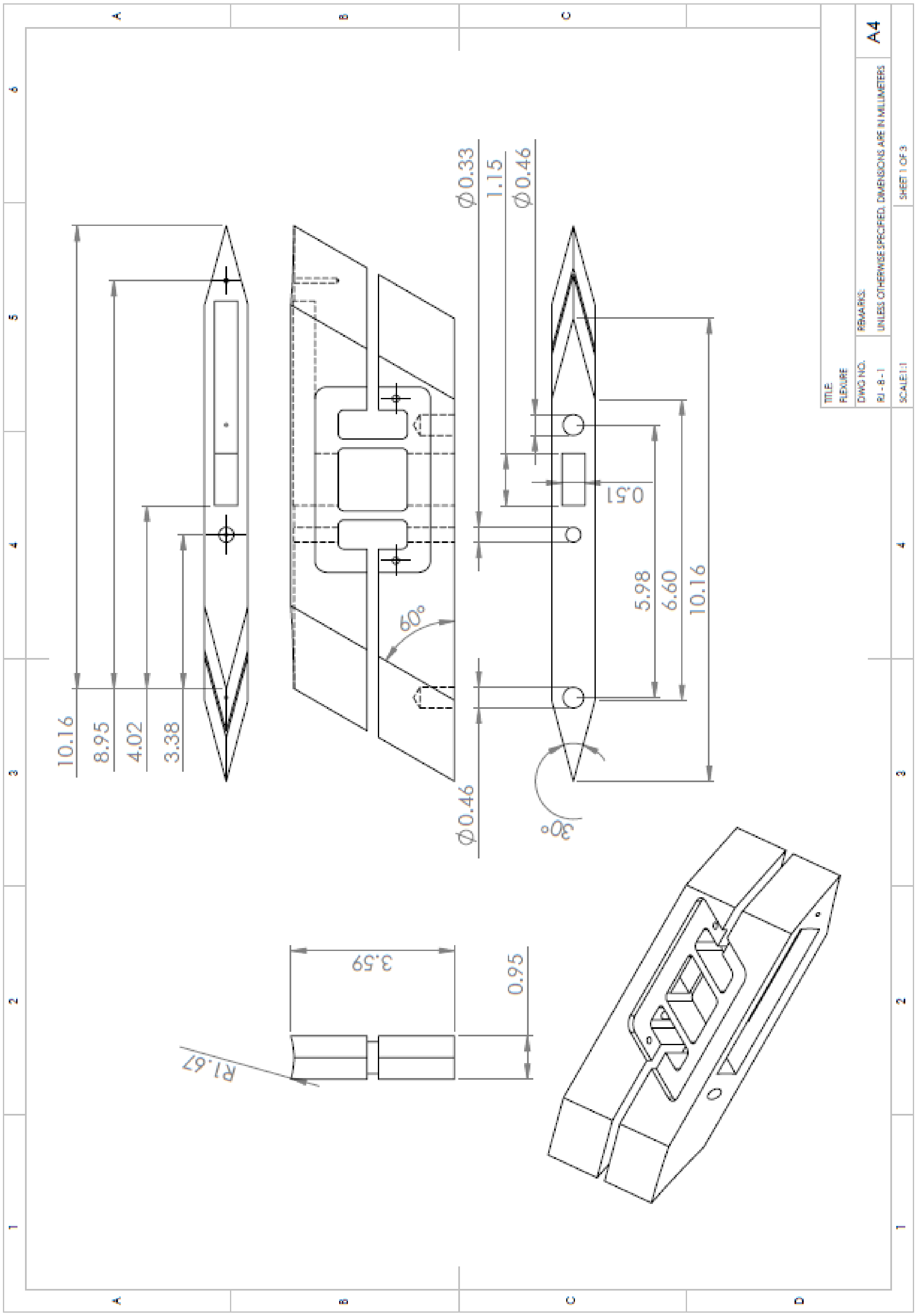

Figure 48. Part drawing: Flexure (RJ – 8 – 1)

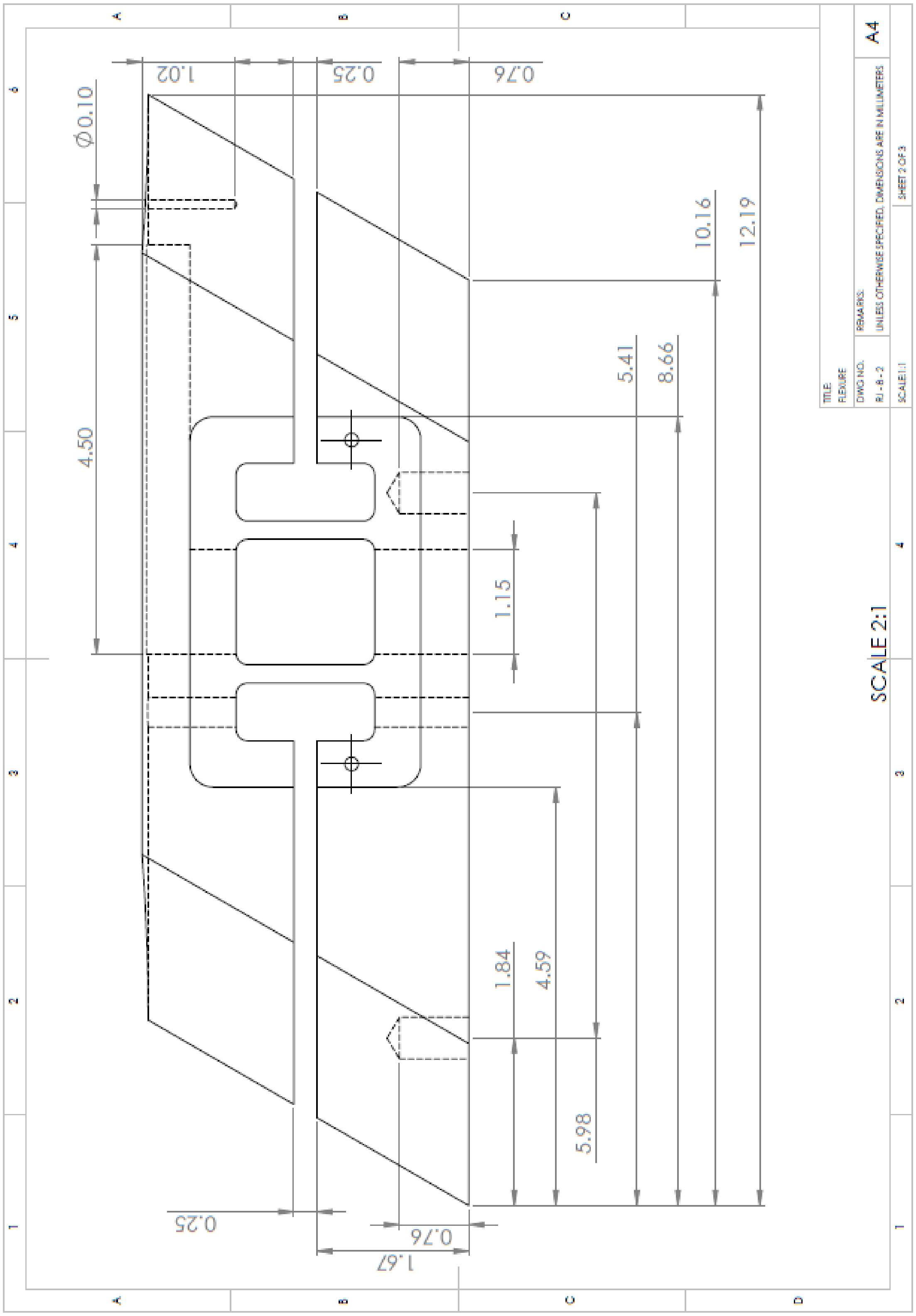

Figure 49. Part drawing: Flexure (RJ – 8 – 2)

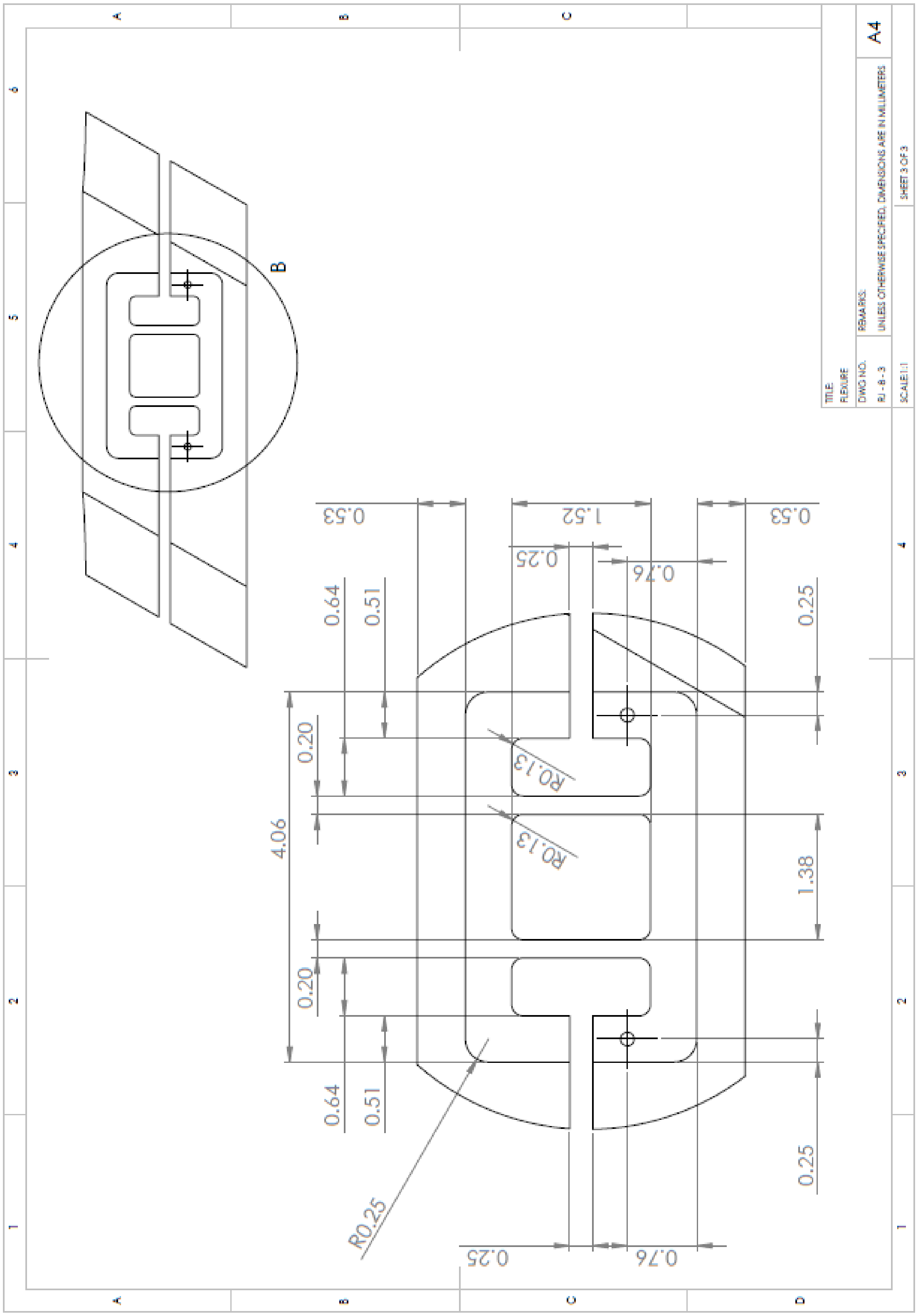

Figure 50. Part drawing: Flexure (RJ – 8 – 3)

THIS PAGE INTENTIONALLY LEFT BLANK

APPENDIX H – Details for Strain Gauges used

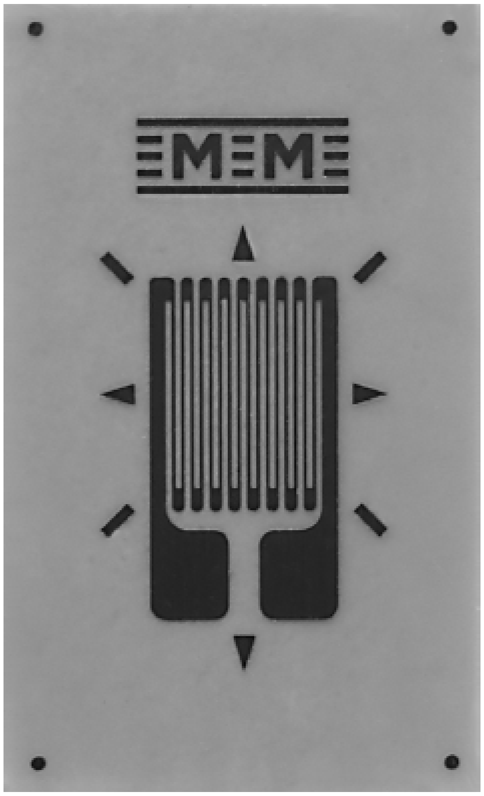

Manufacturer:
Micro-Measurements
(Vishay Precision Group)

Model:
WK – 13 – 062AP – 350

Description:
Fully encapsulated Nickel-Chromium Alloy (K-Alloy)

Operating Temperature Range:
-269°C to 290°C (Normal**)**
-269°C to 400°C (Normal**)**

Resistance:	350 Ω
Fatigue Strain:	2200με
Gauge Length:	1.57 mm
Overall Length:	2.90 mm
Grid Width:	1.57 mm
Overall Width:	1.57 mm
Matrix Length:	6.6 mm
Matrix Width:	4.1 mm

WK Series
WK-Series gages are fully encapsulated K alloy, equipped with integral, high-endurance beryllium copper leadwires. The matrix is a high-temperature epoxy-phenolic resin system reinforced with glass fibers. Overall gage thickness is approximately 0.0028 in [0.071 mm]. WK-Series gages have the widest temperature range and most extensive environmental capability of any general purpose strain gage of the self-temperature-compensated type. Option W is available on many pattern designs, but will lower the excellent cyclic endurance and maximum operating temperature of the basic WK gage. Elevated temperature drift of these gages is very low to +600°F [+315°C], and the main restriction at high temperatures is the limited life of the backing and adhesive due to oxidation and sublimation. Strain limits for WK gages are approximately ±1.5%. High temperature adhesives such as M-Bond 610 are required for full-range performance.

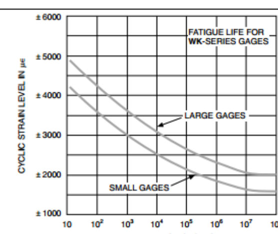

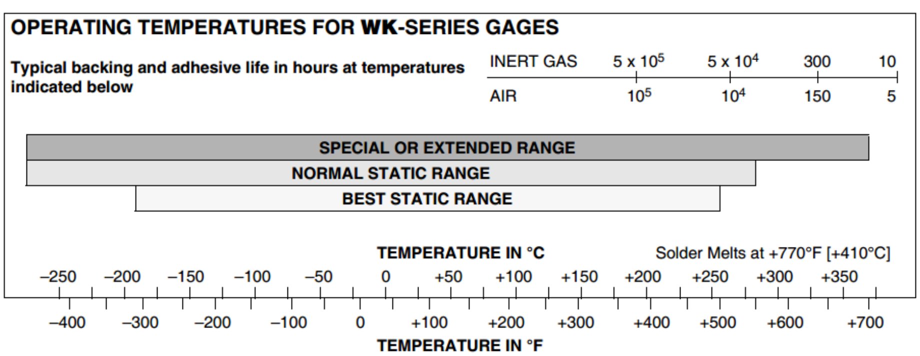

Details used here are extracted from the Manufacturer's Data Sheet, available for download online at: http://www.vishaypg.com/docs/50003/precsg.pdf

THIS PAGE INTENTIONALLY LEFT BLANK

APPENDIX I – DETAILED EXPERIMENT PROCEDURES FOR DRAG MEASUREMENT EXPERIMENT

I1. CALIBRATION OF SIGNALS CONDITIONING SYSTEM

Note: Unless otherwise stated, all PIN references refers to the PIN on the CALEX 8610 Backplane.

1. Set up the signals conditioning system.

a. On the CALEX 163MK Bridgesensor.

i. Set dip switch 1 to OFF.

ii. Set dip switch 2 and 3 to ON, 4 and 5 to OFF.

b. On the CALEX 8610 backplane, set dip switch 6 to ON and 7 to OFF.

c. Connect the 110V A.C. power input to L1, L2 and G.

d. Set the input offset to 0V.

i. Short PIN 2 (Sense+) and PIN 3 (Bridge+).

ii. Short PIN 11(Common) and PIN and PIN 12 (Sense-).

iii. Turn on the power supply.

iv. Monitor the voltage drop across PIN 3 and 10 and tune RP2 on the Bridgesensor until the required excitation voltage to 4V DC is obtained.

v. Turn off the power supply.

2. Set the input offset of the amplifier to 0V.

a. Connect PIN 13 (In-) and PIN 14 (In+) to PIN 10 (Common).

b. Turn on the power supply.

c. Monitor the voltage of PIN 16 (Amplifier Output).

d. On the Bridgesensor, tune RP3 (Input offset trim port) to get a 0V.

e. Turn off the power supply.

f. The input offset is now 0V.

3. Set the gain of the amplifier to 100.

a. Disconnect PIN 14 (In+) from PIN 10 (Common).

b. Feed 1mV into PIN 14 (In+).

c. Turn on the power supply.

d. Monitor the voltage drop across PIN 16 (amplifier output) and PIN 10.

e. Tune RP5 (coarse gain adjustment) and RP4 (fine gain adjustment) on the Bridgesensor until the voltage drop across PIN 16 and PIN 10 is 0.1V.

f. Turn off the power supply.

g. The gain of the amplifier is now set to 100.

I2. LOAD CELL CALIBRATION

1. Set up the load cell as shown in Figure 51.

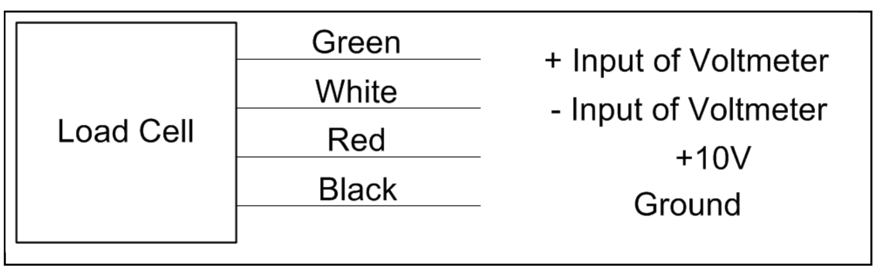

Figure 51. Wiring diagram for load cell calibration

2. Apply a 1kg mass to the load cell and note the voltage response on the voltmeter.

3. Repeat step 2 for 2kg - 5kg mass.

I3. STRAIN GAUGE CALIBRATION

1. Balancing the Wheatstone bridge.

a. Setup the ramjet in the SSWT without the nose cone.

b. Connect the Wheatstone bridge setup to the signals conditioning. system and data acquisition system. (Figure 52)

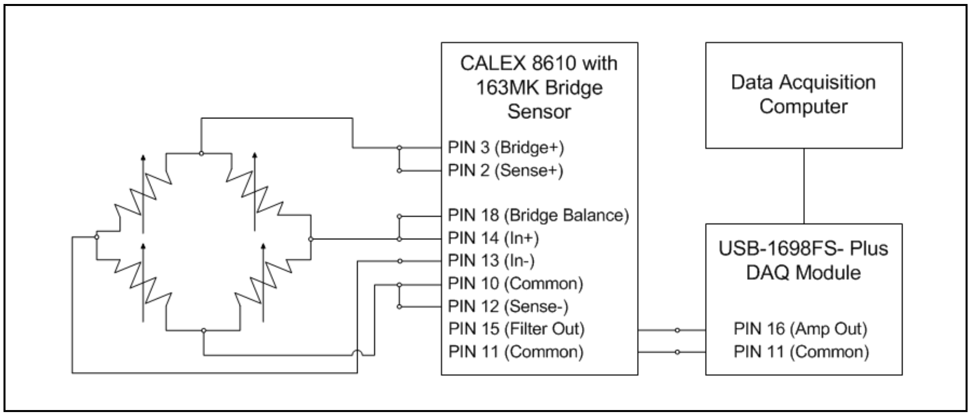

Figure 52. Wiring diagram for bridge balancing

c. Turn on the power supply.

d. Tune RP6 (bridge balance) on the Bridgesensor until 0V is attained.

e. Turn off the power supply.

f. The Wheatstone bridge is now balanced.

2. Calibrate the flexure arms.

a. Set up the load cell circuit as shown in Figure 51.

b. Mount the load cell and thrust fixture into the SSWT (Figure 53).

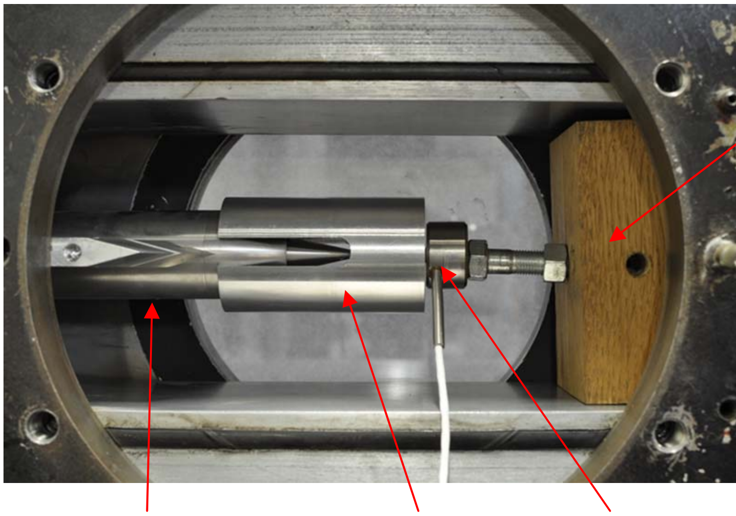

Figure 53. Load cell and thrust fixture mounted in SSWT with ramjet model

c. Turn on the power supply.

d. Turn the jackscrew until the equivalence of a 1kg mass force is observed on the voltmeter.

e Monitor the voltage drop across PIN 15 (Filter out) and PIN 10 (Common).

d. Repeat 2d and 2e with the equivalence of a 2kg, 3kg, 4kg and 5kg mass force.

e. Determine the force and voltage drop relationship for the strain gauges.

I4. DRAG MEASUREMENT

1. Drag measurement.

a. Setup the ramjet in the SSWT.

b. Connect the Wheatstone bridge setup to the signals conditioning system and data acquisition system (Figure 52).

c. Start the SSWT to Mach 4.

d. Log the voltage drop measurements with the TracerDAQ software.

2. Base on the mass-voltage drop relationship obtained in C2, determine the drag force induced on the ramjet and inner flexures.

THIS PAGE INTENTIONALLY LEFT BLANK

APPENDIX J – DETAIL SETUP FOR cfd DRAG prediction

J1. MESH SETUP

The drag analysis uses the same set of meshing parameters with those in the cold-flow analyses. Refer to Appendix A for details.

J2. CFX-PRE SETUP PARAMETERS

Table 49. Default domain for drag analysis

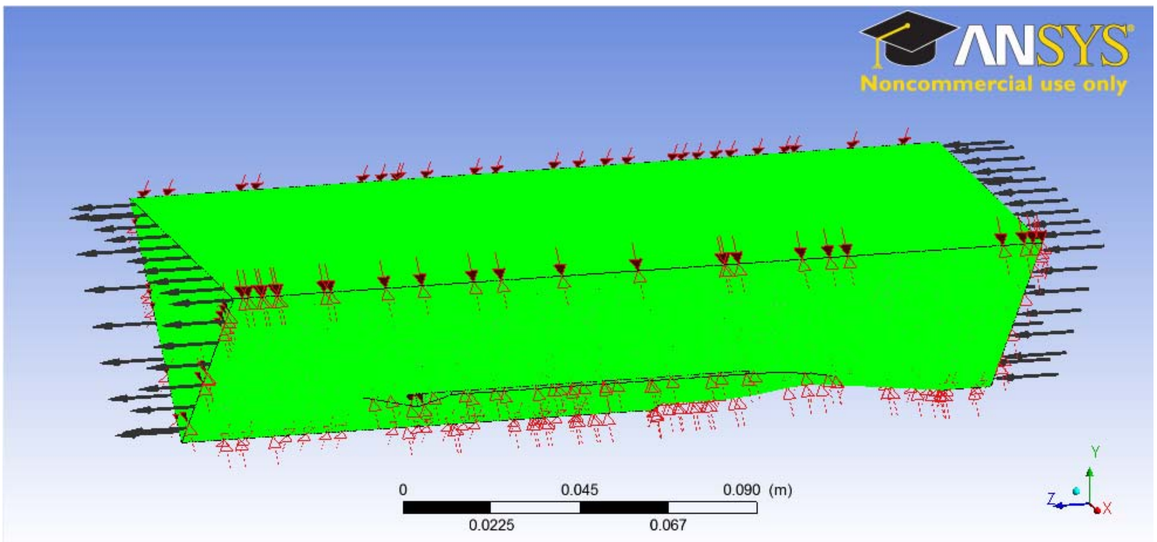

BASIC SETTINGS	
Location and Type	
- Location	<use default>
- Domain Type	Fluid Domain
- Coordinate Frame	Coord 0
Fluid and Particles Definition for Fluid 1	
- Option:	Material Library
- Material	Air Ideal Gas
- Morphology	Continuous Fluid
Domain Models	
- Pressure → Reference Pressure	0 Pa
- Buoyancy Model → Option	Non-Buoyant
- Domain Motion → Option	Stationary
- Mesh Deformation → Option	None

FLUID MODELS	
Heat Transfer → Option	Total Energy
Turbulence - Option - Transitional Turbulence	 Shear Stress Transport Gamma Theta Model
Combustion → Option	None
Thermal Radiation → Option	None

Table 50. Boundary: Flexure – for drag analysis

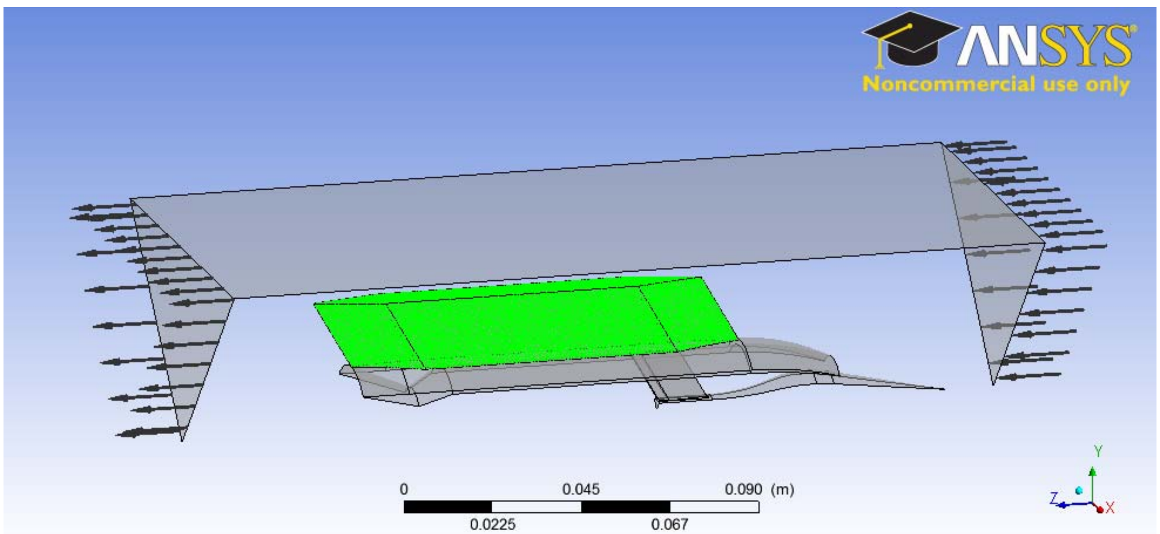

BASIC SETTINGS	
Boundary Type Location	Wall Top
BOUNDARY DETAILS	
Mass and Momentum → Option Heat Transfer → Option	No Slip Wall Adiabatic

3. Other Setup Parameters

The other boundary conditions and setup parameters are the same as those used in the cold-flow analyses. Refer to Appendix A for details.

J3. OTHER NOTES

1. Time-stepping

As seen in the CFX-PRE setup section, a local timescale control with a factor of 3 was used to start the simulation. As the simulation stabilizes, the timescale control was switched to automatic timescale control with a timescale factor of 1. Subsequently, the timescale factor was ramped progressively to a factor of 3 to reduce the time take for the results to converge. These changes in time scaling can be performed on the fly with the “Edit run in progress” function in CFX-POST.

THIS PAGE INTENTIONALLY LEFT BLANK

LIST OF REFERENCES

[1] K. M. Ferguson, *Design and cold flow evaluation of a miniature mach 4 ramjet,* Monterey, CA, 2003.

[2] W. T. Khoo, *Cold flow drag measrement and nmerical performance prediction of a miniature ramjet at mach 4,* Monterey, CA, 2003.

[3] "ANSYS CFX-SOLVER theory guide," [Online]. Available: https://www1.ansys.com/customer/content/documentation/140/cfx_thry.pdf. [Accessed 1 March 2012].

[4] J. E. Bardina, P. G. Huang and T. J. Coakley, *Turbulence modeling validation, testing, and development,* 1997.

[5] F. R. Menter, "Two-equation eddy-viscosity turbulence models for engineering applications," *AIAA Journal,* vol. 32, no. 8, pp. 1598-1605, Aug. 1994.

THIS PAGE INTENTIONALLY LEFT BLANK

INITIAL DISTRIBUTION LIST

1. Defense Technical Information Center
   Ft. Belvoir, Virginia

2. Dudley Knox Library
   Naval Postgraduate School
   Monterey, California

3. Hobson, Garth
   Department of Mechanical and Aerospace Engineering
   Naval Postgraduate School
   Monterey, California

4. Brophy, Christopher
   Department of Mechanical and Aerospace Engineering
   Naval Postgraduate School
   Monterey, California

5. COL Lim Soon Chia
   Defence Research and Technology Office
   Ministry of Defence
   Singapore

6. Yeo Tat Soon
   Temasek Defence Systems Institute
   National University of Singapore
   Singapore

7. Tan Lai Poh
   Temasek Defence Systems Institute
   National University of Singapore
   Singapore